PORTLAND CEMENT pca ASSOCIATION

Research and Development
Construction Technology Laboratories

PB 281 733

50272-101

REPORT DOCUMENTATION PAGE	1. REPORT NO. NSF/RA-760844	2.	3. Recipient's Accession No.
4. Title and Subtitle Earthquake Resistant Structural Walls - Tests of Coupling Beams (Progress Report)			5. Report Date Oct. 29, 1976
			6.
7. Author(s) C.B. Barney, K.N. Shiu, B.G. Rabbat, A.E. Fiorato			8. Performing Organization Rept. No.
9. Performing Organization Name and Address Portland Cement Association Construction Technology Laboratories Old Orchard Road Skokie, Illinois 60076			10. Project/Task/Work Unit No.
			11. Contract(C) or Grant(G) No. (C) GI43880 (G)
12. Sponsoring Organization Name and Address Applied Science and Research Applications (ASRA) National Science Foundation 1800 G Street, N.W. Washington, D.C. 20550			13. Type of Report & Period Covered Progress
			14.

15. Supplementary Notes

16. Abstract (Limit: 200 words)

Design criteria for reinforced concrete structural walls used as lateral bracing in earthquake resistant buildings are being developed. Tests are conducted to investigate the behavior of reinforced concrete coupling beams under reversing loads. This report covers test details and preliminary results for the first six coupling beam tests. Four specimens with diagonal reinforcement and two with no diagonal reinforcement were tested. The specimens were subjected to in-plane reversing loads. Instrumentation was applied to determine loads, deformations, and strains. The geometry, reinforcement details, material properties, and construction procedures are described. Results indicate that all specimens had considerable ductility. Beams with diagonal reinforcement demonstrated improved behavior as compared to beams with straight bars. Two specimens without diagonal reinforcement exhibited rapid loss of strength after the peak load was reached. Cumulative ductility was also lower.

17. Document Analysis   a. Descriptors

Earthquake resistant structures	Tests	Design standards
Beams (supports)	Structural design	
Structural members	Construction	
Walls	Buildings	

b. Identifiers/Open-Ended Terms

Coupling beams

c. COSATI Field/Group

18. Availability Statement NTIS.	19. Security Class (This Report)	21. No. of Pages 142
	20. Security Class (This Page)	22. Price A07-A01

(See ANSI–Z39.18)   See Instructions on Reverse   OPTIONAL FORM 272 (4
(Formerly NTIS–35)
Department of C...

i

Report to
THE NATIONAL SCIENCE FOUNDATION
(RANN)
Grant No. GI-43880

EARTHQUAKE RESISTANT STRUCTURAL WALLS -
TESTS OF COUPLING BEAMS
(Progress Report)

By: G. B. Barney, K. N. Shiu,
        B. G. Rabbat, and A. E. Fiorato

Date: October 29, 1976

EARTHQUAKE RESISTANT STRUCTURAL WALLS -
TESTS OF COUPLING BEAMS (Progress Report)

by

G. B. Barney, K. N. Shiu, B. G. Rabbat, and A. E. Fiorato*

INTRODUCTION

Background

The Portland Cement Association is carrying out a program to develop design criteria for reinforced concrete structural walls used as lateral bracing in earthquake resistant buildings. Of primary concern in this investigation is the ductility, energy dissipation capacity, and strength of the walls. The combined analytical and experimental investigation is sponsored in part by the National Science Foundation under Grant GI-43880.

As part of this program, tests are being conducted to investigate the behavior of reinforced concrete coupling beams under reversing loads. Coupling beams are frequently used to join adjacent structural walls. For buildings in earthquake regions, these beams are required to withstand large inelastic deformations.

Structural wall systems, combining isolated structural walls with coupling beams, will be tested in another part of the program.

This progress report covers test details and preliminary test results for the first six coupling beam tests.

*Respectively, Structural Engineer, Associate Structural Engineer, Structural Engineer, and Senior Structural Engineer, Structural Development Section, Portland Cement Association, Skokie, Illinois.

Objective and Scope

The objectives of this investigation are:

1. To provide information for selecting details of coupling beams for use in tests of structural wall systems.

2. To determine load-deformation characterictics of coupling beams with various reinforcing details.

3. To determine the ductility and energy dissipation capacities of coupling beams subjected to reversing loads.

4. To determine strengths of coupling beams subjected to reversing loads.

Six coupling beam specimens have been tested. Details of each specimen and test results are reported in the following sections.

The test specimens represent approximately 1/3-scale models of coupling beams. However, no specific prototypes were modeled. Normal weight concrete and deformed reinforcing bars were used in the specimen. The specimens were subjected to in-plane reversing loads. Instrumentation was applied to determine loads, deformations, and strains.

Variables

Variables included in the test program were type and amount of diagonal reinforcement and size of confined concrete core. Four specimens with diagonal reinforcement and two with no diagonal reinforcement were tested. All speci-

mens had a span-to-depth ratio of 2.5. Further tests are planned to investigate beams with different span-to-depth ratios.

A summary of the specimens tested to date is given in Table 1. Hoops constructed of D-3 deformed bars were used in each specimen to provide confinement. Two core sizes were considered. Specimens C1, C2 and C3 were tested with a core size of 2.63x6.16 in. (67x157 mm.), out to out of hoops. The core size for Specimens C4, C5 and C6 was 3.50x6.16 in. (89x157 mm.).

TEST SPECIMENS

This section reports the geometry, reinforcement details, and material properties for the six specimens tested. Construction procedures are also described.

Specimen Description
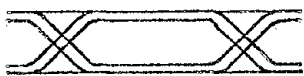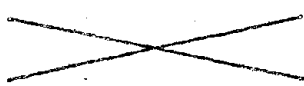
Each test specimen consisted of two coupling beams framing into rigid abutment walls at each end as shown in Fig. 1. The end condition imposed by the abutments simulated the effect of the walls in a structural wall system.

Coupling beams had rectangular cross sections 4-in. (102-mm.) wide and 6.67-in. (169-mm.) deep. The beams had lengths of 16.67 in. (423 mm.). The L-shaped abutments were 4-in. (102 mm.) thick.

Specimen Design

The specimens were designed assuming a concrete design compressive strength of 3000 psi (20.7 MPa) and reinforcing steel yield stress of 60,000 psi (413.7 MPa). Strain hardening

TABLE 1 –   TEST SPECIMENS

Specimen	Core Width a (in.)	Diagonal Reinforcement
C1	2.63	
C2	2.63	
C3	2.63	
C4	3.50	
C5	3.50	
C6	3.50	

1 in. = 25.4mm.

16.67" (423 mm.)
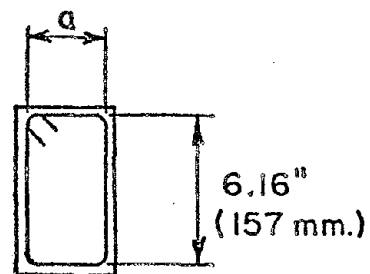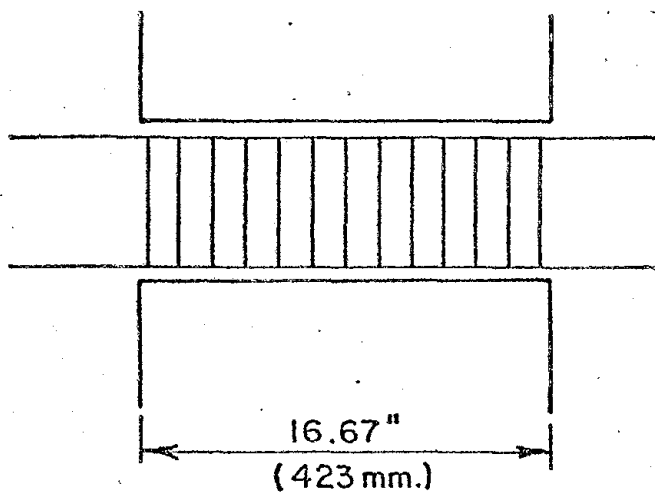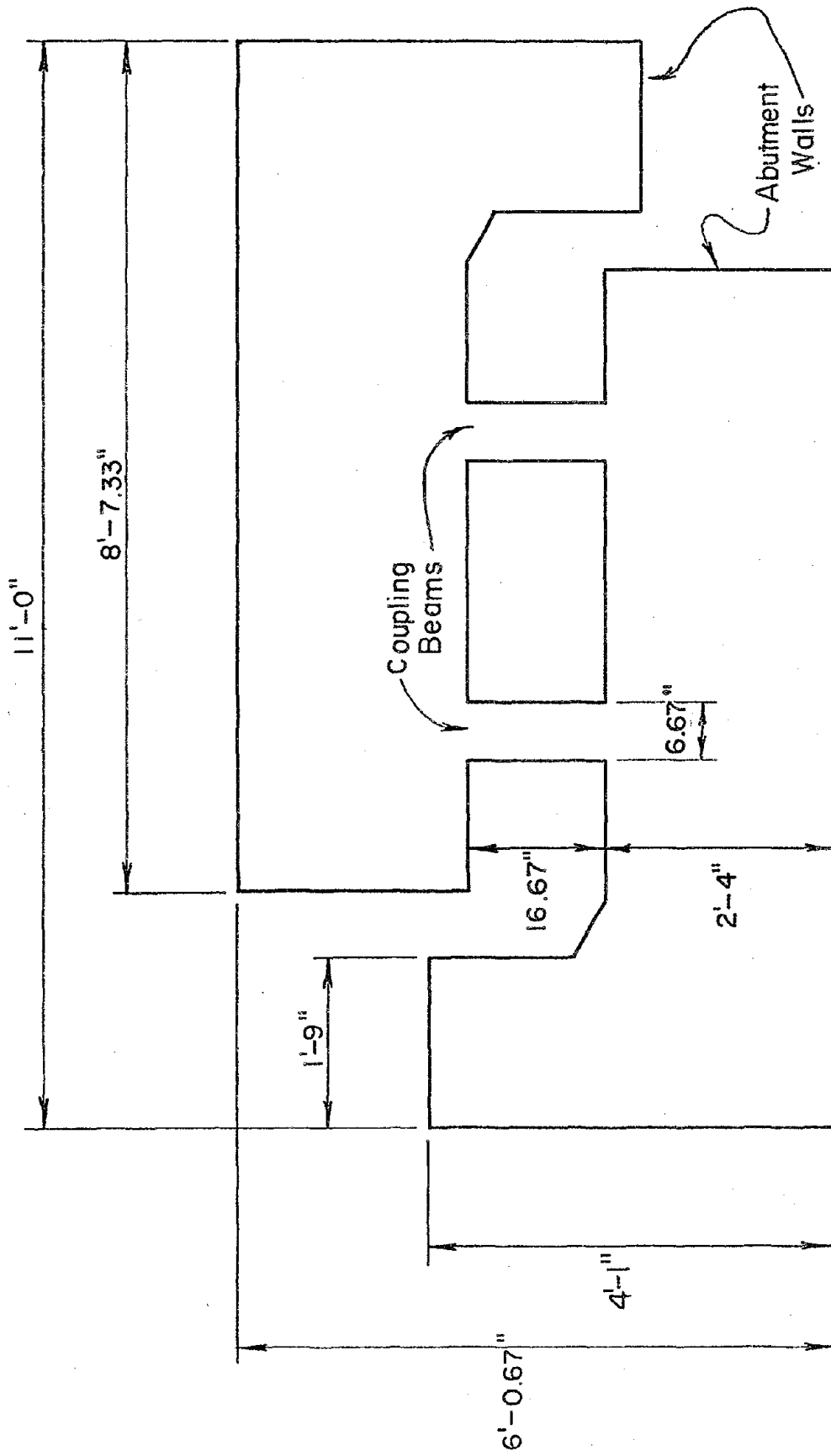
6.16" (157 mm.)

Fig. 1 Specimen Geometry

1" = 25.4 mm.

Abutment Walls

Coupling Beams

11'-0"

8'-7.33"

6.67"

16.67"

2'-4"

1'-9"

4'-1"

6'-0.67"

in the reinforcing steel was assumed to increase the ultimate stress by 50% above the yield stress.

The results of tests reported by Bertero and Popov[1] indicated that satisfactory behavior was obtained for coupling beams with special reinforcement subjected to nominal shear stresses as high as $6\sqrt{f'_c}$ ($0.50\sqrt{f'_c}$). The beams in their investigation had shear span to depth ratios similar to those described in this report. For this investigation, beams with even higher maximum nominal shear stresses were tested. Specimens were designed so that nominal shear stresses as high as $9\sqrt{f'_c}$ ($0.75\sqrt{f'_c}$) could be expected. Shear stresses were calculated from Eq. 11-3 of the 1971 ACI Building Code[2] with $\phi = 1$. Shear reinforcement was proportioned using Eq. 11-13 of the ACI Code[2] assuming $v_c = 0$. Flexural steel was selected to be compatible with the required level of shear stress, assuming 50% strain hardening. Embedment of flexural steel was 50% greater than that required by the ACI Code[2] to allow for additional bar forces caused by strain hardening.

Diagonal reinforcement in Specimens C1, C3 and C4 was designed to carry the ultimate shear force without yielding. The reinforcement was provided to reduce the amount of shear deformation in the hinging regions. Concrete was assumed to carry no shear. Hoops were provided in all specimens in accordance with Section A.5 of the ACI Code[2].

The abutments were reinforced similar to structural walls. Realistic anchorage for coupling beam flexural

16.67"

0.33"   12 @ 1.33" = 16"   0.33"

A   B

6 mm Bars

D-3 Deformed Wire

A   B

a) ELEVATION

4"

6.67"

D-3 Deformed Wire

$\frac{11}{16}$"CL

6 mm Bar

$\frac{11}{16}$"CL

$\frac{1}{4}$"CL

b) SECTION A-A
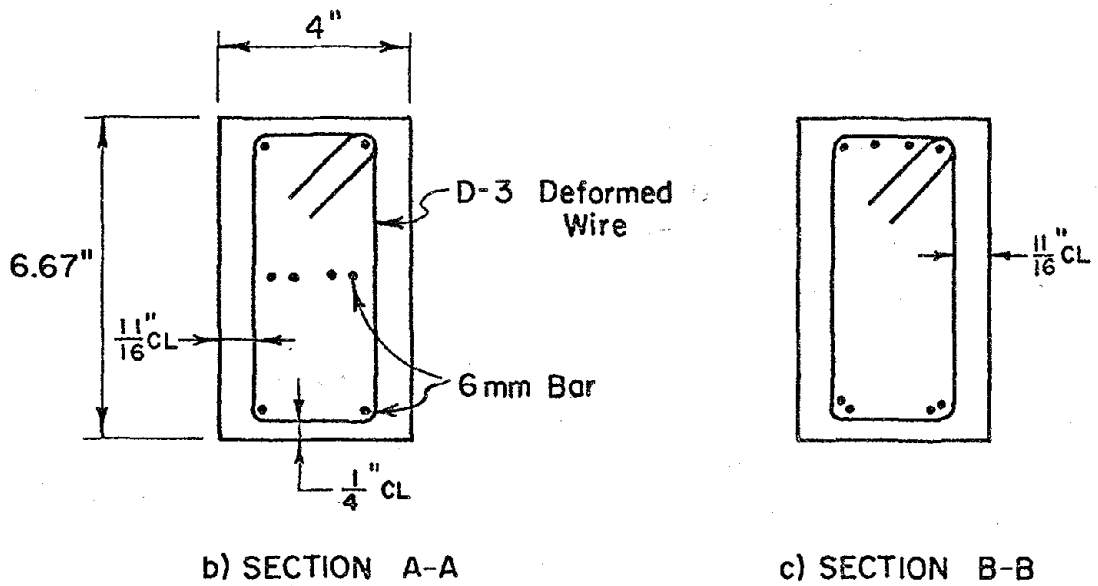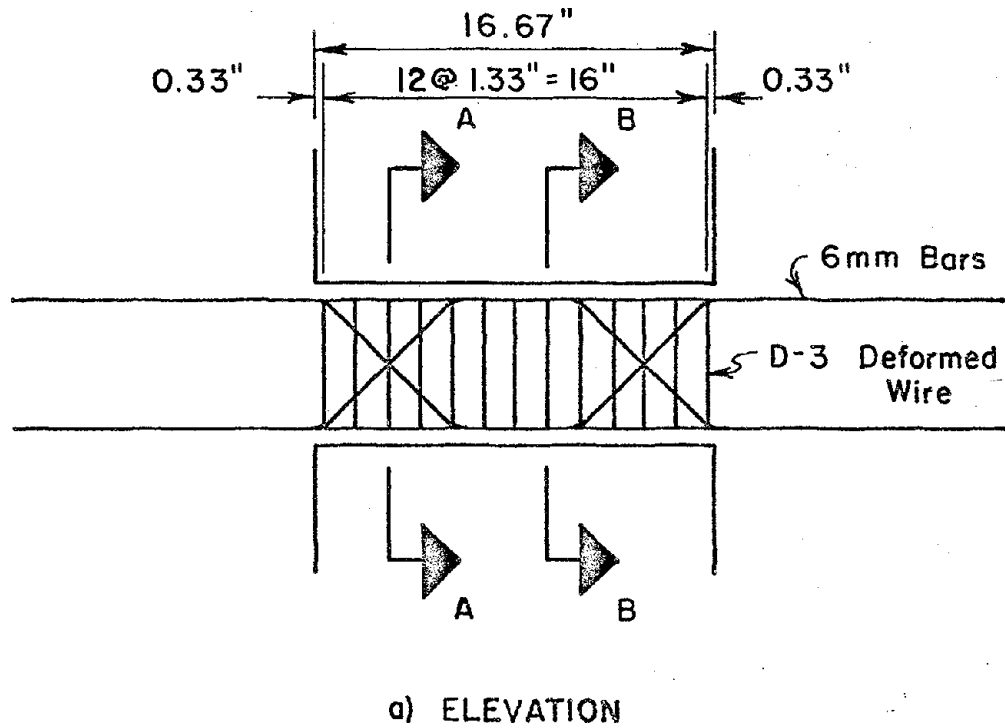
c) SECTION B-B

1"= 25.4 mm.

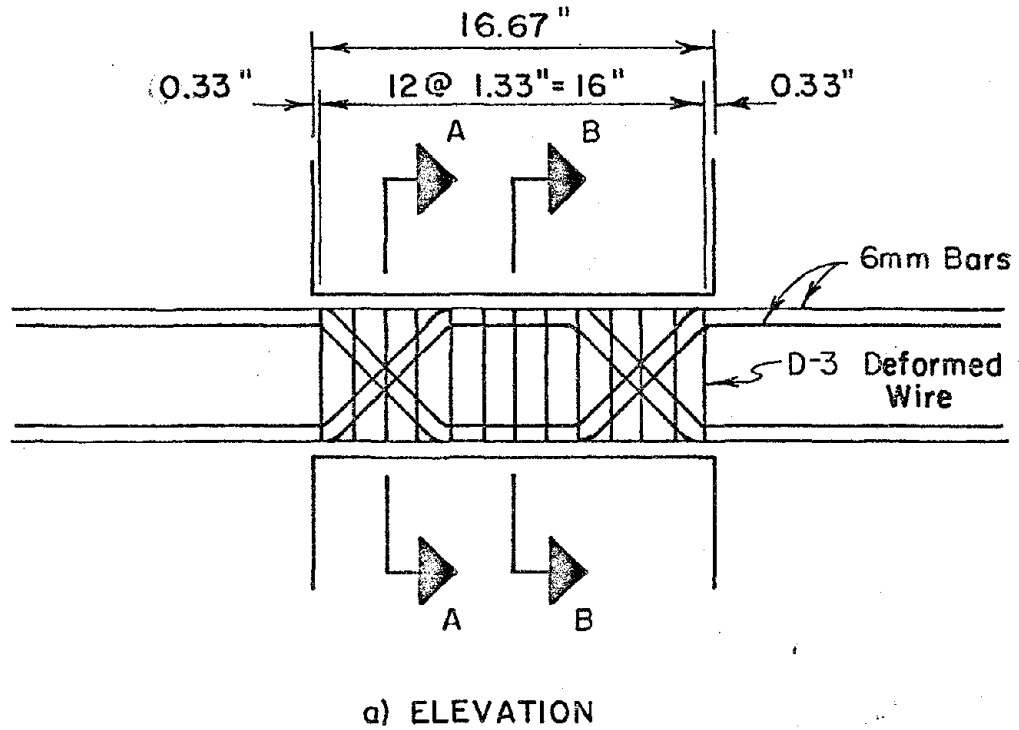Fig. 2   Reinforcement Details for Specimen Cl
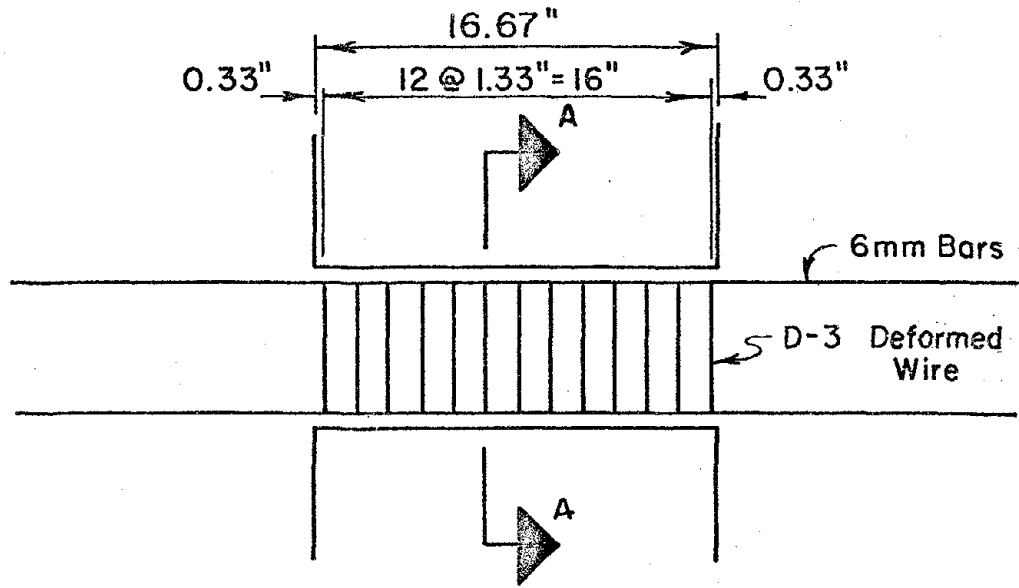
a) ELEVATION
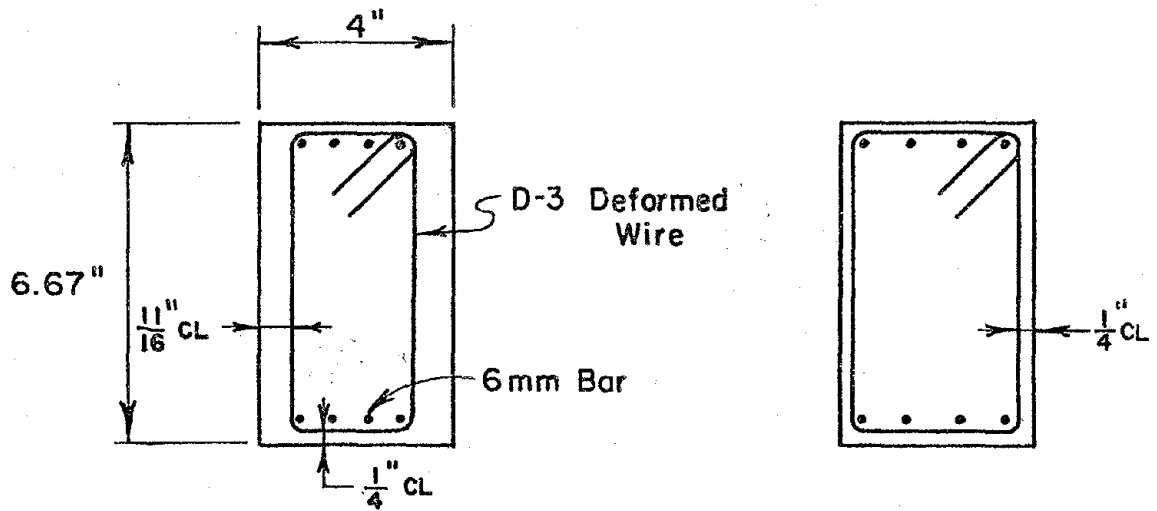
b) SECTION A-A FOR
SPECIMEN C2

c) SECTION B-B FOR
SPECIMEN C5

1" = 25.4 mm.
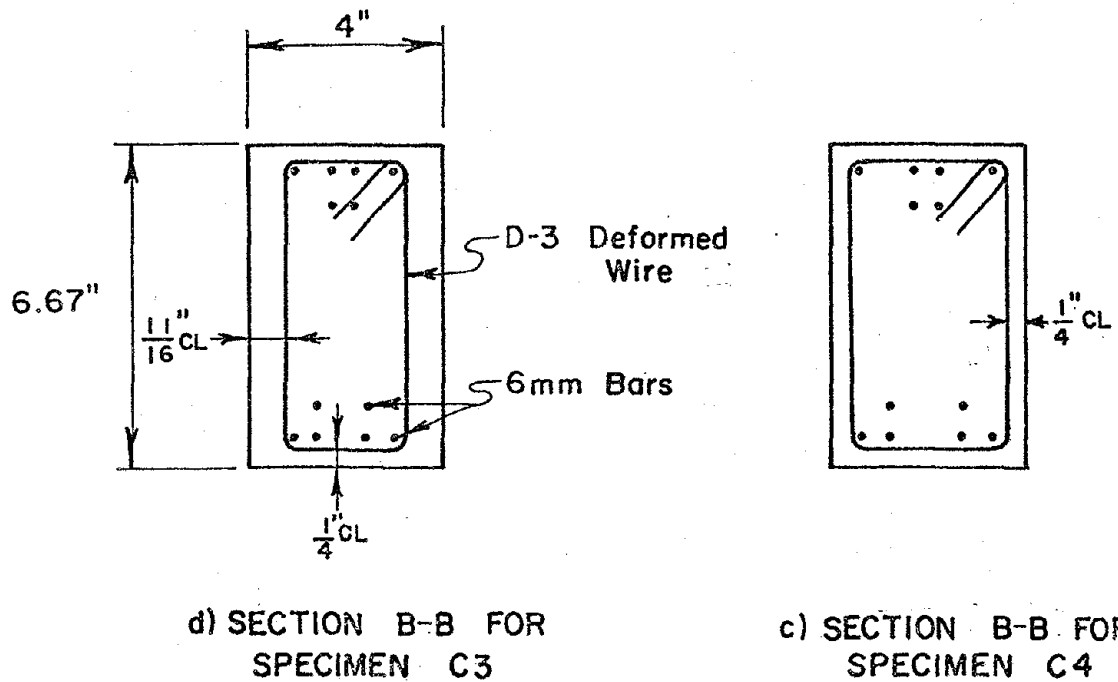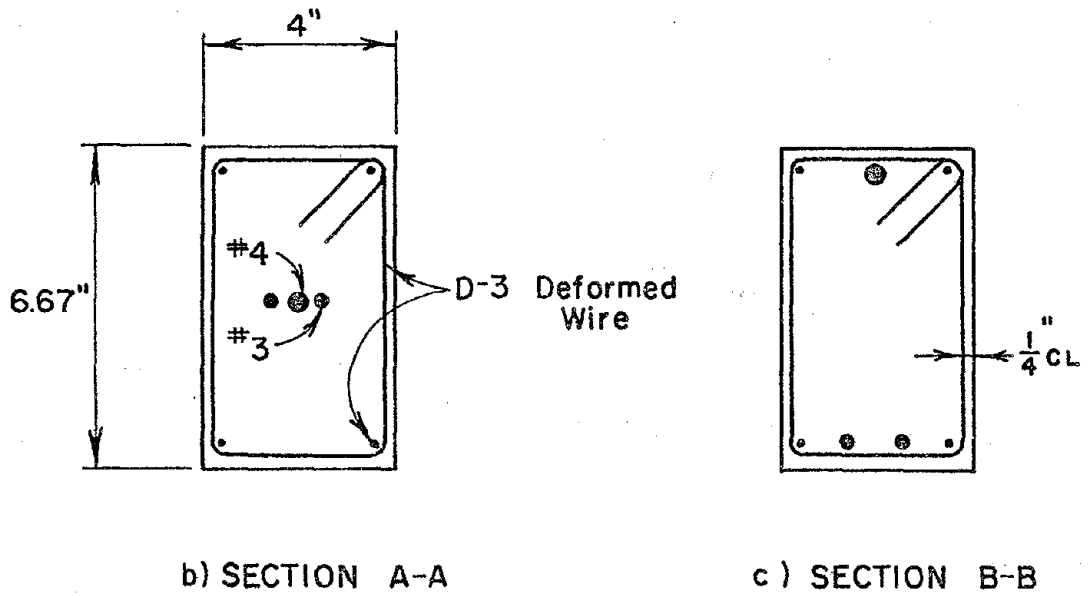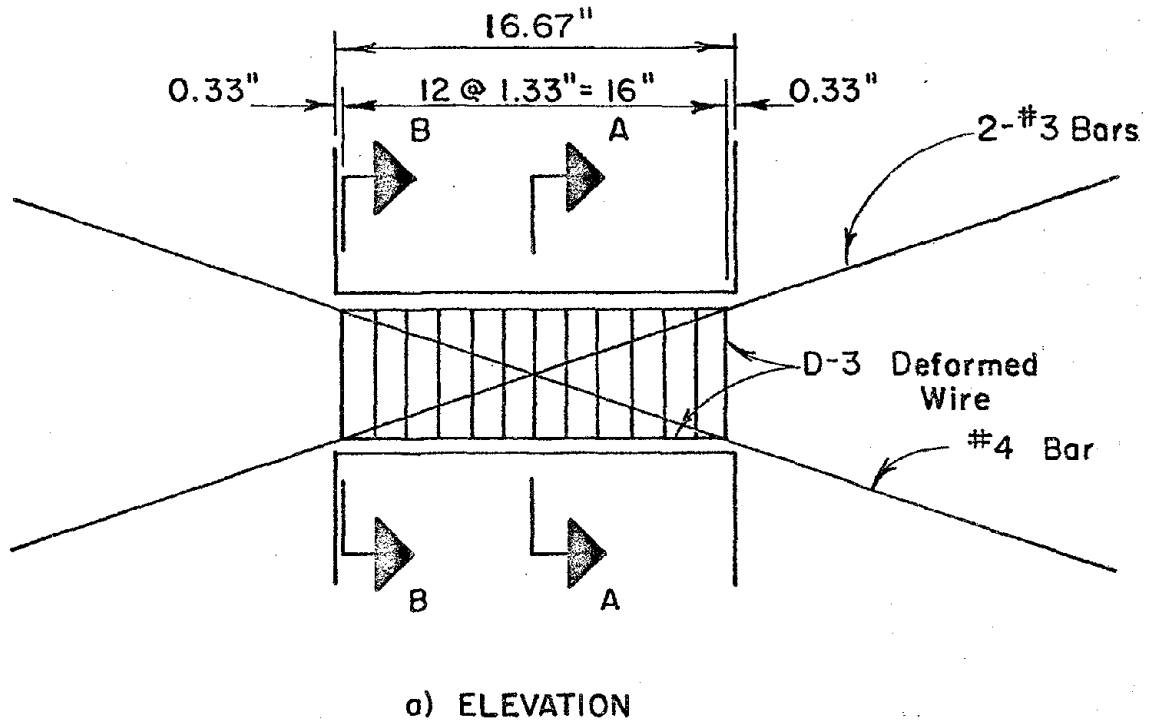
Fig. 3   Reinforcement Details for Specimens C2 and C5

a) ELEVATION

b) SECTION A-A' FOR
SPECIMEN C3

c) SECTION B-B FOR
SPECIMEN C4
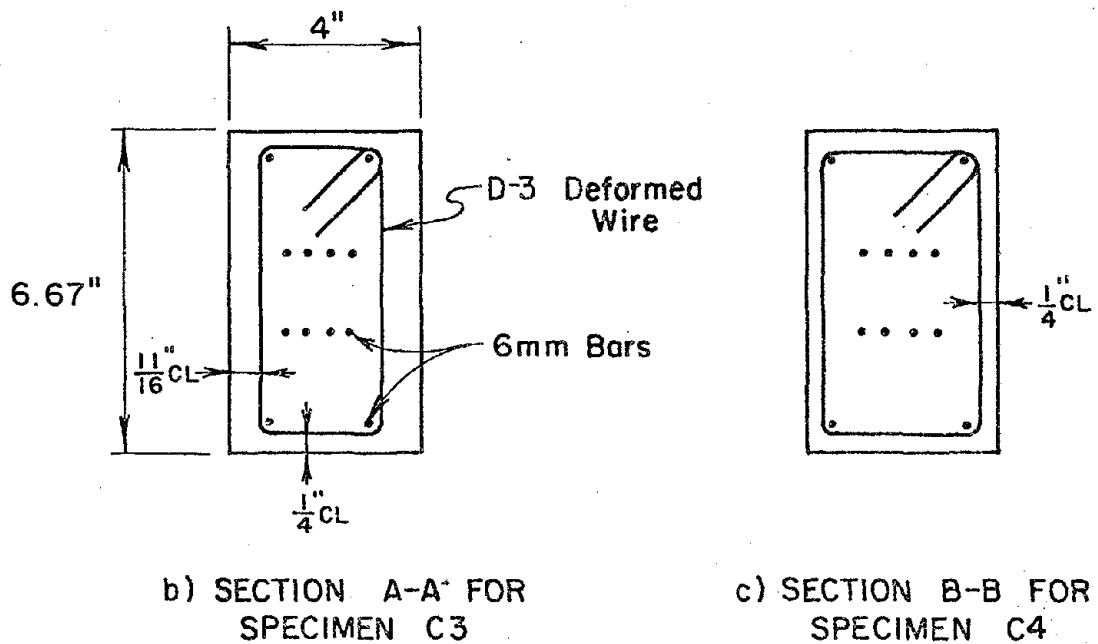
1"=25.4 mm.

Fig. 4 Reinforcement Details for Specimens C3 and C4

d) SECTION B-B FOR
SPECIMEN C3

c) SECTION B-B FOR
SPECIMEN C4

1" = 25.4 mm.

Fig. 4 (cont.)   Reinforcement Details for Specimens C3 and C4

a) ELEVATION

b) SECTION A-A   c) SECTION B-B

1"= 25.4 mm.

Fig. 5   Reinforcement Details for Specimen C6
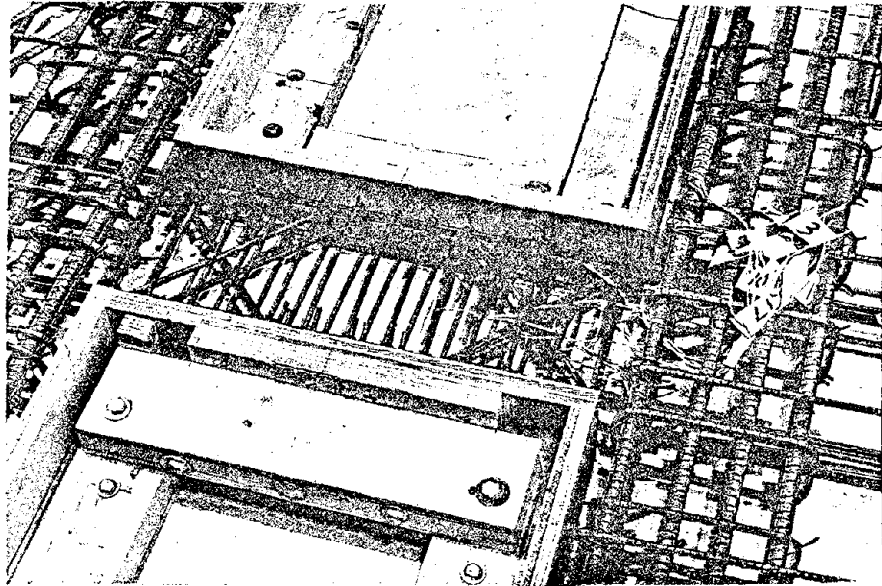
Fig. 6   Reinforcement for Specimen C1
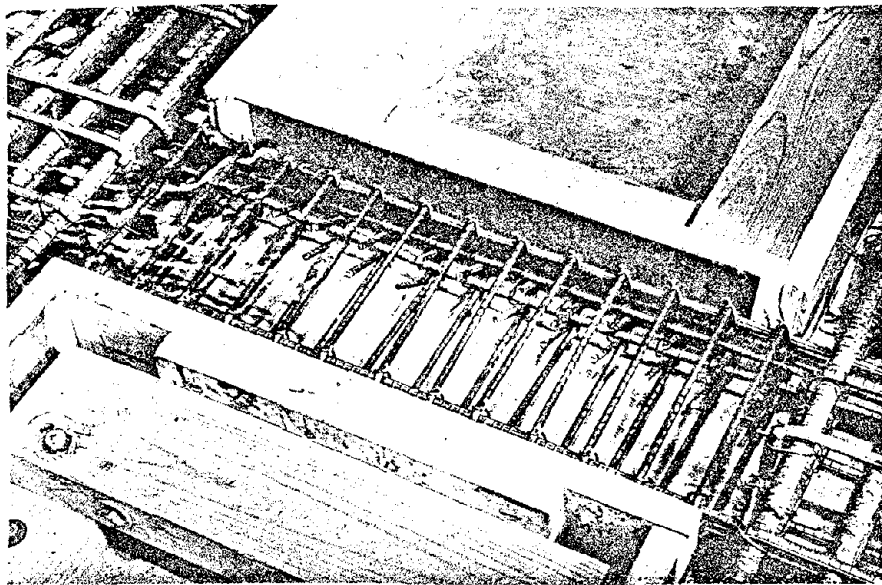
Fig. 7   Reinforcement for Specimens C2 and C5
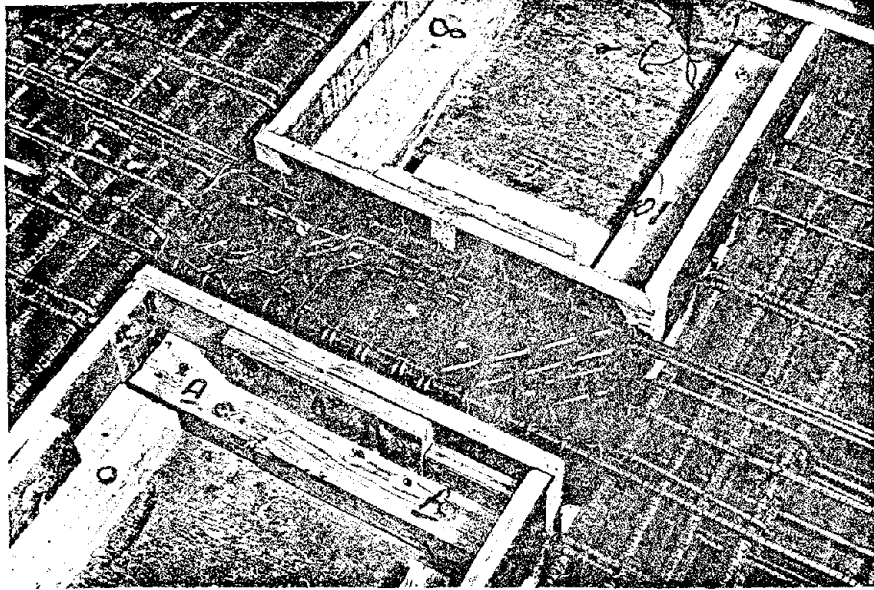
Fig. 8   Reinforcement for Specimens C3 and C4
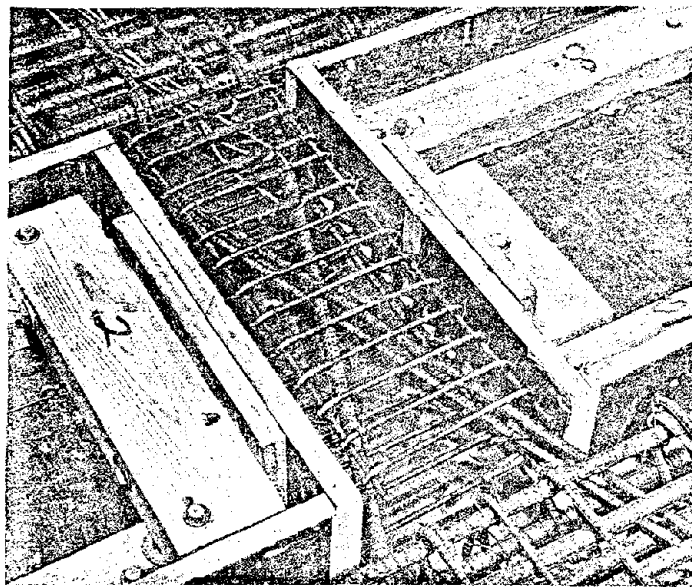
Fig. 9   Reinforcement for Specimen C6

reinforcement was provided. The width of the abutments was selected to limit cracking.

Reinforcement

Details for the steel reinforcement in Specimens C1 through C6 are shown in Figs. 2 through 9. Primary flexural reinforcement in all specimens except Specimen C6 was provided by four 6-mm.bars top and bottom.

For Specimen C1, two bars from both the top and bottom steel were bent at 45 degrees in the hinging regions to provide restraint against shear deformations. The diagonal bars at each end crossed at a single point. This arrangement is shown in Figs. 2 and 6.

Specimens C3 and C4 contained two additional 6-mm.bars top and bottom bent at 45 degrees to provide additional diagonals in the hinging regions. This is shown in Figs. 4 and 8.

The primary reinforcement in Specimen C6 was provided by diagonal steel. Two No. 3 bars were placed on one diagonal and one No. 4 bar on the other, as shown in Figs. 5 and 9.

Specimens C2 and C5 contained no diagonal reinforcement. Details for these specimens are shown in Figs. 3 and 7.

Size D-3 deformed wire was used for hoops in all specimens. These were spaced at 1.33 in. (33.8 mm.) to provide confinement and shear reinforcement capable of resisting the applied shear force. This spacing corresponds to the maximum allowed in full-scale structures by Section A.5 of the ACI

Code[2].

Reinforcing steel properties for each specimen are shown in Table 2. Representative stress-strain curves are shown in Fig. 10.

Concrete

The design compressive strength of the concrete used in the test specimens was 3000 psi (20.7 MPa). The mix consisted of Type I cement, sand, and aggregate with a maximum size of 3/8 in. (9.5 mm.).

Material properties were determined from tests on 6x12-in. (152.4x304.8-mm.) cylinders. Concrete properties are contained in Table 2. A representative stress-strain curve is shown in Fig. 11.

Construction of Test Specimens

Specimens were cast in a horizontal position using the forming system shown in Fig. 12. Reinforcing cages for the abutments and coupling beams were constructed separately and then placed in the form. Before casting, lifting eyes and inserts for attaching external instrumentation were placed in position.

Each specimen was cast from four batches of concrete. Concrete for both coupling beams in each specimen was taken from the same batch. After casting, the specimens were covered with a sheet of polyethelene plastic and allowed to cure for four days. The specimens were then stripped and moved to the test location. Testing normally began on the fourteenth day after casting.

TABLE 2 — MATERIAL PROPERTIES

Material	Property	Specimen No.					
		C1	C2	C3	C4	C5	C6
D-3* Deformed Wire	f_y (ksi)	70.0	69.3	69.3	70.8	71.1	71.4
	f_{su} (ksi)	76.3	75.0	75.1	75.0	75.1	75.1
	E_s (ksi)	32,400	30,000	29,400	31,300	31,100	31,000
6mm** Bar	f_y (ksi)	69.2	74.9	73.6	66.0	66.3	-
	f_{su} (ksi)	98.0	99.8	98.8	89.7	88.8	-
	E_s (ksi)	31,400	30,000	30,600	30,000	30,000	-
No.3 Bar	f_y (ksi)	-	-	-	-	-	70.7
	f_{su} (ksi)	-	-	-	-	-	104.7
	E_s (ksi)	-	-	-	-	-	30,200
No.4 Bar	f_y (ksi)	-	-	-	-	-	59.2
	f_{su} (ksi)	-	-	-	-	-	103.0
	E_s (ksi)	-	-	-	-	-	31,000
Concrete	f'_c (psi)	2940	3050	2970	3490	3140	2520
	E_c (ksi)	3180	2910	3040	3170	2730	2780

*Area = 0.03 sq. in. = 19.4 sq. mm.

**Area = 0.05 sq. in. = 32.3 sq. mm.

1 ksi = 6.895 x 10^{-6} MPa

1 psi = 6.895 x 10^{-3} MPa
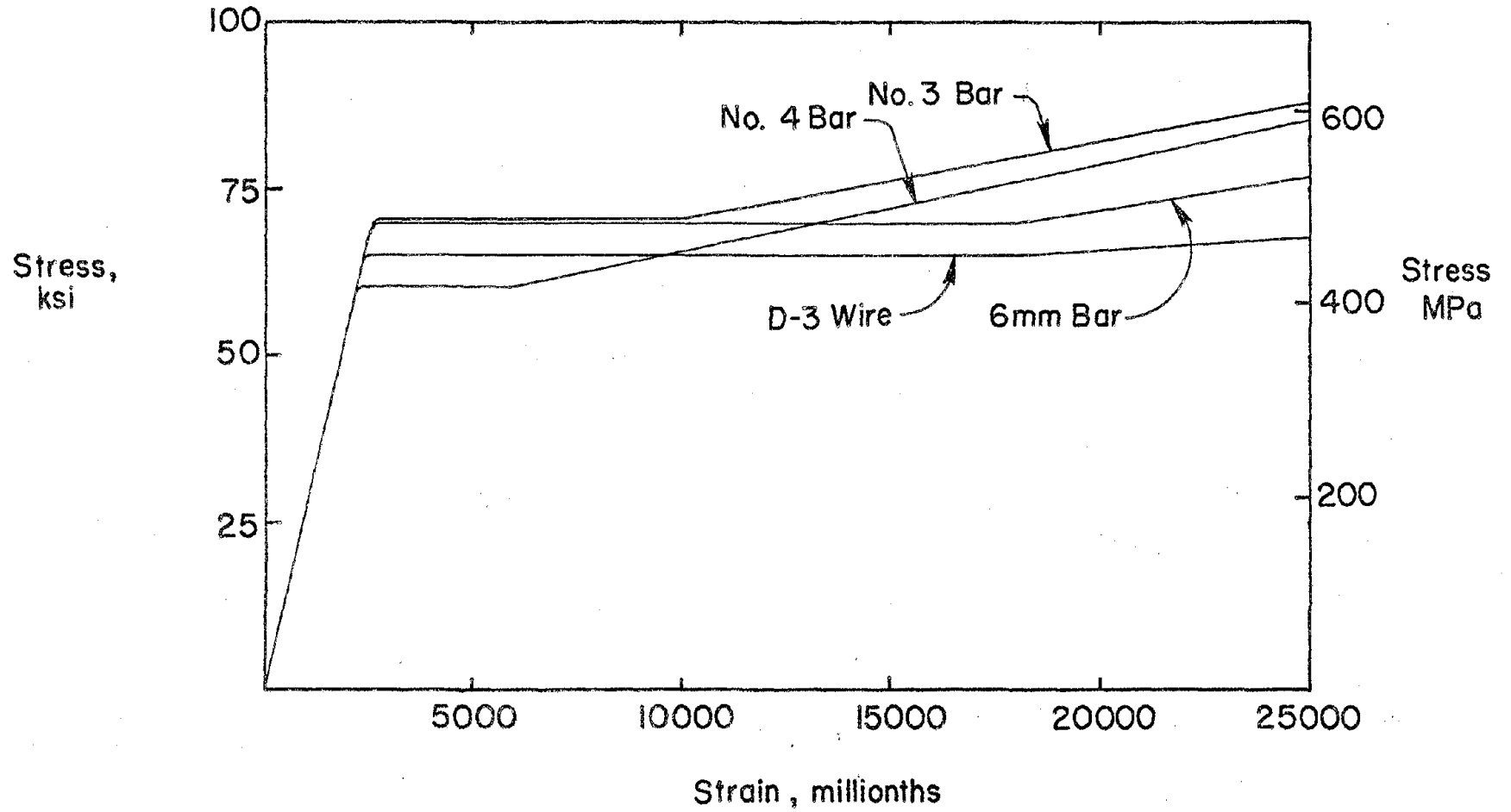
Fig. 10 Stress versus Strain Relationships for Reinforcement
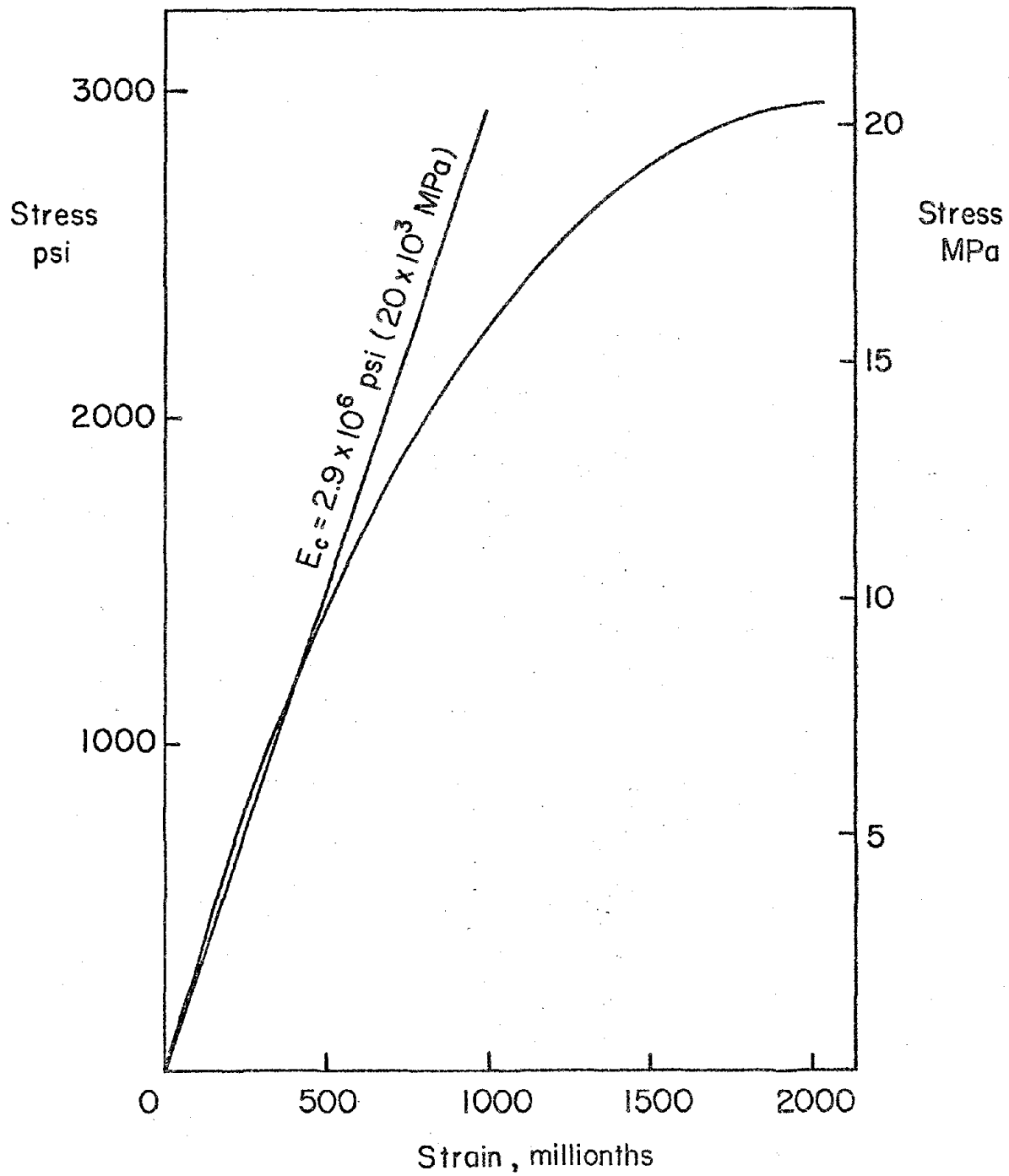
Fig. 11   Stress versus Strain Relationship for Concrete
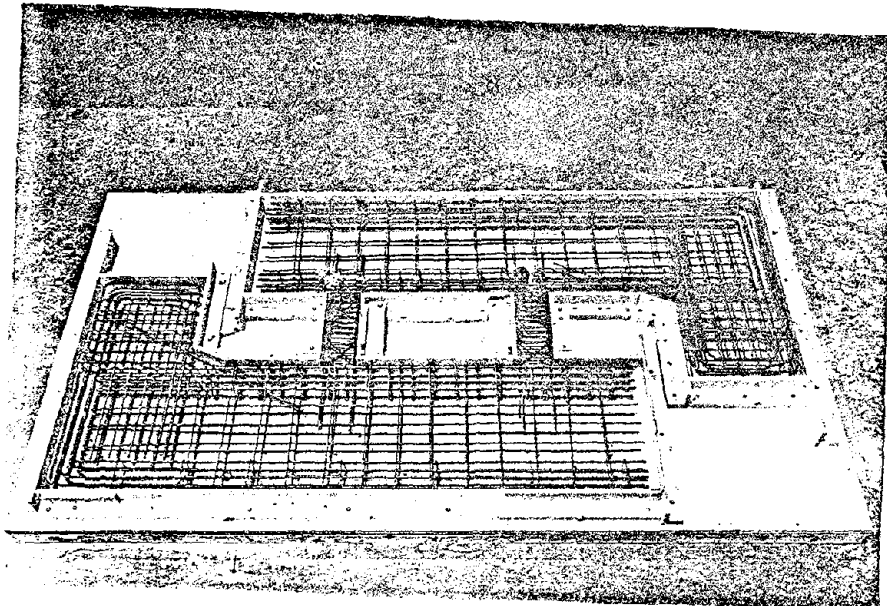
Fig. 12 Specimen Prior to Casting
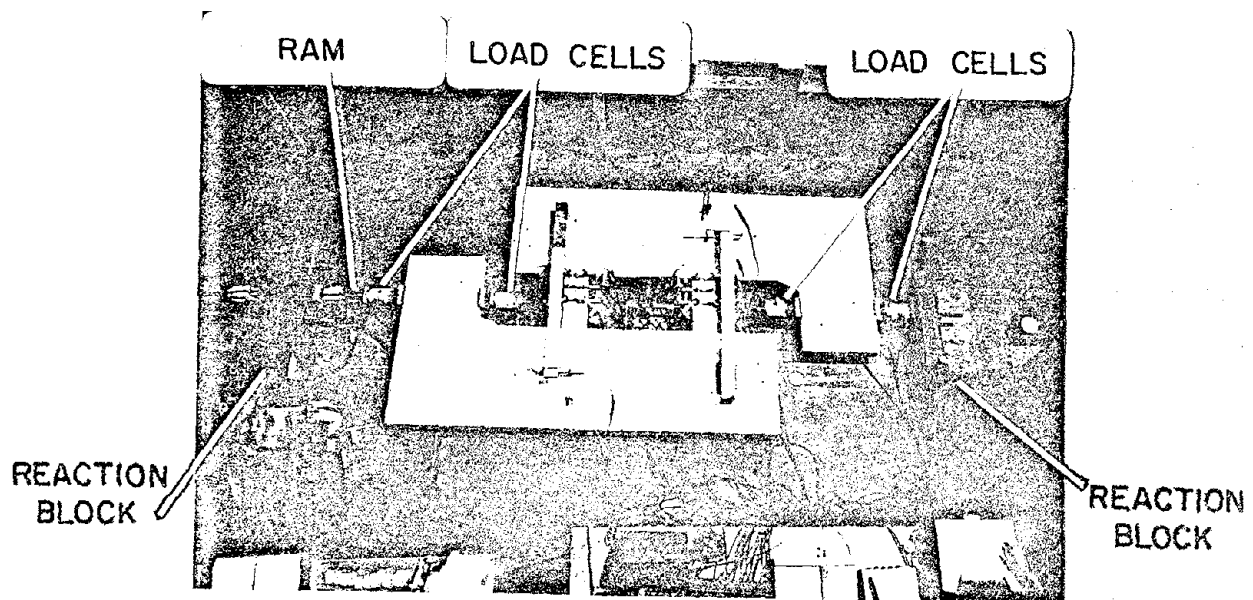
Fig. 13 Specimen Prepared for Testing

TEST PROCEDURES

Details of the test program are presented in this section. A description of the test setup and loading procedures used during testing are discussed. Instrumentation used on the specimens is described.

Test Setup

An overhead photograph of a specimen setup for testing is shown in Fig. 13. For testing, specimens were placed parallel to the laboratory floor and supported on thrust bearings. Reaction blocks to resist applied forces were post-tensioned to the floor on each side of the specimen. With one end of the specimen fixed, hydraulic rams were used to apply load at the opposite end. This loading scheme is illustrated in Fig. 14. The line of action of the applied forces passed through the midlength of the coupling beams to minimize the possibility of axial forces occurring in the beams. Two roller guides prevented the specimens from rotating.

Magnitude of the applied force was controlled by a hydraulic pump. A four-way valve in the hydraulic line was used to direct pressure to one of two rams to either push or pull on the specimen. Lateral movement at the live end of the specimens was prevented by fixtures post-tensioned to the laboratory floor. Locations of the guides are shown in Fig. 14.
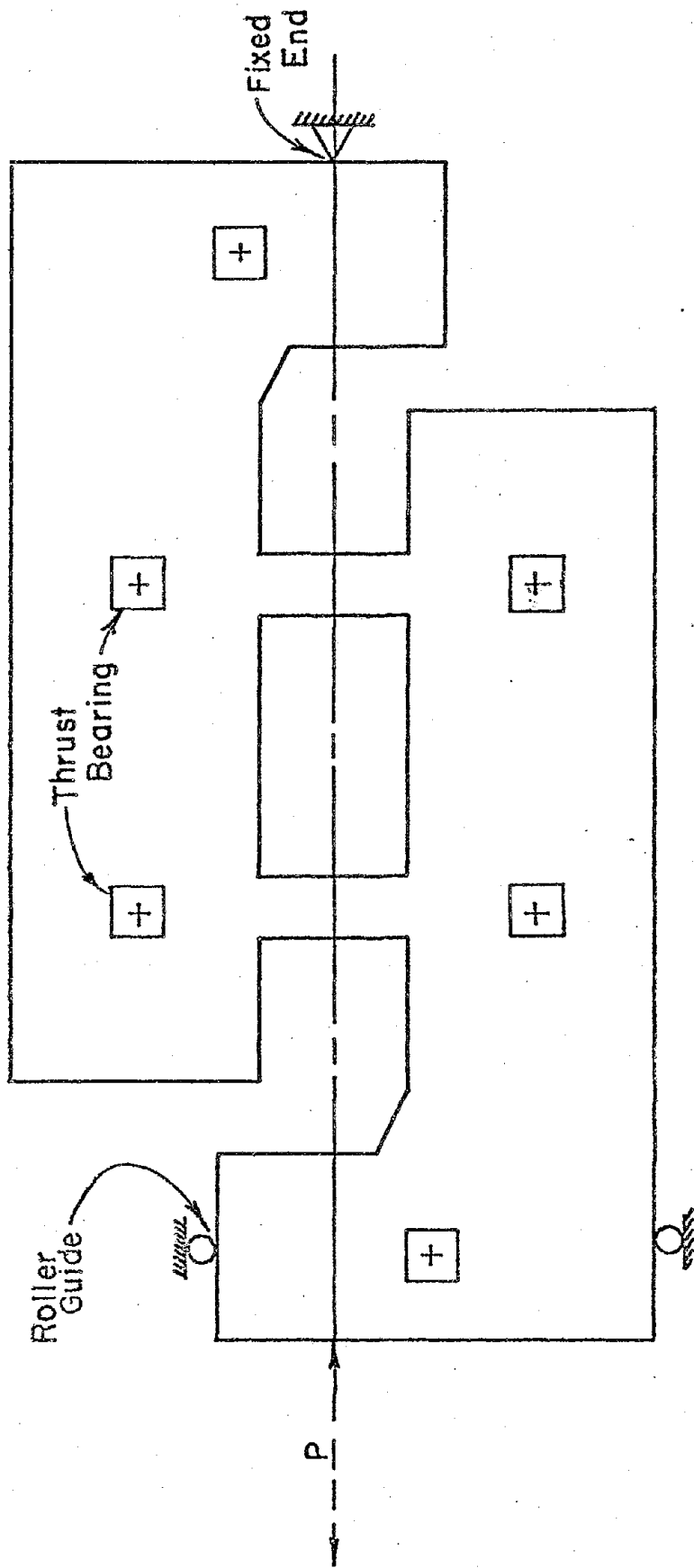
Fig. 14 Specimen Loading

Instrumentation

Test specimens were instrumented to measure loads,
deformations and strains. Readings from each sensing device
were recorded by a VIDAR digital data acquisition system
interfaced with an HP9830A calculator. The data were stored
on tape cassettes for subsequent analysis.

Loads were recorded by load cells located at both the
fixed and live ends of the specimens as shown in Fig. 13.
This arrangement provided a means for determing losses
caused by friction in the thrust-bearing supports. This
loss was generally less than 2% of the applied loads. Two
load cells were used at each end so that forces applied in
both directions were recorded.

Displacements in most specimens were recorded by 6-in.
(152 mm.) DCDT's at three locations. One DCDT was attached
to brackets on the inside face of each rigid abutment midway
between the coupling beams, as shown in Fig. 15. This
measured the relative lateral displacement of the ends of
the coupling beams.

Lateral and longitudinal displacement were also measured
at each coupling beam location. Wooden 2x4-in. (51x102-mm.)
arms parallel to each coupling beam were bolted to one rigid
abutment with the free end extending across to the other
abutment. Six inch (152 mm.) DCDT's were bolted to the
other abutment and attached to the free end of the arms.
This arrangement is shown in Fig. 15.
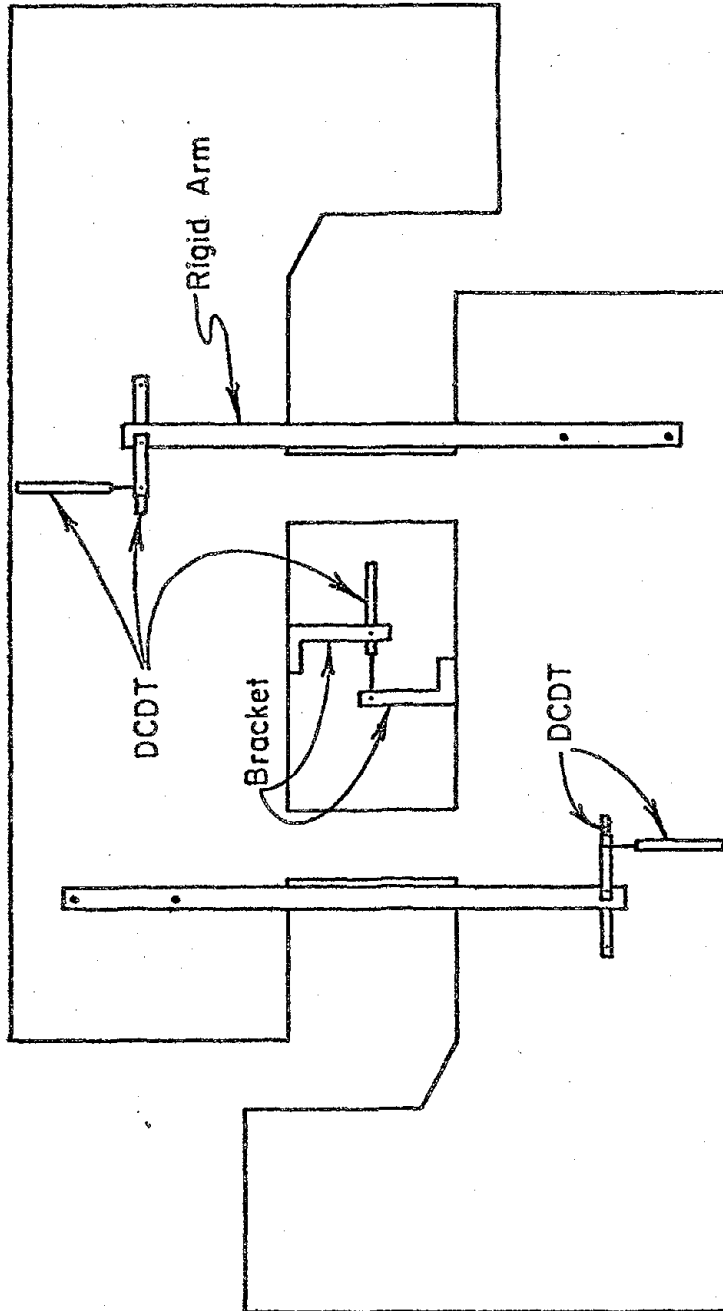
Fig. 15 DCDT Locations

In all specimens, except C1, rotations in two regions of each coupling beam were determined from 4-in. (102 mm.) potentiometers. Two threaded rods were embedded at each of three cross sections in each beam. The cross sections were spaced at 4-in. (102 mm.) intervals with the first section located at the intersection of the beam with the abutment wall. For convenience, the regions between these cross sections are referred to as the base region and the internal region, as shown in Fig. 16. Steel brackets were fastened to the threaded rods at each section. Potentiometers were attached near the ends of adjacent brackets. This setup is illustrated in Fig. 16.

Shear deformations in the same two regions of each coupling beam were determined from 6-in. (152 mm.) LVDT's. The LVDT locations are shown schematically in Fig. 17.

Electrical resistance strain gages were attached to the reinforcing steel in all specimens. Strains were measured on the flexural steel, diagonal steel, and hoops. The location of strain gages is shown in Fig. 18.

A continuous record of load versus deflection was recorded during each test by an X-Y plotter. Load was measured by pressure cells placed in the hydraulic line. The relative lateral deflection between rigid abutments was recorded by a DCDT attached to brackets on each abutment as shown in Fig. 15.

Loading

Prior to yielding in a specimen, loading was controlled
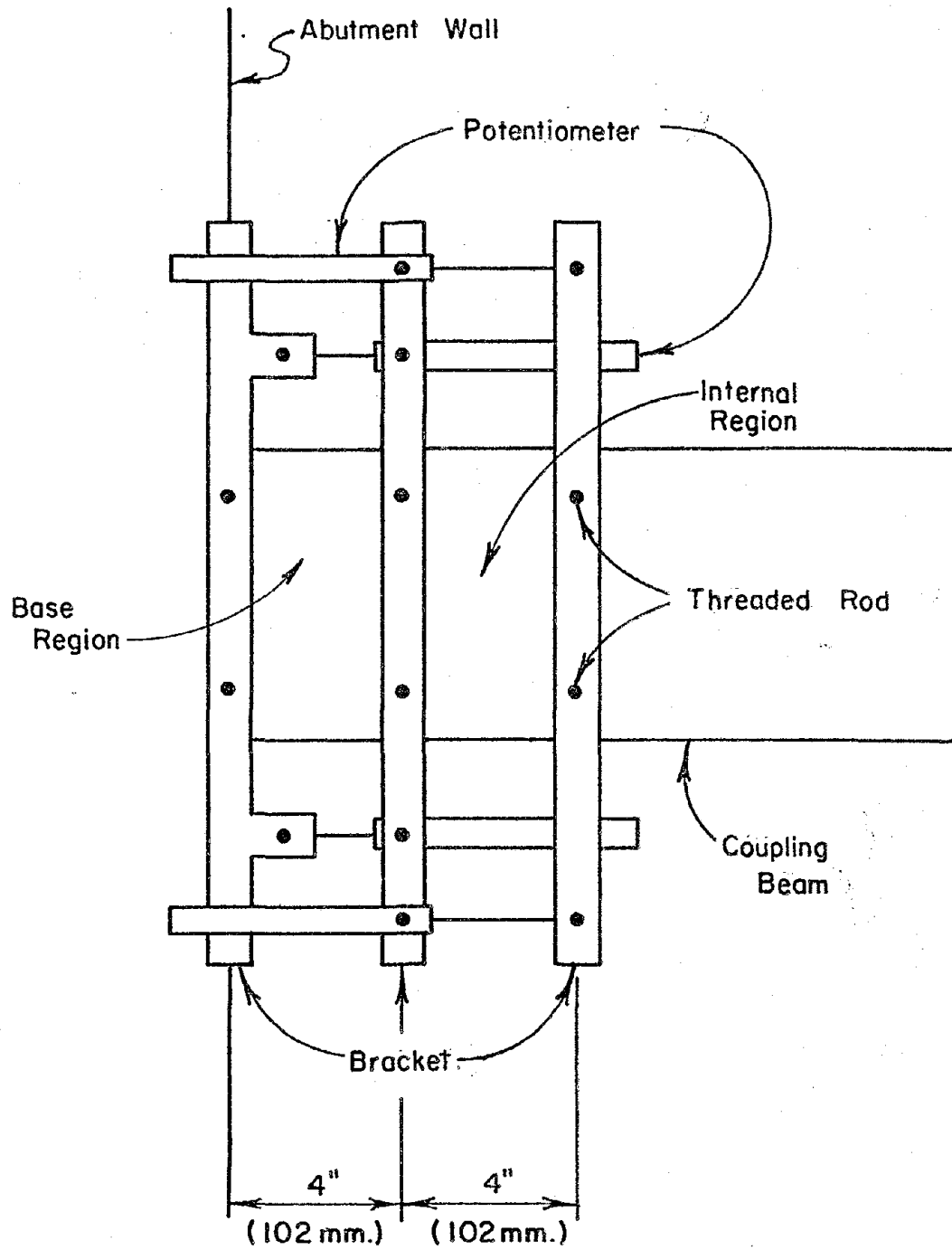
Fig. 16 Potentiometer Locations for Rotation Measurements
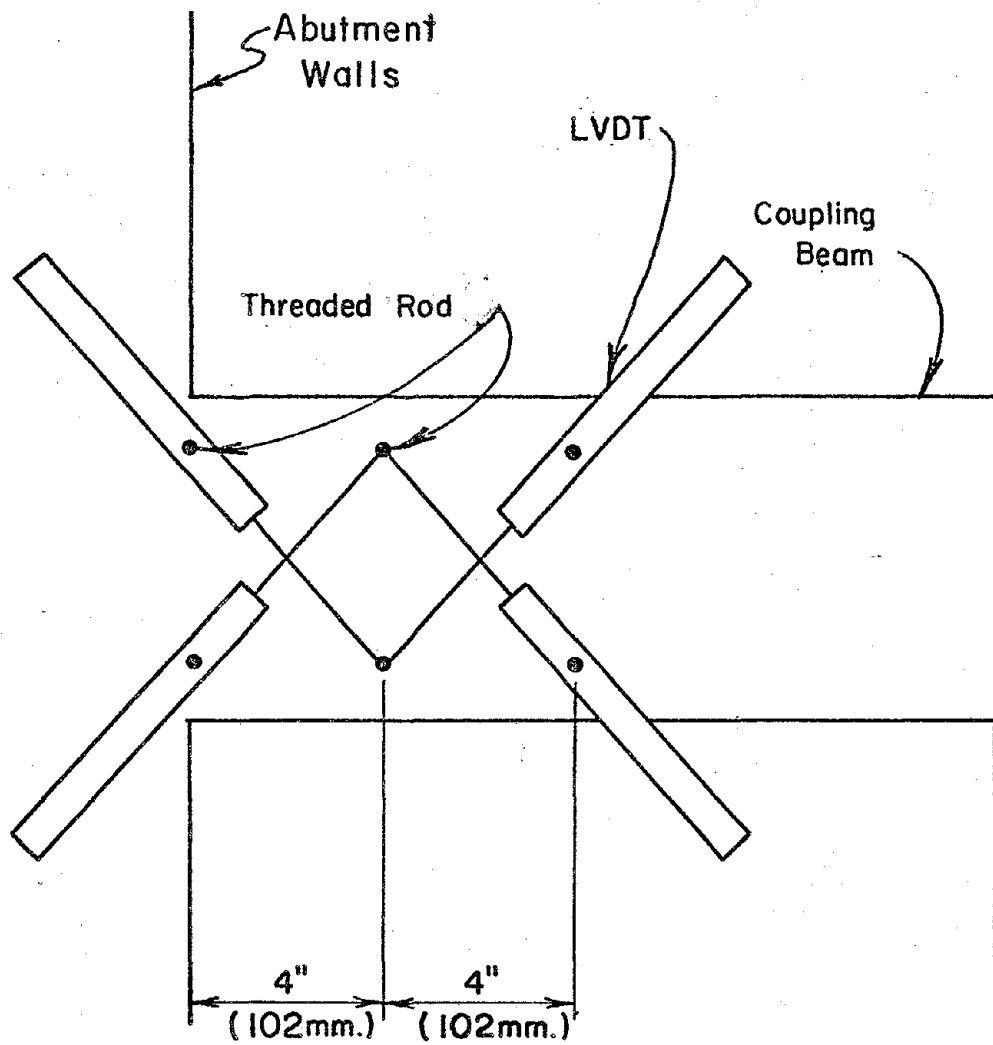
Fig. 17 LVDT Locations for Shear Distortion Measurements
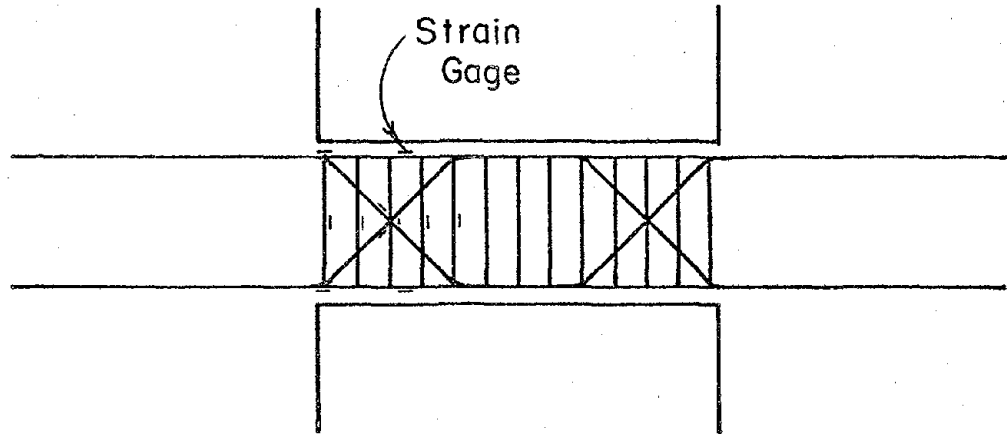
a) Specimen C 1
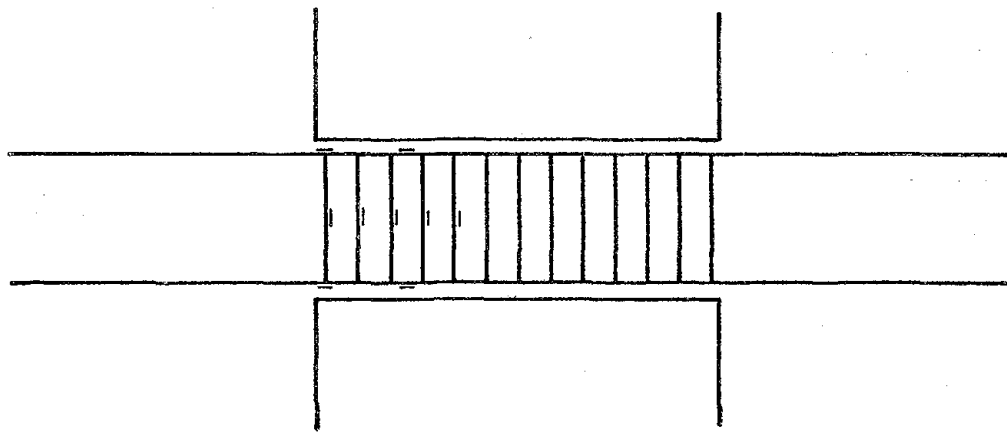
b) Specimen C2 and C5

Fig. 18 Strain Gage Locations
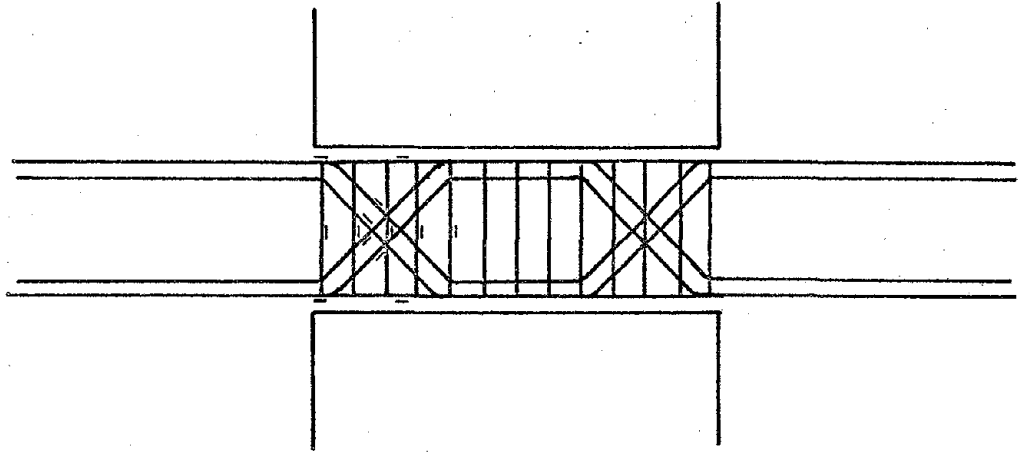
c) Specimens C3 and C4
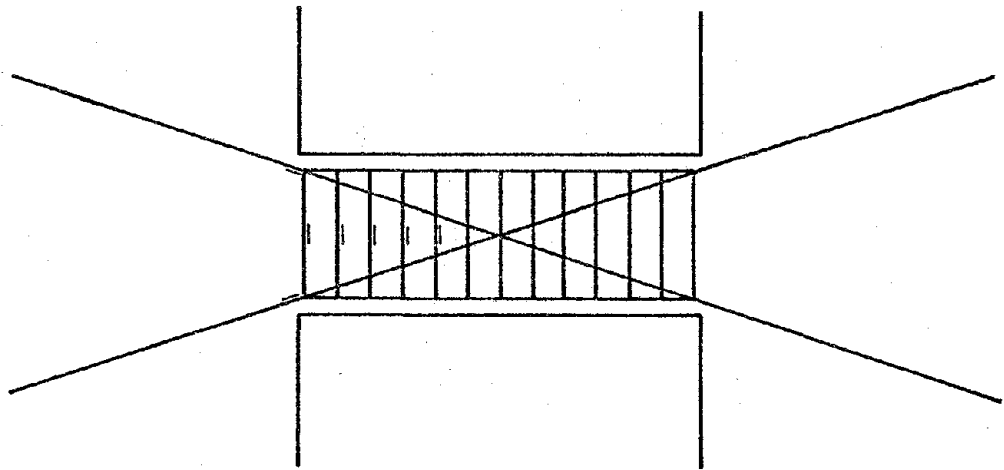
d) Specimen C6

Fig. 18 (cont.) Strain Gage Locations

by the magniture of applied force. After yielding, loading
was controlled by the deflection imposed on the specimens.
Load and deflection histories for each specimen are shown in
Appendix A.

After each predetermined level of force or displacement
was applied, data was recorded by the VIDAR digital data
acquisition system. Each of these readings is defined as a
load stage. A set of load stages corresponding to con-
secutive and equal applications of force or displacement in
the positive and negative directions is defined as a load
cycle. Each cycle started and ended with zero load. In-
elastic load cycles are defined as load cycles after measured
yielding in the primary reinforcement. Three consecutive
load cycles having the same magnitude of maximum force or
displacement are defined as a load increment. These terms
are illustrated graphically in Fig. 19.

Maximum displacements in the first load cycle of each
increment after yielding were reached in three load stages.
Maximum displacements in subsequent load cycles of the same
increment were reached in one load stage.

After each load stage, specimens were inspected vis-
ually for cracking and evidence of distress. Cracks were
marked with a felt tip pen. Photographs were taken at each
load stage to provide a permanent record of crack develop-
ment.

TEST RESULTS

A description of the behavior of each specimen observed
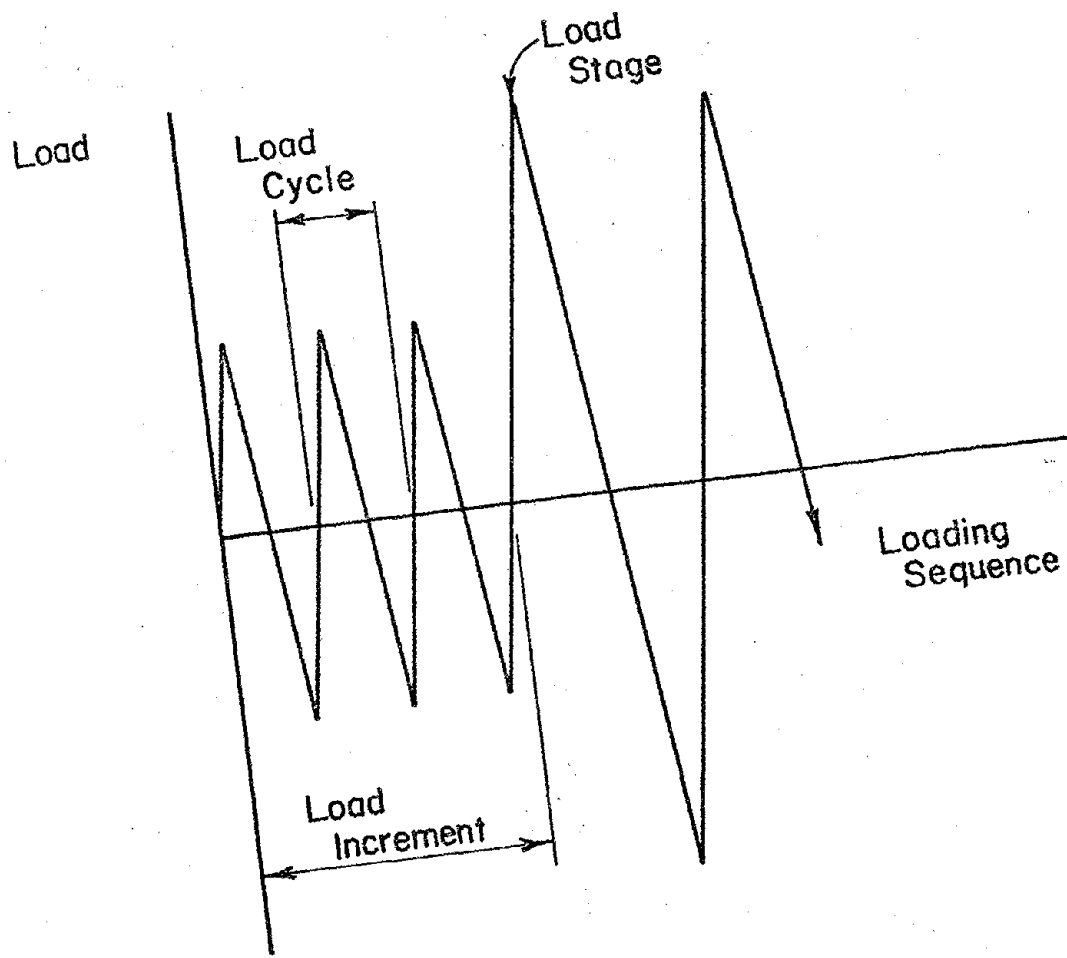
Fig. 19 Definition of Loading Terms

during testing is contained in this section. Principal test results are contained in Table 3. These results include yield loads and displacements, peak loads and maximum displacements, and peak nominal shear stresses. Shear stresses were calculated from Eq. 11-3 of the ACI Code[2] assuming $\phi = 1$.

Behavior of Test Specimens

Specimen C1

Details for Specimen C1 are shown in Fig. 2. Diagonal reinforcement was provided in the hinging regions. Core size was 2.63x6.16 in. (67x157 mm.).

A continuous plot of load versus deflection taken during the test is presented in Fig. 20.

Cracking in this specimen was first observed in the tension zones at the ends of each beam during the seventh load cycle at an applied load of 3.3 kips (14.7 KN.) per beam. Yielding of the flexural reinforcement occurred during the seventeenth load cycle at a load of 8.1 kips (36.0 KN.) per beam. The recorded deflection at yield was 0.16 in. (4.1 mm.). Flexural cracking at the yield load had extended across the full depth of each beam at the ends. Flexure-shear cracks were also observed at sections located between 3 and 6 in. (76 and 154 mm.) from the ends of the beams.

Yielding of the diagonal reinforcement occurred at a load of 8.9 kips (39.6 KN.) per beam during the third inelastic load cycle.

A maximum load of 9.2 kips (40.9 KN.) per beam was carried by the specimen during the ninth inelastic load

TABLE 3 - PRINCIPAL TEST RESULTS

Specimen	Yield Load (kips)	Peak Load (kips)	Yield Displacement (in.)	Maximum* Displacement (in.)	Max.Displ. / Yield Displ.	Peak Shear Stress (psi)
C1	8.1	9.2	0.16	1.28	8.0	$7.0 \sqrt{f'_c}$
C2	10.2	10.3	0.23	1.28	5.6	$7.7 \sqrt{f'_c}$
C3	10.2	11.8	0.15	1.40	9.3	$9.0 \sqrt{f'_c}$
C4	10.0	11.5	0.14	1.40	10.0	$8.0 \sqrt{f'_c}$
C5	9.2	9.4	0.19	1.28	6.7	$6.8 \sqrt{f'_c}$
C6	7.8	13.4	0.11	1.00	9.1	$10.9 \sqrt{f'_c}$

*Maximum displacement corresponds to the last load application.

1 kip = 4.448×10^{-3} N

1 in. = 25.4 mm.

$1 \sqrt{psi}$ = $0.083036 \sqrt{MPa}$
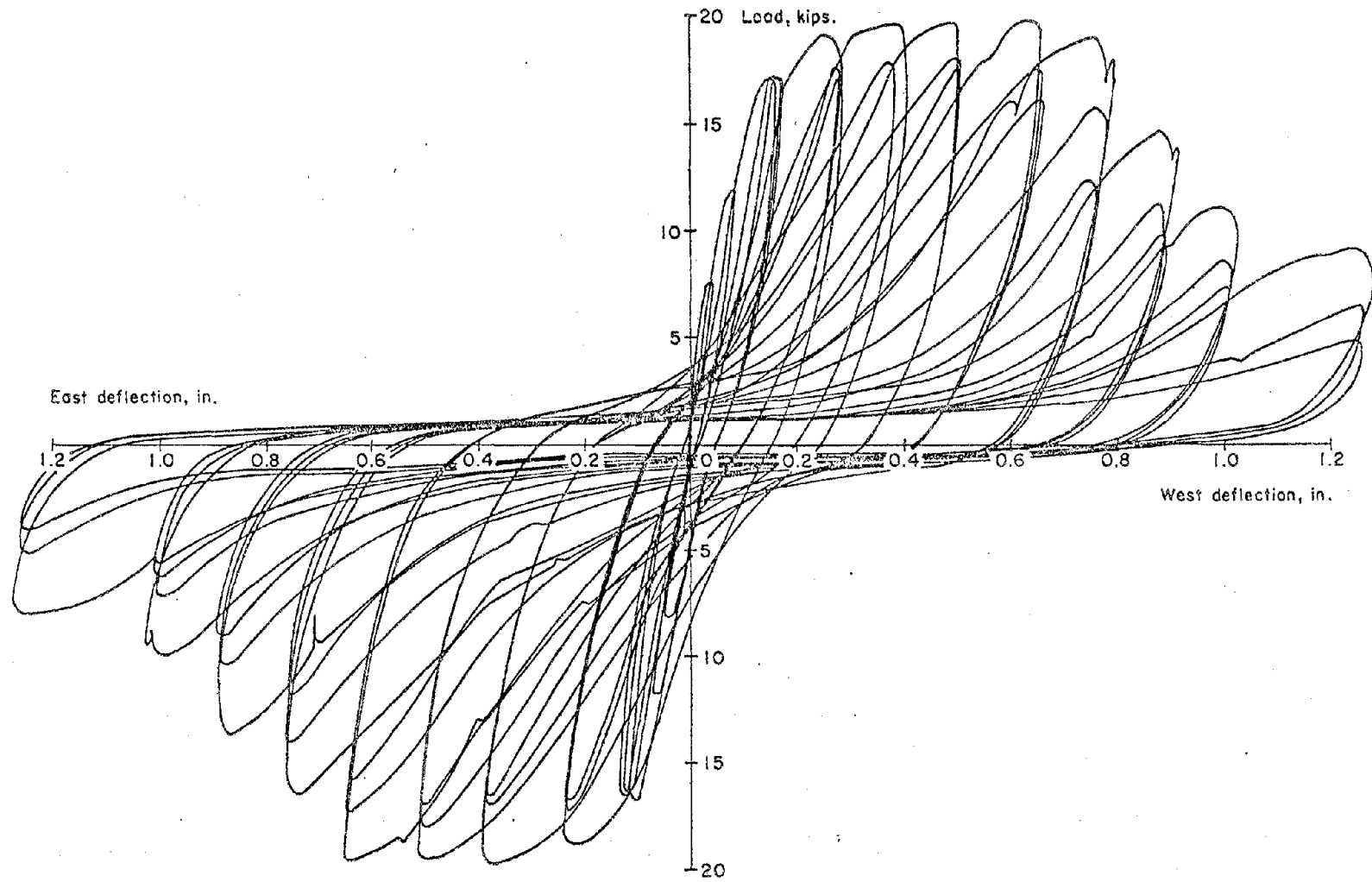
Fig. 20 Load versus Deflection for Specimen Cl

cycle. The nominal shear stress at this load was $7.0\sqrt{f_c'}$
$(0.58\sqrt{f_c'})$. The corresponding deflection was measured as
0.55 in. (14.0 mm.).

The concrete cover in the hinging regions began spal-
ling at an applied load of 9.1 kips (40.5 KN.) per beam.
This occurred at a deflection of 0.71 in. (18.0 mm.) during
the twelfth inelastic load cycle.

In the third loading cycle at the maximum imposed
deflection of 1.82 in. (46 mm.), a load of 0.9 kips (4.0
KN.) per beam was recorded. This represents a loss of 91%
in the load carrying capacity of the specimen. The test was
terminated after this load was applied. A total of 29
inelastic cycles were applied to the specimen. Failure was
attributed to the gradual loss of shear capacity in the
hinging regions.

Photographs of the beams at the end of the test are
shown in Fig. 21. Spalling concrete in the shell around the
confined core exposed the reinforcement. Deterioration of
the concrete in the confined core can also be seen in the
hinging regions.

Specimen C2

Specimen C2, having the same core size as Specimen C1,
was tested without diagonal reinforcement. Details for this
specimen are shown in Fig. 3. A continuous record of load
versus deflection recorded during the test is shown in Fig.
22.
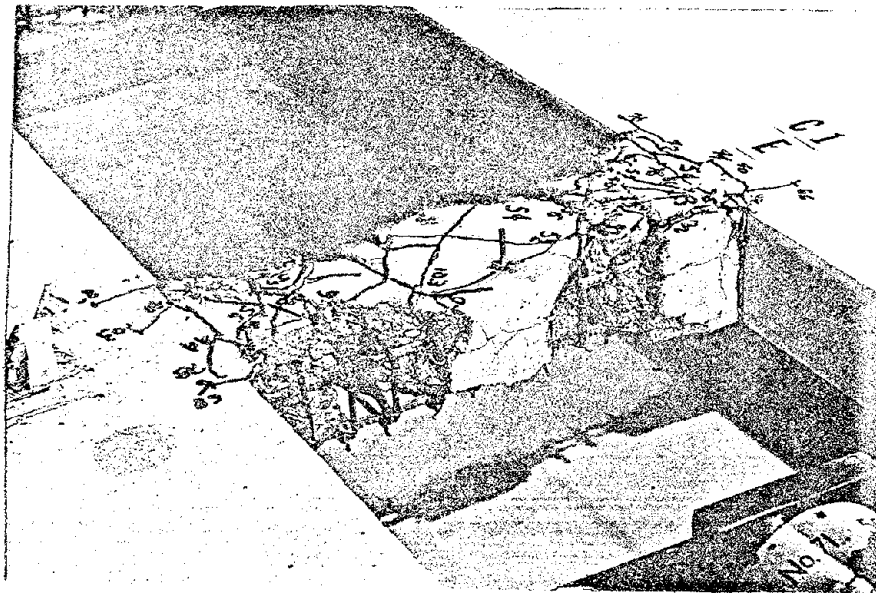
a) East Beam
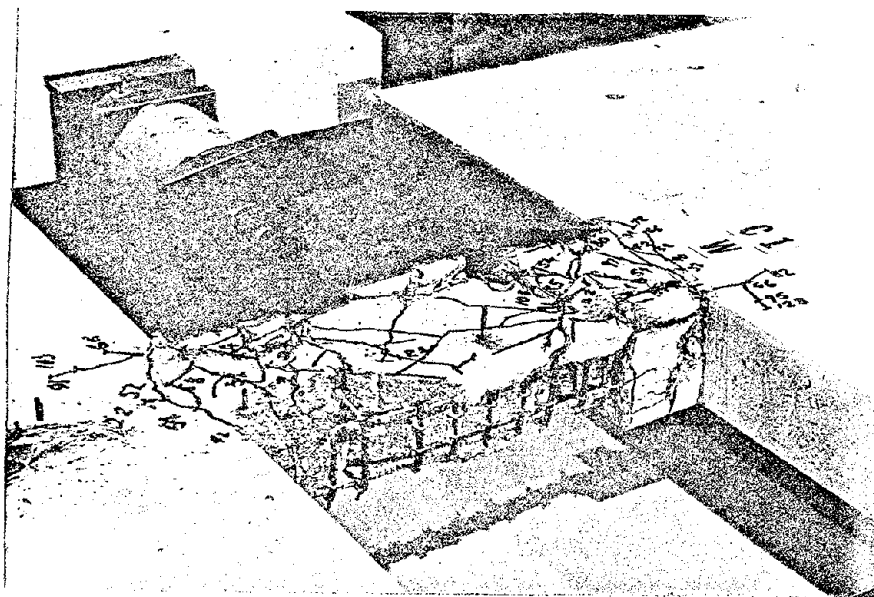
b) West Beam

Fig. 21 Specimen C1 After Testing to Destruction
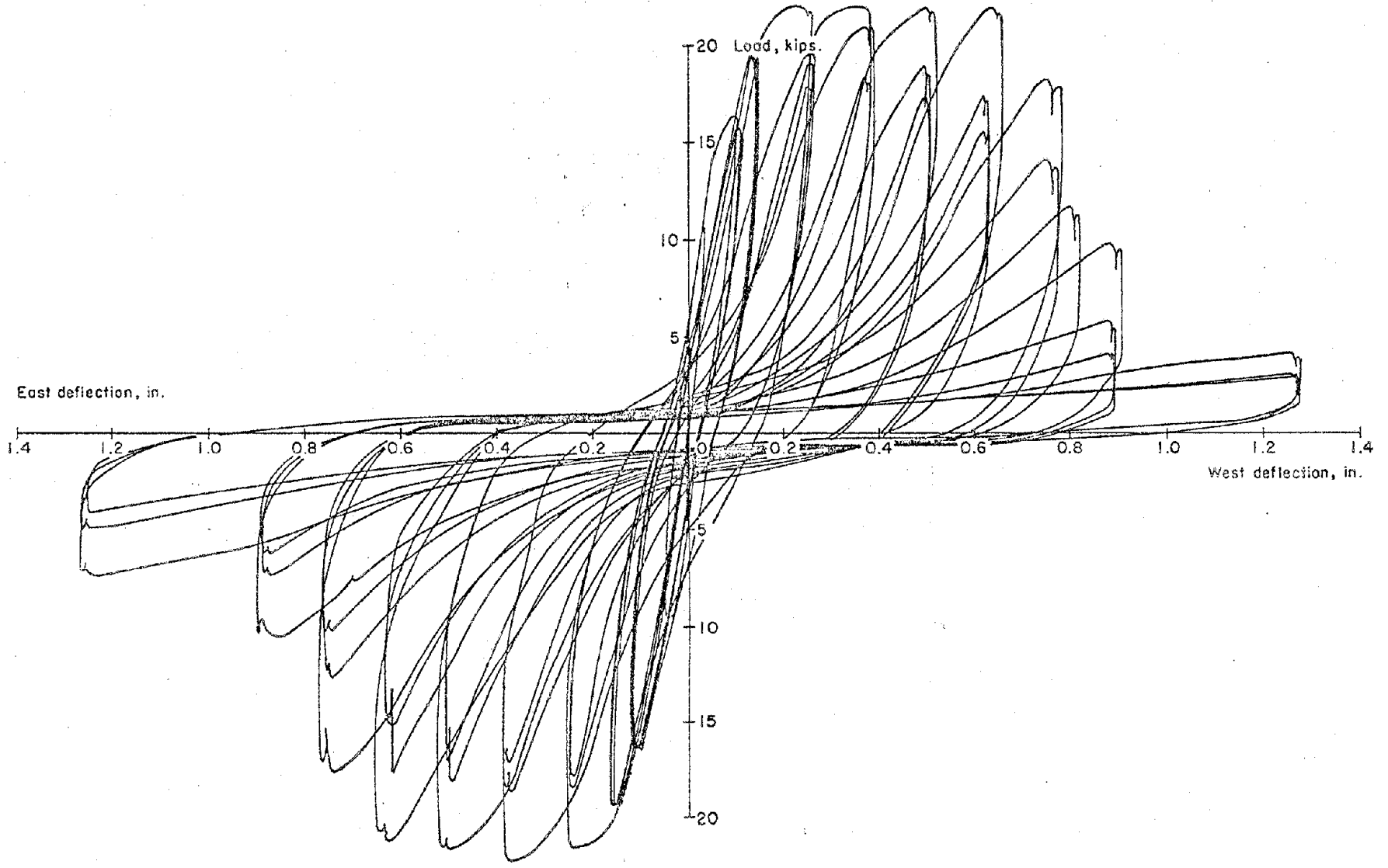
Fig. 22   Load versus Deflection for Specimen C2

First cracking in this specimen occured during the fourth load cycle at a load of 1.9 kips (8.5 KN.) per beam. Yielding of the flexural reinforcement was recorded during the sixteenth load cycle at a load of 10.2 kips (45.4 KN.) per beam. Deflection at first yield reached 0.23 in. (5.8 mm.). The reversing loads caused flexural cracks extending across the full depth of the beams at the ends. Diagonal cracking in both directions also appeared in the end regions of both beams.

The maximum load of 10.3 kips (45.8 KN.) per beam carried by Specimen C2 occurred during the seventh inelastic load cycle. Nominal shear stress at this load was $7.7 \sqrt{f_c'}$ $(0.64 \sqrt{f_c'})$. Deflection at this load was measured as 0.41 in. (10.4 mm.).

Spalling of the concrete shell surrounding the confined core began in the hinging region at a load of 5.9 kips (26.2 KN.) per beam during the fourteenth inelastic load cycle. Deflection at this load was 0.74 in. (18.8 mm.).

During the final load cycle the capacity of the specimen at an imposed deflection of 1.28 in. (32.5 mm.) was 1.7 kips (7.6 KN.) per beam. This represented an 84% reduction from the recorded peak load. A total of 21 inelastic load cycles were applied to the specimen.

Photographs of the beams after testing are shown in Fig. 23. The extent of spalling in the concrete shell can
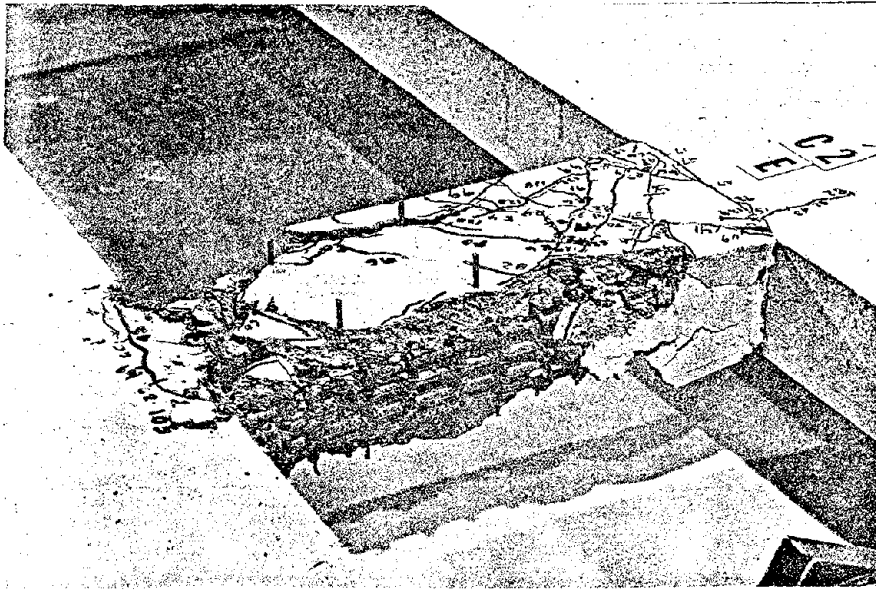
a) East Beam
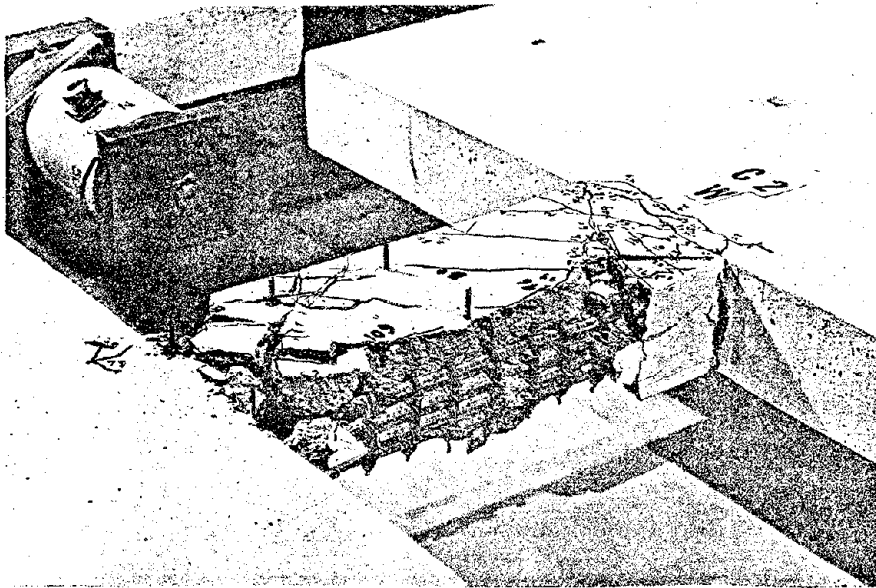
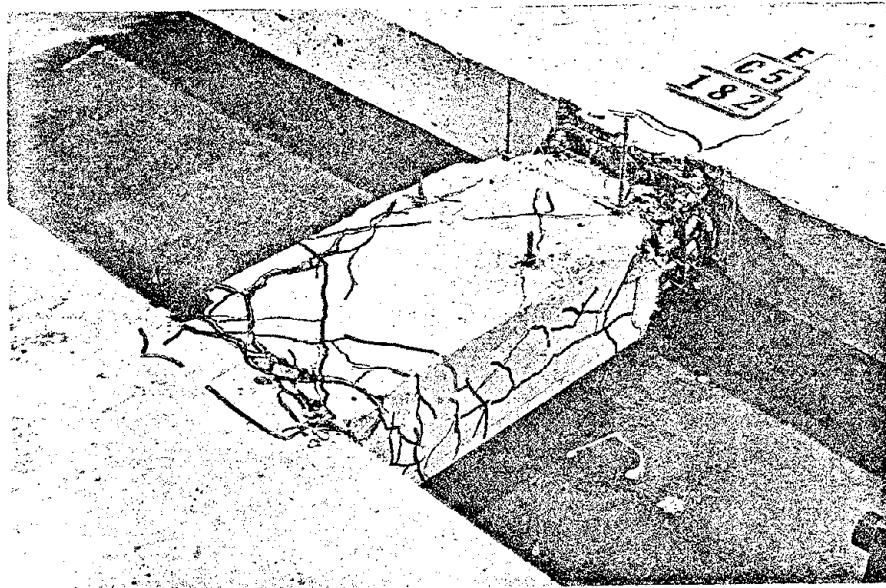b) West Beam

Fig. 23   Specimen C2 After Testing to Destruction

be seen. Loss of strength appeared to be caused primarily by "sliding shear" at the interface between the beam and the face of the abutment wall. Concrete deterioration in this region is shown in the photographs.

Specimen C3

Specimen C3 contained double diagonal reinforcement in the hinging regions of the beams. Core area was the same as for Specimens C1 and C2. Details are shown in Fig. 4. A continuous record of load versus deflection is shown in Fig. 24.

Cracking in this specimen first occurred during the seventh load cycle at a load of 2.9 kips (12.9 KN.) per beam. Yielding of the main flexural reinforcement occurred during the thirteenth load cycle at a load of 10.2 kips (45.4 KN.) per beam and a deflection of 0.15 in. (3.8 mm.) At this level, flexural cracks in each beam extended across the full depth at the ends. Furthermore, a diagonal crack extending across more than half the depth at approximately the 1/3-point in the span of the east beam was also observed.

Maximum load carried by the specimen was 11.8 kips (52.5 KN.) per beam during the seventh inelastic load cycle. Nominal shear stress at this load was $9.0\sqrt{f_c'}$ ($0.75\sqrt{f_c'}$). The deflection recorded at this load was 0.36 in. (9.1 mm.). Yielding of the diagonal reinforcement also occurred during
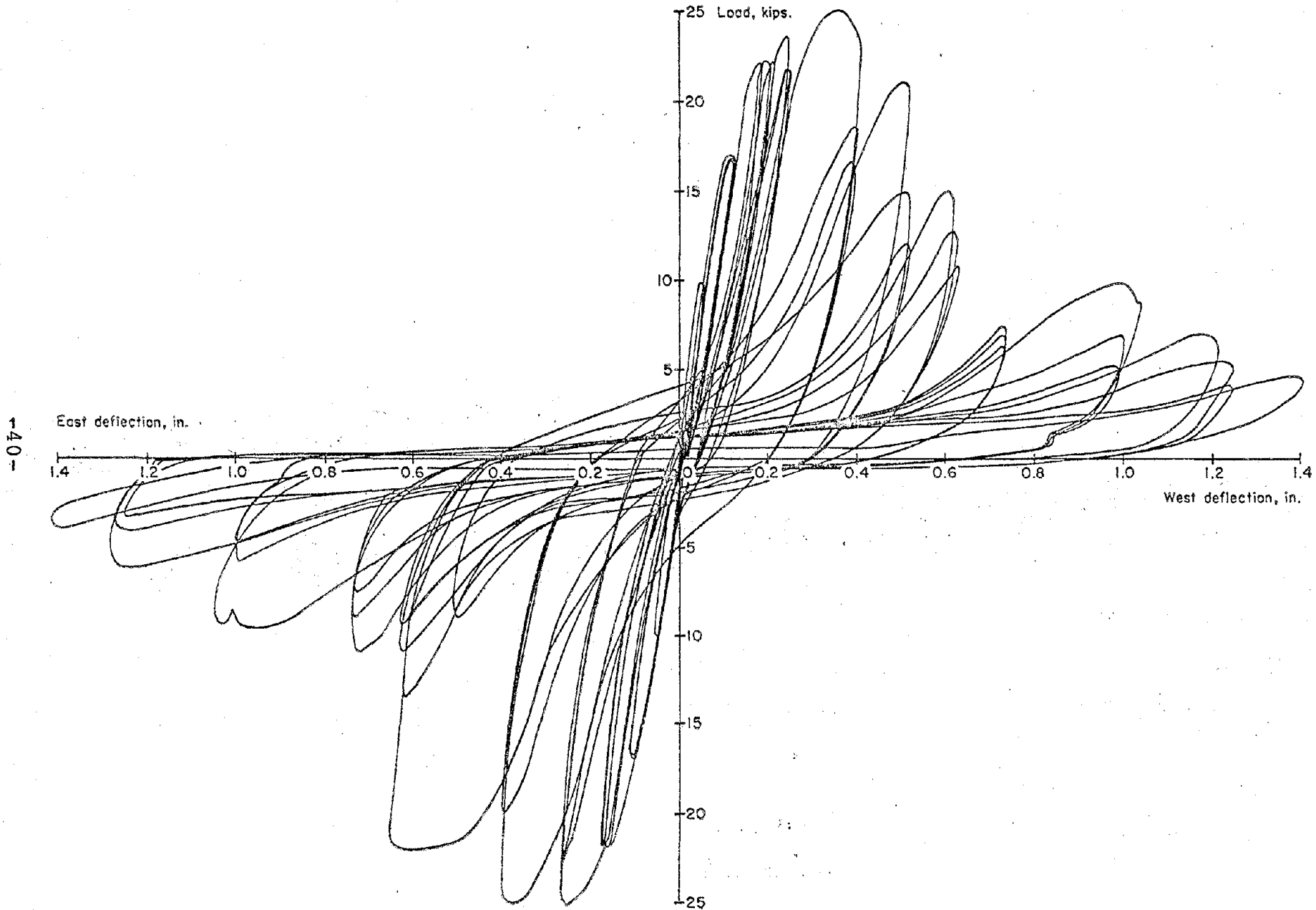
Fig. 24   Load versus Deflection for Specimen C3

this load cycle at a load of 11.2 kips (49.8 KN.) per beam.

A photograph of the specimen under maximum load is shown in Fig. 25. Cracking is much more severe in the east beam.

Spalling of the concrete shell surrounding the confined core began at a load of 18.3 kips (81.4 KN.) during the tenth inelastic load cycle. Deflection at this load was 0.74 in. (18.8 mm.).

During the final load cycle at an imposed deflection of 1.45 in. (36.8 mm.), the specimen carried a load of 1.4 kips (6.2 KN.) per beam. This represented a loss of 88% from the peak load. A total of 25 inelastic load cycles were applied to the specimen.

Photographs of the beams after testing are shown in Fig. 26. The difference in behavior of the two beams is apparent. The diagonal crack that formed in the east beam caused the complete deterioration of the concrete core in the center of the span. The west beam behaved in a similar manner to Specimen C1. Deterioration occurred in the hinging regions at the ends of the beam.

Specimen C4

Specimen C4 was similar to Specimen C3 except that the size of the confined concrete core was increased to 3.50x 6.16 in. (89x157 mm.). As a result of this increased core size, it was necessary to place the straight flexural bars
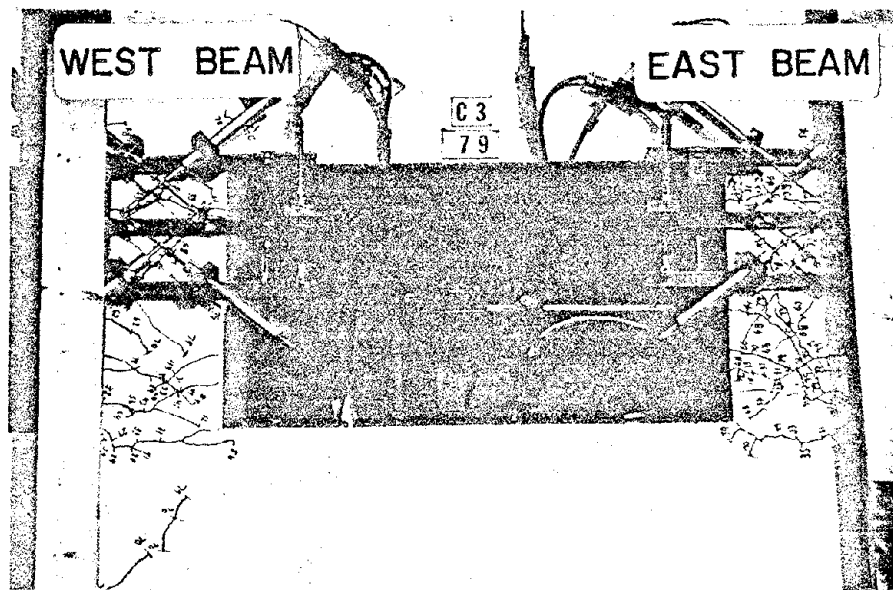
Fig. 25   Specimen C3 at Peak Load
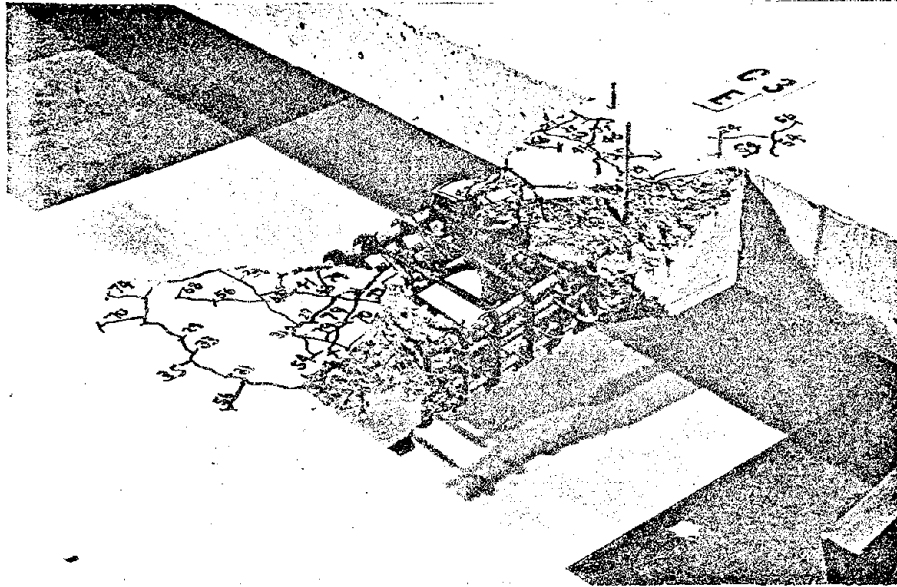
a) East Beam
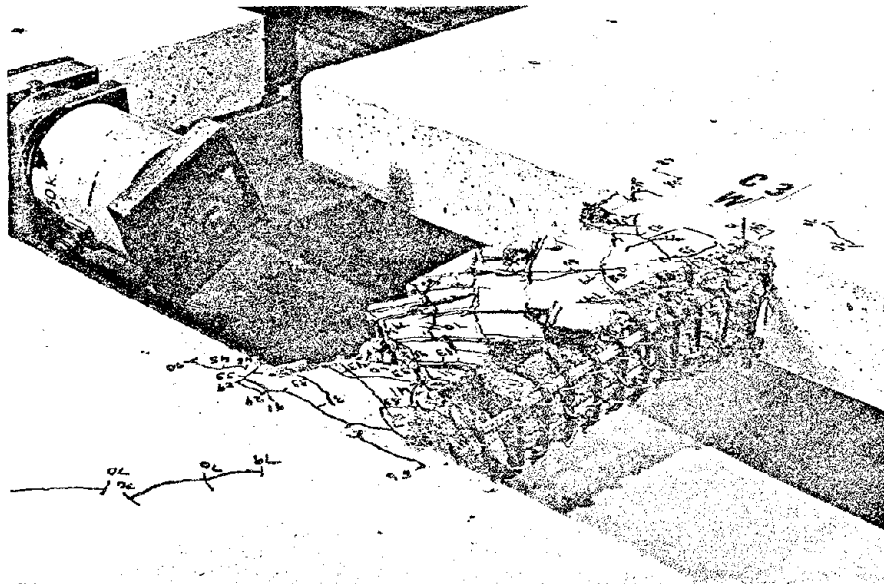
b) West Beam

Fig. 26   Specimen C3 After Testing to Destruction

outside the simulated wall reinforcement in the abutment walls. Therefore, these bars were not anchored in confined concrete. Details of this specimen are shown in Fig. 4. This anchorage detail, although satisfactory for the test specimen, is not recommended for field practice.

A continuous record of load versus deflection is shown in Fig. 27.

Cracking was first observed in this specimen during the seventh load cycle at a load of 4.0 kips (17.8 KN.) per beam. Flexural reinforcement yielded during the sixteenth load cycle at a load of 10.0 kips (44.5 KN.) per beam and a deflection of 0.14 in. (3.6 mm.). At this load, flexural cracks extended across the full depth of both beams at the ends. Diagonal cracks had also formed at approximately the 1/4-points of the span in both beams. Yielding of the diagonal reinforcement occurred at a load of 11.4 kips (50.7 KN.) per beam during the fourth inelastic load cycle.

A peak load of 11.5 kips (51.2 KN.) per beam was recorded for Specimen C4 during the seventh inelastic load cycle. Nominal shear stress at this load was $8.0\sqrt{f_c'}$ $(0.66\sqrt{f_c'})$. Deflection at this load was 0.40 in. (10.2 mm.).

A maximum deflection of 1.57 in. (39.9 mm.) was imposed on the specimen during the seventh inelastic load cycle. The measured load was 2.4 kips (10.7 KN.) per beam. This represented a loss of 79% in load capacity.

Spalling of the concrete shell in the hinging region
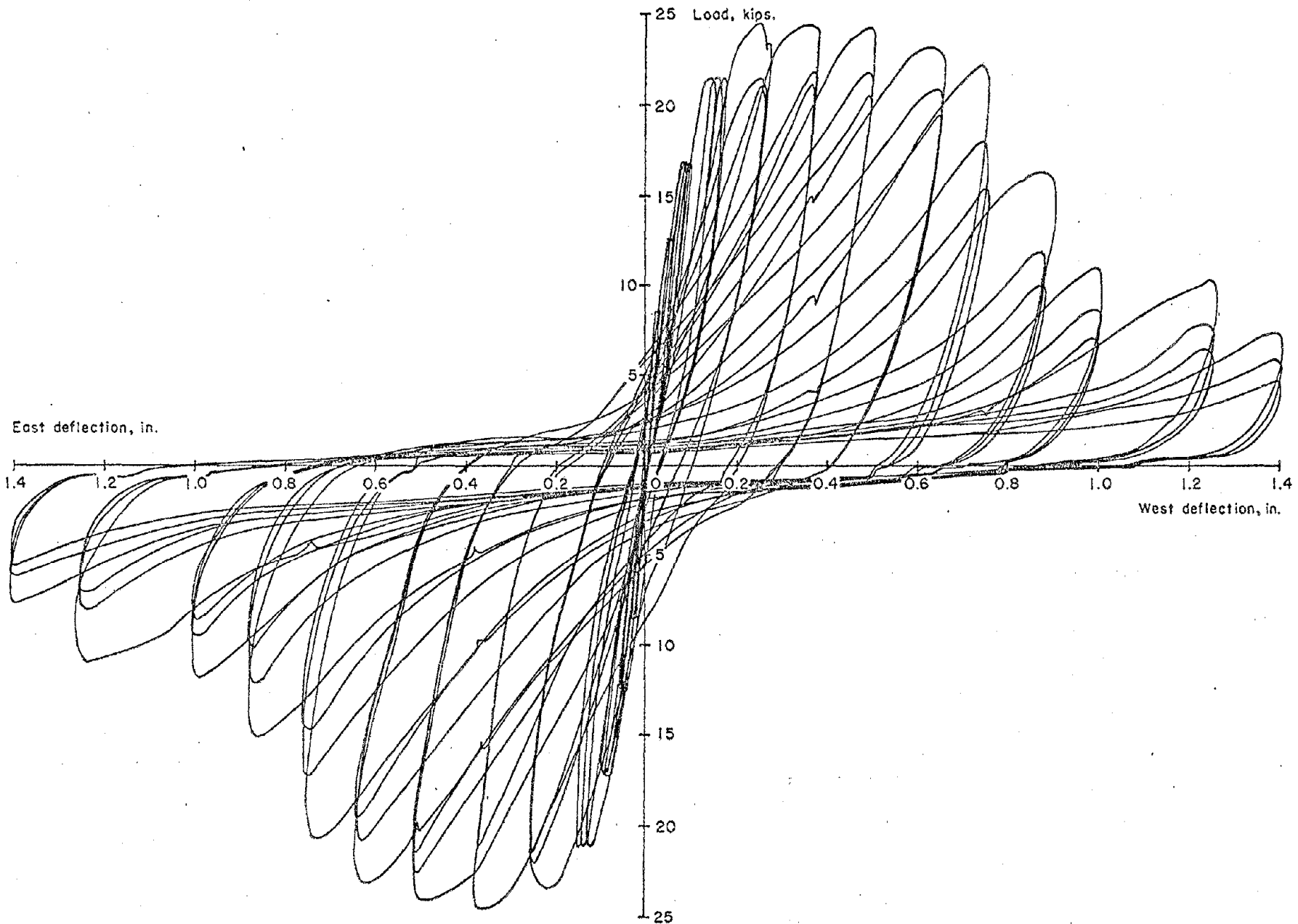
Fig. 27   Load versus Deflection for Specimen C4

was first observed at a load of 10.9 kips (48.5 KN.) per beam during the thirteenth inelastic load cycle. The corresponding deflection was 0.67 in. (17.0 mm.).

Photographs of the beams after testing are shown in Fig. 28. More cracks in the abutment walls near the beam ends than in previous specimens can be seen. These are associated with stresses in the embedment zone of the coupling beam flexural steel. These cracks appeared prior to yield. However, no bond failure was observed.

Specimen C5

Specimen C5 was similar to Specimen C2 except that the size of the confined concrete core was increased to 3.50x 6.16 in. (89x157 mm.). As in Specimen C4, the larger core size required that the top and bottom reinforcing bars be placed outside the steel in the rigid abutments. Details are shown in Fig. 3. Again, this anchorage detail is not recommended for field practice.

A continuous plot of load versus deflection is shown in Fig. 29.

First cracking in this specimen occurred during the seventh load cycle at a load of 3.7 kips (16.5 KN.) per beam. Yielding took place during the sixteenth load cycle at an applied load of 9.2 kips (40.9 KN.) per beam. The measured deflection at yield was 0.19 in. (4.8 mm.). Full depth flexural cracks and some diagonal cracks had formed at the yield load.
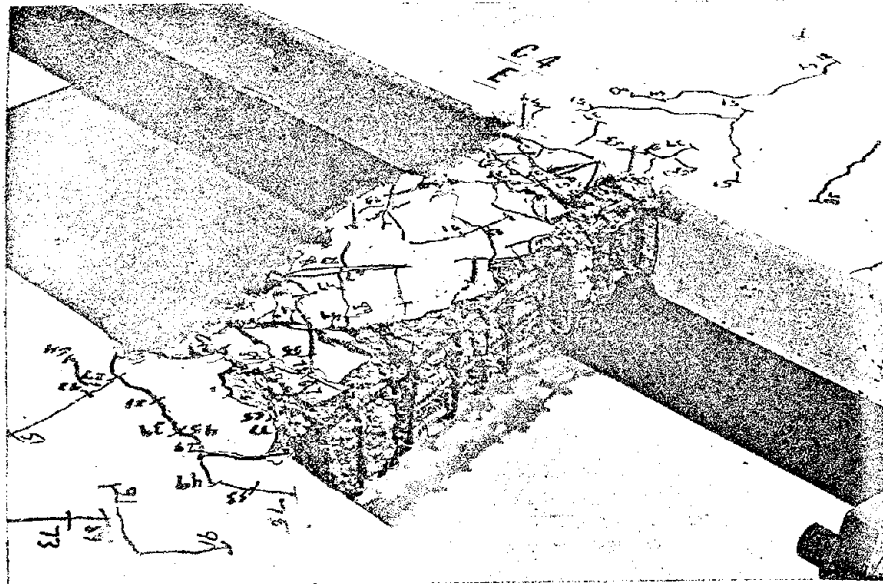
a) East Beam
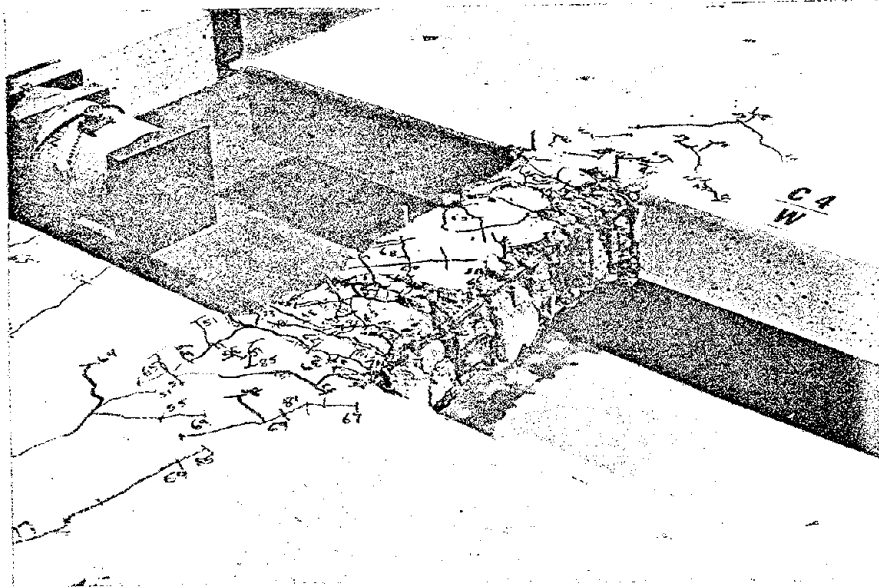
b) West Beam

Fig. 28   Specimen C4 After Testing to Destruction
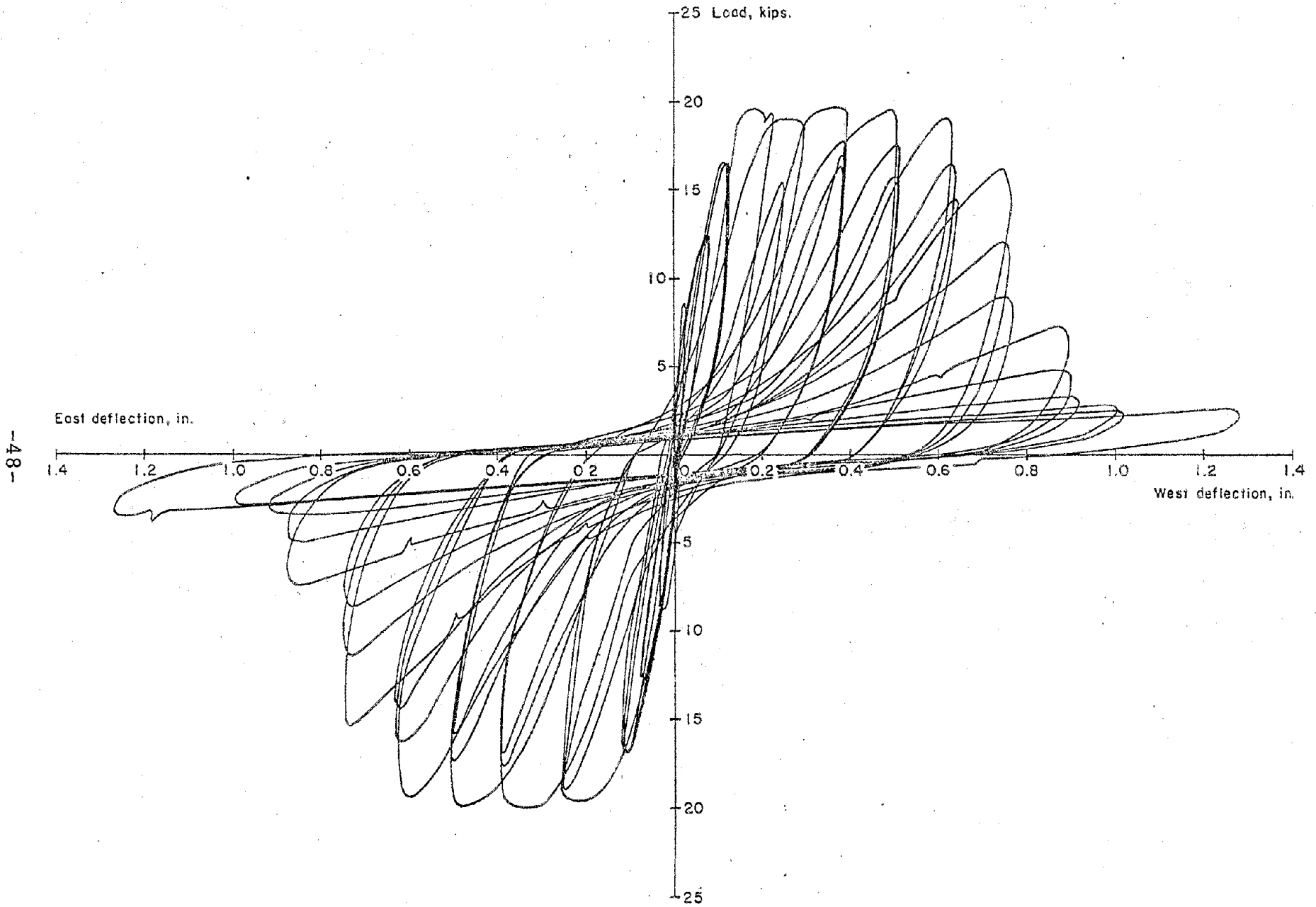
Fig. 29 Load versus Deflection for Specimen C5

The maximum load carried by Specimen C5 was 9.4 kips (41.8 KN.) per beam during the fourth inelastic load cycle. Nominal shear stress at this load was $6.8 \sqrt{f_c'}$ $(0.56 \sqrt{f_c'})$. Deflection at this load level was 0.35 in. (8.9 mm.).

Spalling of the concrete shell in the hinging region began at a load of 7.7 kips (34.3 KN.) per beam during the eleventh inelastic load cycle. Deflection at this load level was 0.59 in. (15.0 mm).

The test was terminated after 22 inelastic load cycles had been applied to the specimen. Maximum deflection was 1.30 in. (33.0 mm.). The final load applied to the specimen was 1.4 kips (6.2 KN.) per beam. This represented a loss in capacity of 85%.

Photographs of the beams after test are shown in Fig. 30. Most of the concrete deterioration in each of these beams occurred at one end. Extensive crushing of the confined concrete in the core of the west beam was observed. Failure was attributed to "sliding shear" at the interface between the beam ends and the face of the abutment wall. Cracking in the abutment walls near the ends of the beams was less severe in this specimen than in Specimen C4.

Specimen C6

Specimen C6 was tested with diagonal steel as primary reinforcement. Two No. 3 bars formed one diagonal and one No. 4 bar formed the other. Symmetry was maintained by

a) East Beam
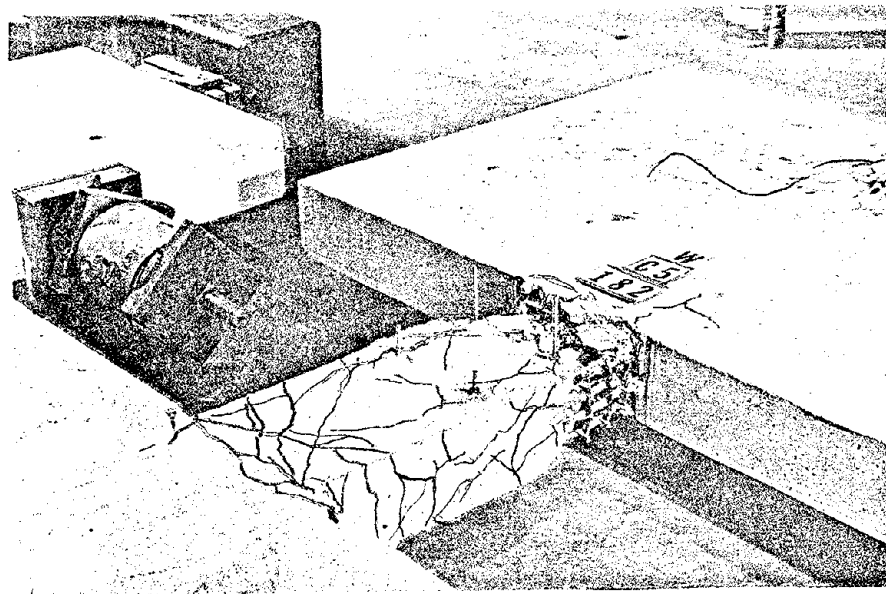
b) West Beam

Fig. 30   Specimen C5 After Testing to Destruction

passing the No. 4 bar between the No. 3 bars at the point
of intersection. Details are shown in Fig. 5.

A continuous plot of load versus deflection is shown in
Fig. 31. The loops for the individual load cycles do not
show the same pinching effect that was characteristic of
the other specimens. Furthermore, this specimen maintained
its load capacity for many more cycles of loading.

First cracking in this specimen occurred during the
seventh load cycle at an applied load of 3.7 kips (16.5 KN.)
per beam. Yielding in the primary reinforcement occurred
during the thirteenth load cycle at an applied load of 7.8
kips (34.7 KN.) per beam. Deflection at yield was 0.11 in.
(2.8 mm.) Full depth cracks and some diagonal cracks had
formed at the yield load.

Spalling of the concrete shell in the hinging region
was first observed during the tenth inelastic load cycle at
a load of 8.8 kips (39.1 KN.) per beam. Deflection at this
load level was 0.35 in. (8.9 mm.).

The maximum load carried by Speciemen C6 was 13.4 kips
(59.6 KN.) per beam during the sixteenth inelastic load
cycle. Nominal shear stress at this load was $10.9 \sqrt{f'_c}$
($0.91 \sqrt{f'_c}$). Deflection at this load level was 0.75 in.
(19.1 mm.).

As load was being applied in the positive direction
during the twenty first inelastic load cycle, twisting was
observed in the east beam about its longitudinal axis.

Load, kips

East deflection, in.

West deflection, in.

30

20

10

1.2 1.0 0.8 0.6 0.4 0.2   0.2 0.4 0.6 0.8 1.0 1.2

10

20

30
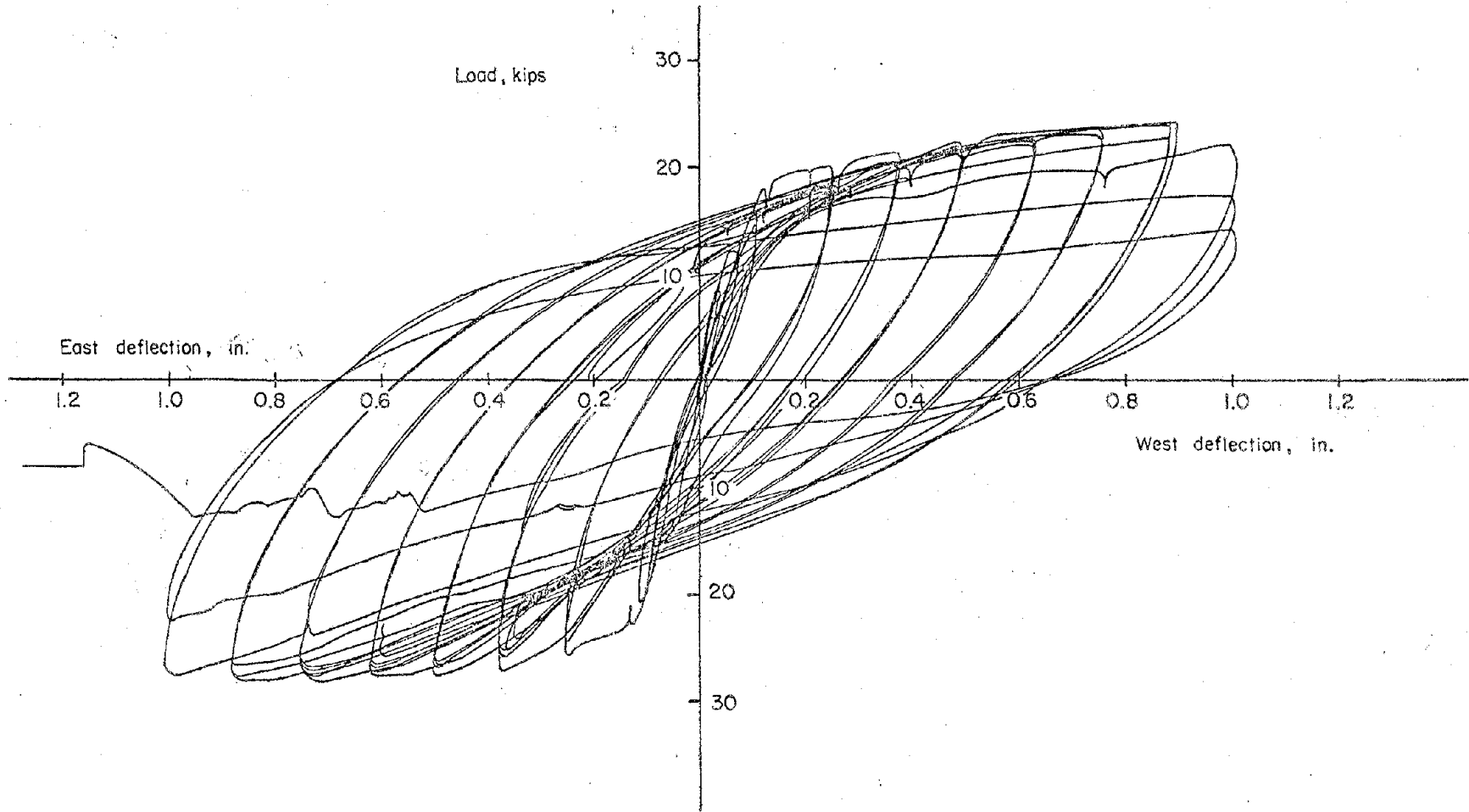
Fig. 31   Load versus Deflection for Specimen C6

Deflection at this level was 0.88 in. (22.4 mm.). Examination of the specimen after the test revealed that the diagonal reinforcement was approximately 1/4 in. (6.4 mm.) off center at the north end of the beam. The internal forces in the beam were therefore not symmetric and the beam twisted.

As load was applied during the twenty second inelastic load cycle, further twisting of the east beam occurred and twisting of the west beam was observed. As deflection was increased to 1.00 in. (25.4 mm.), buckling of the exposed No. 3 bars at the end of the beam was observed. The first decrease in load capacity with increasing deflection occurred during this load cycle. External instrumentation was removed from the east beam to prevent damage to the gages.

During application of load in the negative direction during the twenty third inelastic load cycle, fracture of a No. 3 bar occurred on the north side of the east beam. The maximum deflection of 1.00 in. (25.4 mm.) was imposed during this load cycle. Applied load had dropped to 10.4 kips (46.3 KN.) per beam. The test was terminated during the twenty fourth inelastic load cycle when the remaining No. 3 bars fractured.

Photographs of the beams after the test are shown in Fig. 32.

Evaluation of Test Results

In this section the behavior of the six specimens is
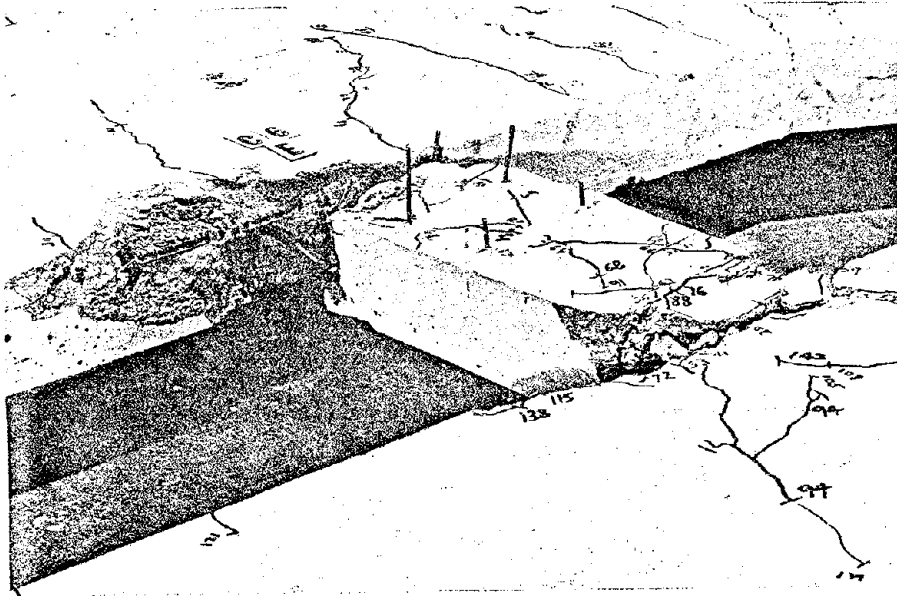
a) East Beam
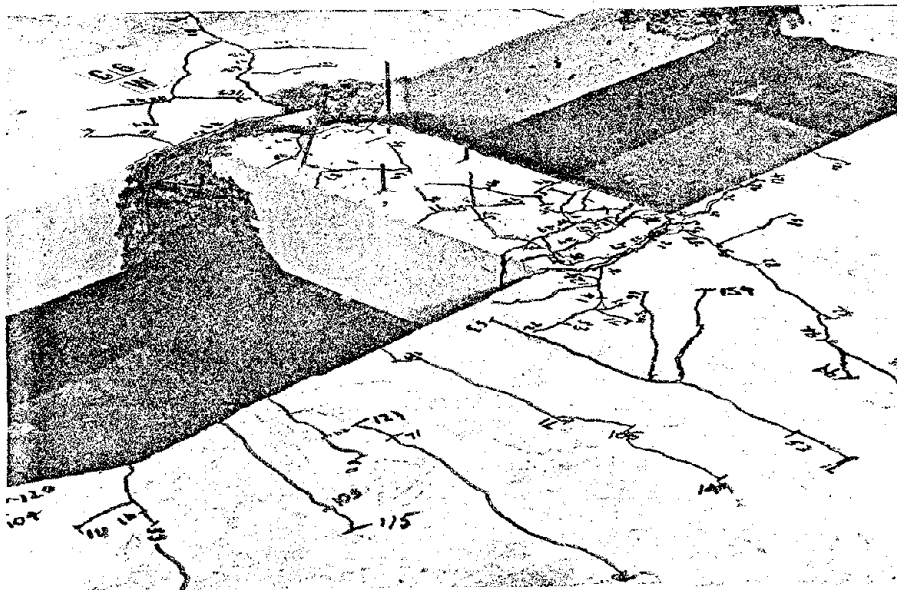
b) West Beam

Fig. 32   Specimen C6 After Testing to Destruction

compared. A comparison is also made between calculated and measured response of the specimens. Data for the individual tests is presented in Appendix A.

Strength

Table 4 shows a comparison between calculated and measured values of yield load and ultimate load. Calculated values for each specimen were determined using strain compatibility analysis and measured material properties. Monotonic loading was assumed.

A comparison of calculated load versus deflection relationships for monotonic loading with the load versus deflection envelopes determined from test results for each specimen is shown in Fig. 33 through Fig. 38. Calculated values were determined from moment-area theorems. Moment versus curvature relationships for each specimen were derived from a strain compatibility analysis using measured material properties. Plane sections were assumed to remain plane and shear distortions were neglected. Except for Specimen C6, beams having diagonal reinforcement were assumed to have a constant cross section within the limits of the diagonals. The section was taken at the point where the diagonals crossed. For Specimen C6, each half of the beam was divided into two regions of equal length. The section properties of the interior regions were determined at the point of crossing of the diagonals. The exterior regions were analyzed for

TABLE 4 — COMPARISON OF CALCULATED AND OBSERVED LOADS

Specimen	Yield Load			Maximum Load		
	Observed (kips)	Calculated (kips)	Observed/Calculated	Observed (kips)	Calculated (kips)	Observed/Calculated
C1	8.1	9.0	0.90	9.2	10.8	0.86
C2	10.2	9.8	1.04	10.3	11.8	0.87
C3	10.2	9.8	1.04	11.8	12.3	0.96
C4	10.0	9.5	1.05	11.5	12.3	0.94
C5	9.2	8.8	1.05	9.4	10.6	0.89
C6	7.8	10.7	.73	13.4	12.7	1.06
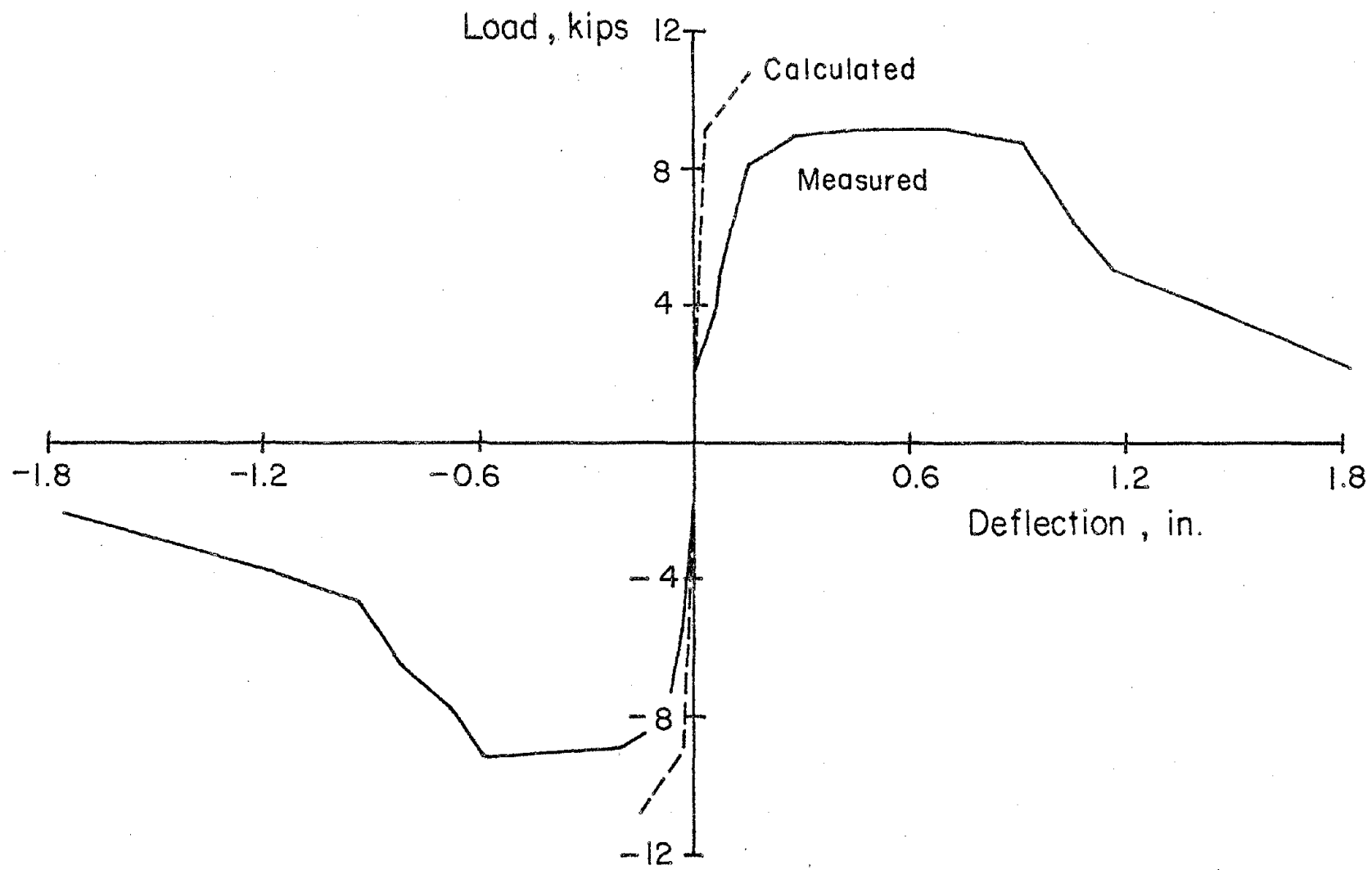
Fig. 33 Calculated and Measured Load versus Deflection Envelopes for Specimen Cl
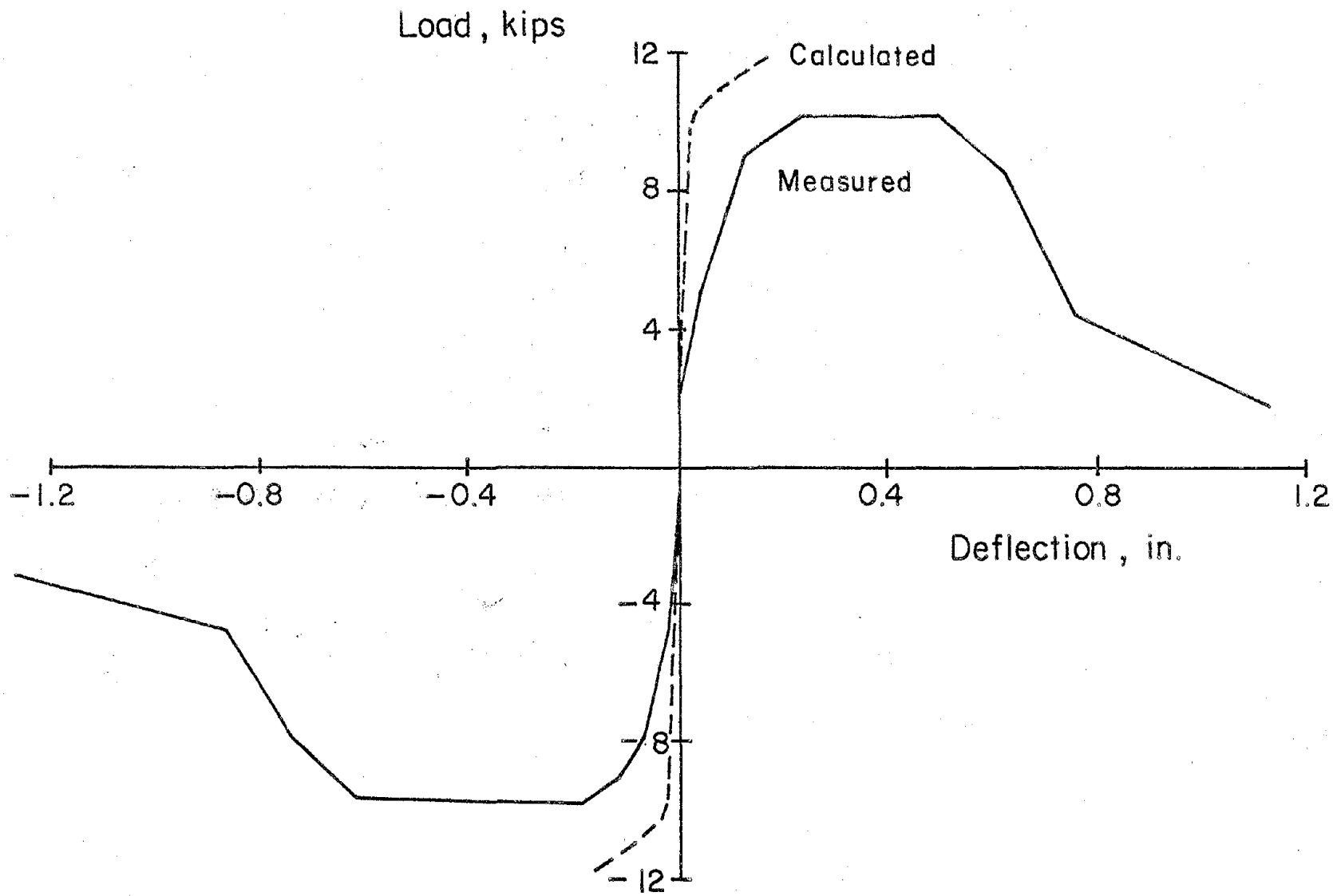
Fig. 34   Calculated and Measured Load versus Deflection Envelopes for Specimen C2
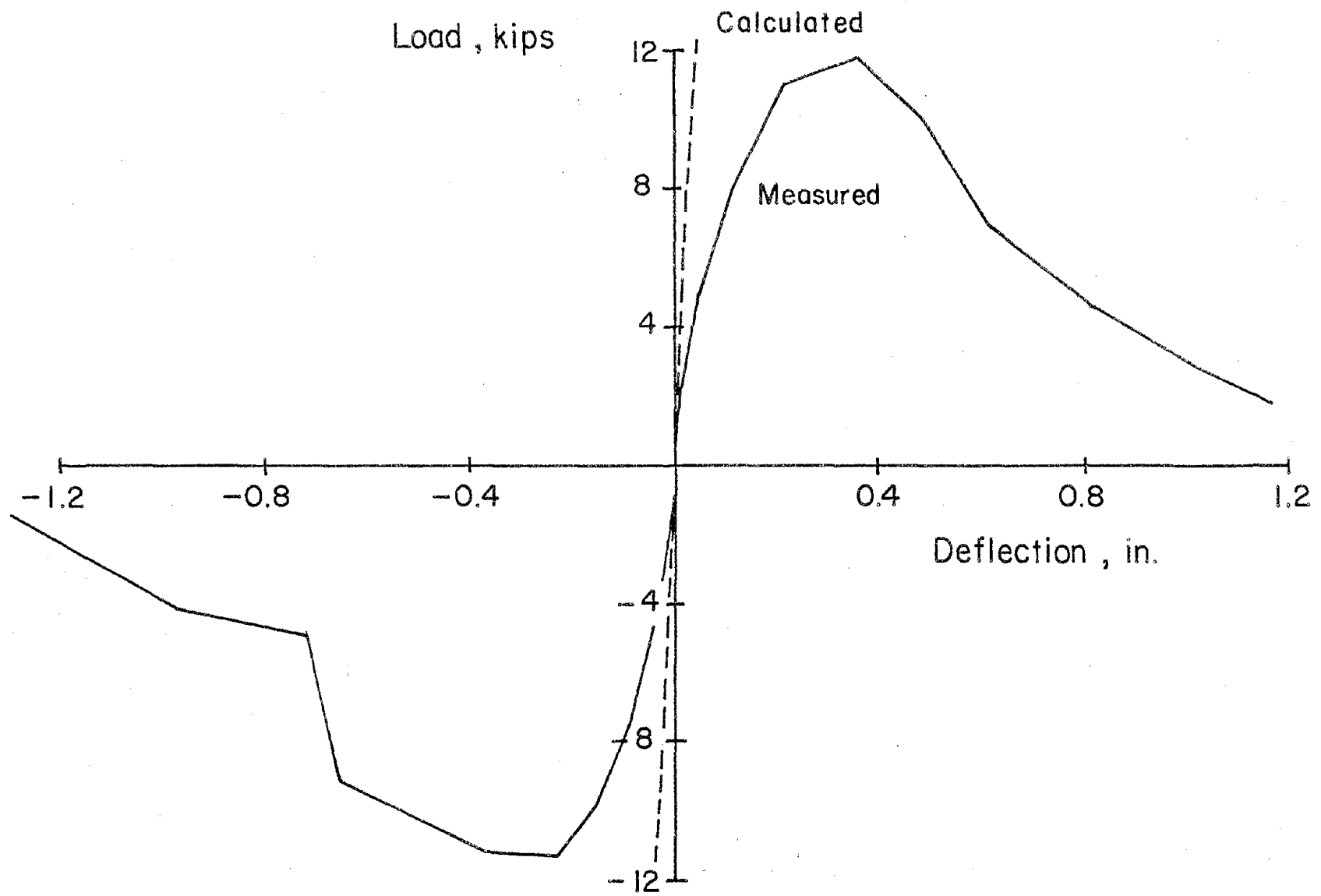
Fig. 35   Calculated and Measured Load versus Deflection Envelopes for Specimen C3
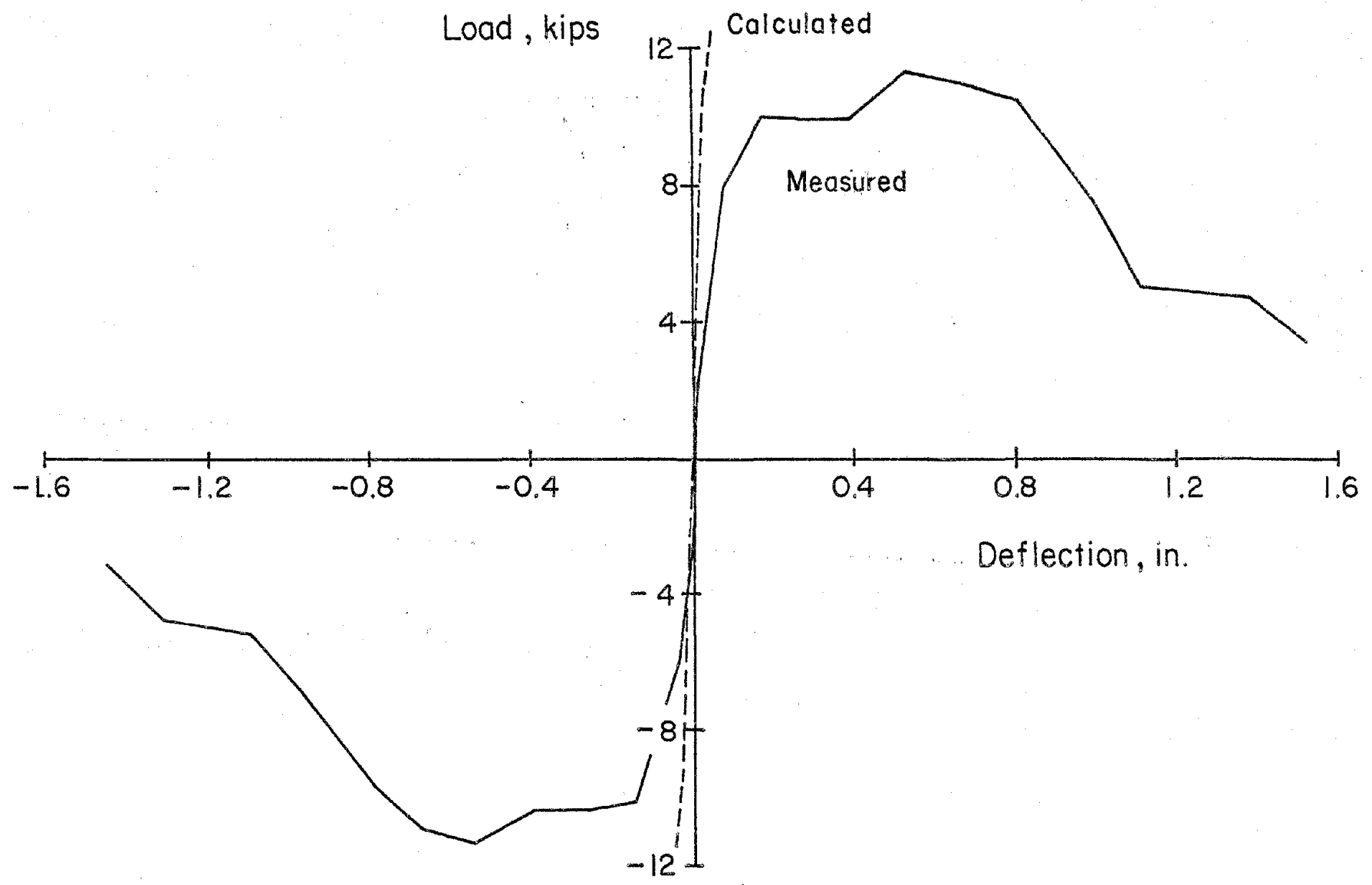
Fig. 36   Calculated and Measured Load versus Deflection Envelopes for Specimen C4

Load , kips
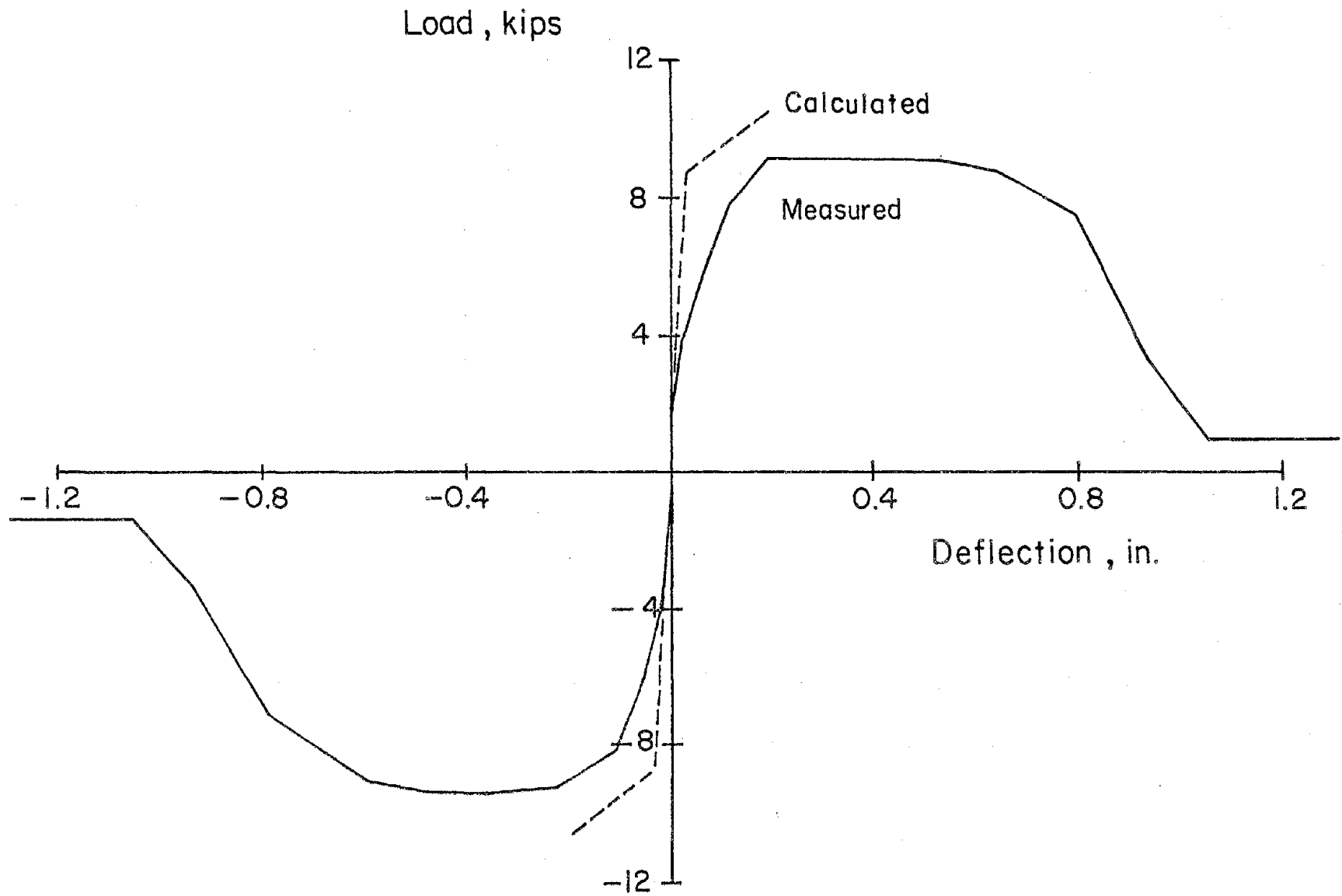
Fig. 37 Calculated and Measured Load versus Deflection Envelopes for Specimen C5
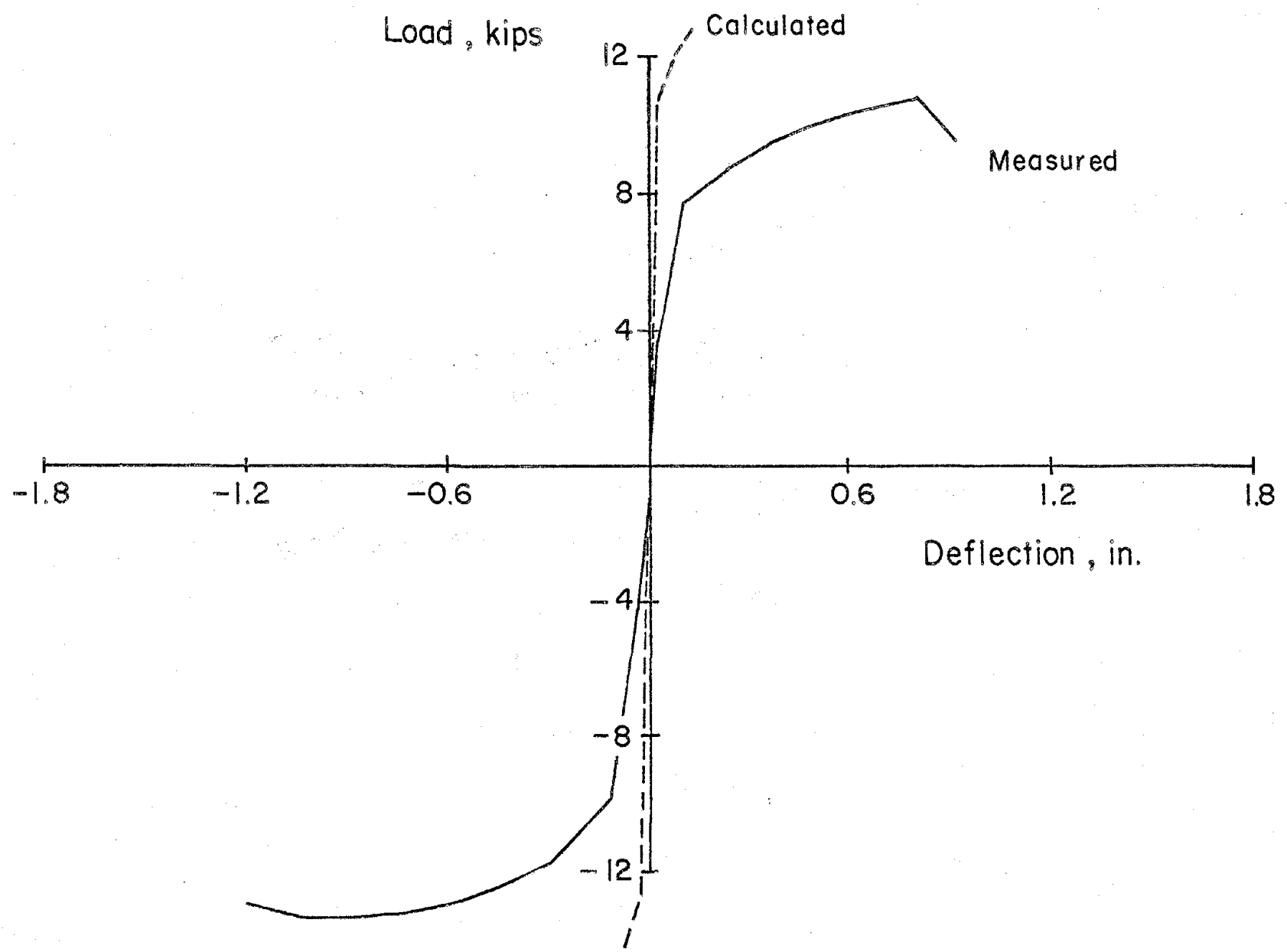
Fig. 38 Calculated and Measured Load versus Deflection Envelopes for Specimen C6

the cross sections at the ends of the beam.

For all specimens, the measured maximum load is less than the calculated maximum. The measured maximum load generally occurred at a larger deflection than that predicted. This is attributed to degradation in the specimen caused by cyclic loading.

A comparison of the load versus deflection envelopes for the six specimens is shown in Fig. 39. Each of the specimens exhibited significant loss of strength at increased deflection after the peak load was reached.

Specimens C2 and C5 with no diagonal reinforcement showed the greatest loss of strength. Peak loads in these specimens occurred at deflections of 0.41 in. (10.4 mm.) and 0.35 in. (8.9 mm.), respectively. These deflections correspond to 1.8 times the yield deflection for both specimens.

Specimens C1 and C4 had diagonal reinforcement in the hinging regions. These specimens showed better load retention characteristics after reaching peak load than Specimens C2 and C5. Peak loads in Specimens C1 and C4 occurred at deflections of 0.55 in. (14.0 mm.) and 0.40 in. (10.2 mm.), respectively. These deflections correspond to 3.4 and 2.9 times the respective yield deflection. Specimen C3 showed the most severe strength loss. However, as previously reported, one of the beams in this specimen deteriorated rapidly at its midspan after yielding. This accounts for the relatively poor performance of this specimen.

Load , kips
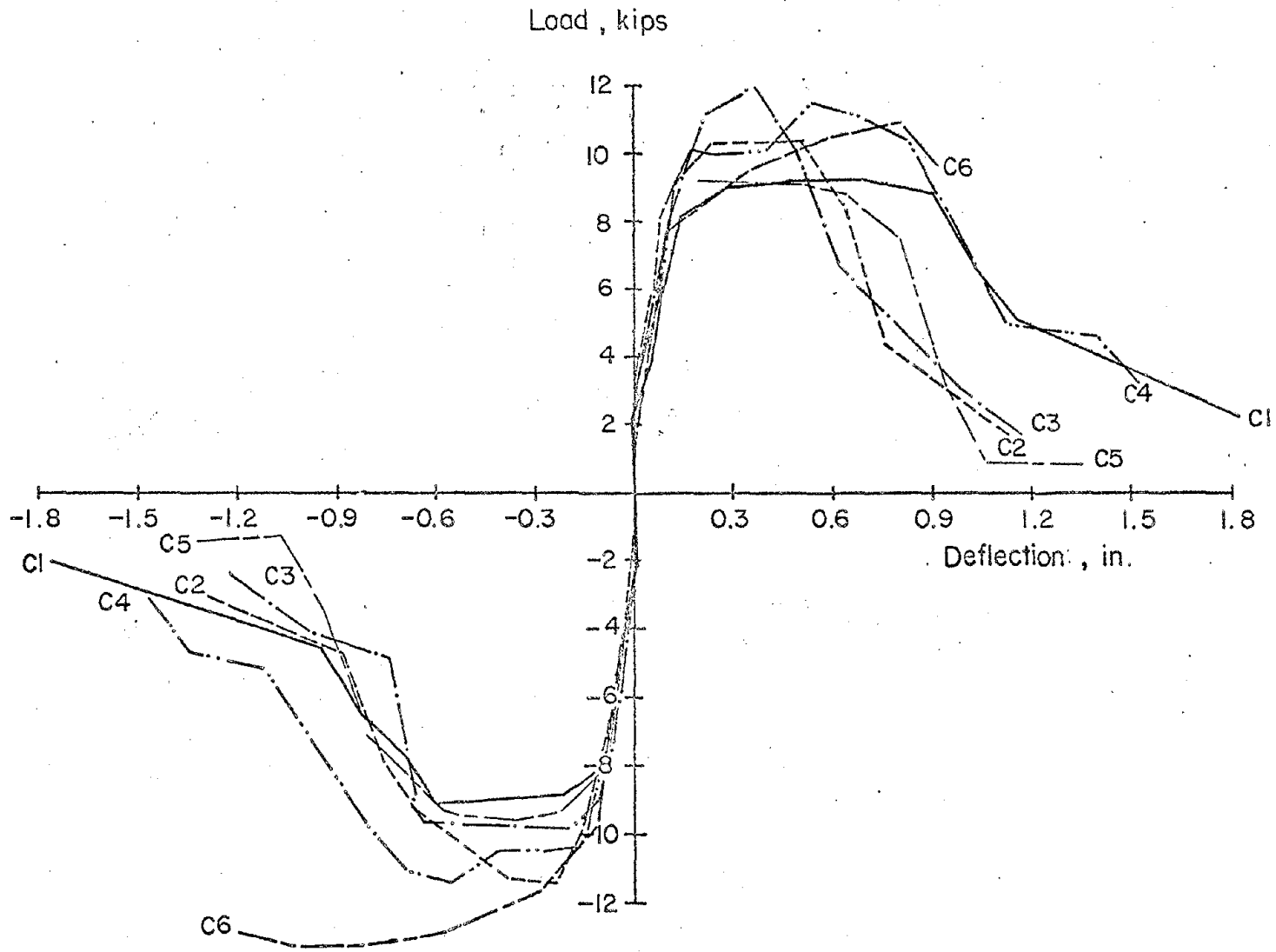
Fig. 39   Load versus Deflection Envelope for Specimens C1 to C6

Specimen C6, with cross-beam diagonal reinforcement, showed superior strength. Since the diagonals in this specimen were not identical, the capacity was different for each direction of loading. The strength of the specimen increased with each new load increment up to an imposed deflection of 0.88 in. (22.4 mm.). This is approximately 8 times the yield deflection. Fracture of the diagonal reinforcement and loss of strength occurred at a deflection of 1.00 in. (25.4 mm.).

Cumulative Deflection Ductility

The cumulative deflection ductility of a coupling beam specimen at the nth load cycle is defined as

$$C_n = \sum_{i=1}^{n} \frac{\Delta_i}{\Delta_y} \qquad (1)$$

where Δ_y is the deflection measured at first yield with respect to zero deflection and Δ_i is the peak deflection during load cycle i. Deflection is measured as shown in Fig. 40. Cumulative ductility is calculated separately for positive and negative loadings.

A comparison of cumulative deflection ductility versus load for Specimens C1, C2 and C3 is shown in Fig. 41. These specimens all had the smaller core size. Specimen C1 with single diagonal reinforcement in the hinging regions showed the greatest ductility and least drop in load capacity.

$$C_n = \sum_{i=1}^{n} \frac{\Delta i}{\Delta y}$$
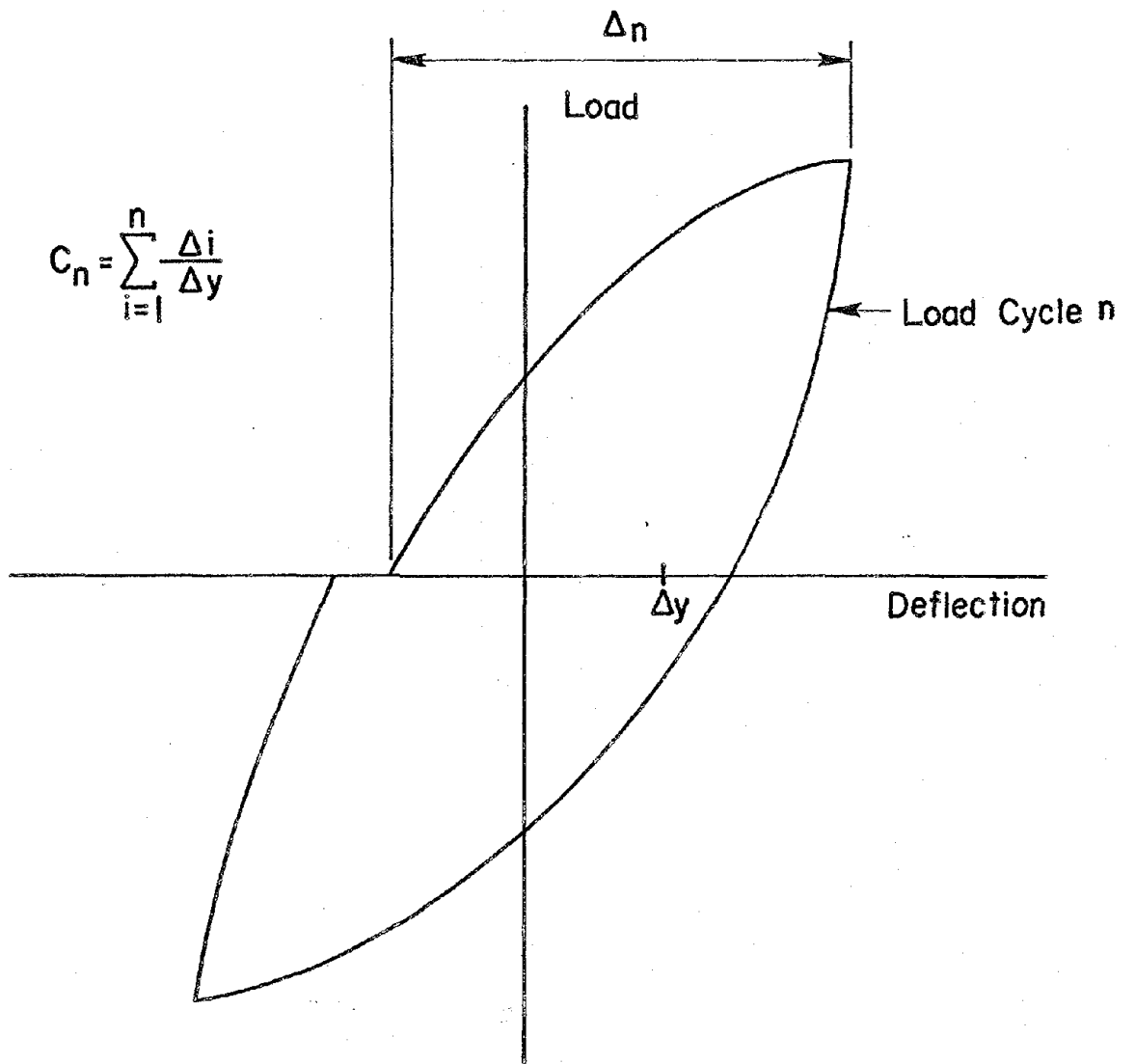
Fig. 40   Definition of Cumulative Ductility

Load , kips

12

10

8

6

4

2

C2

C3

Cl

C3

C2

Cl

-240 -200 -160 -120 -80 -40 0 40 80 120 160 200 240

Cumulative Ductility
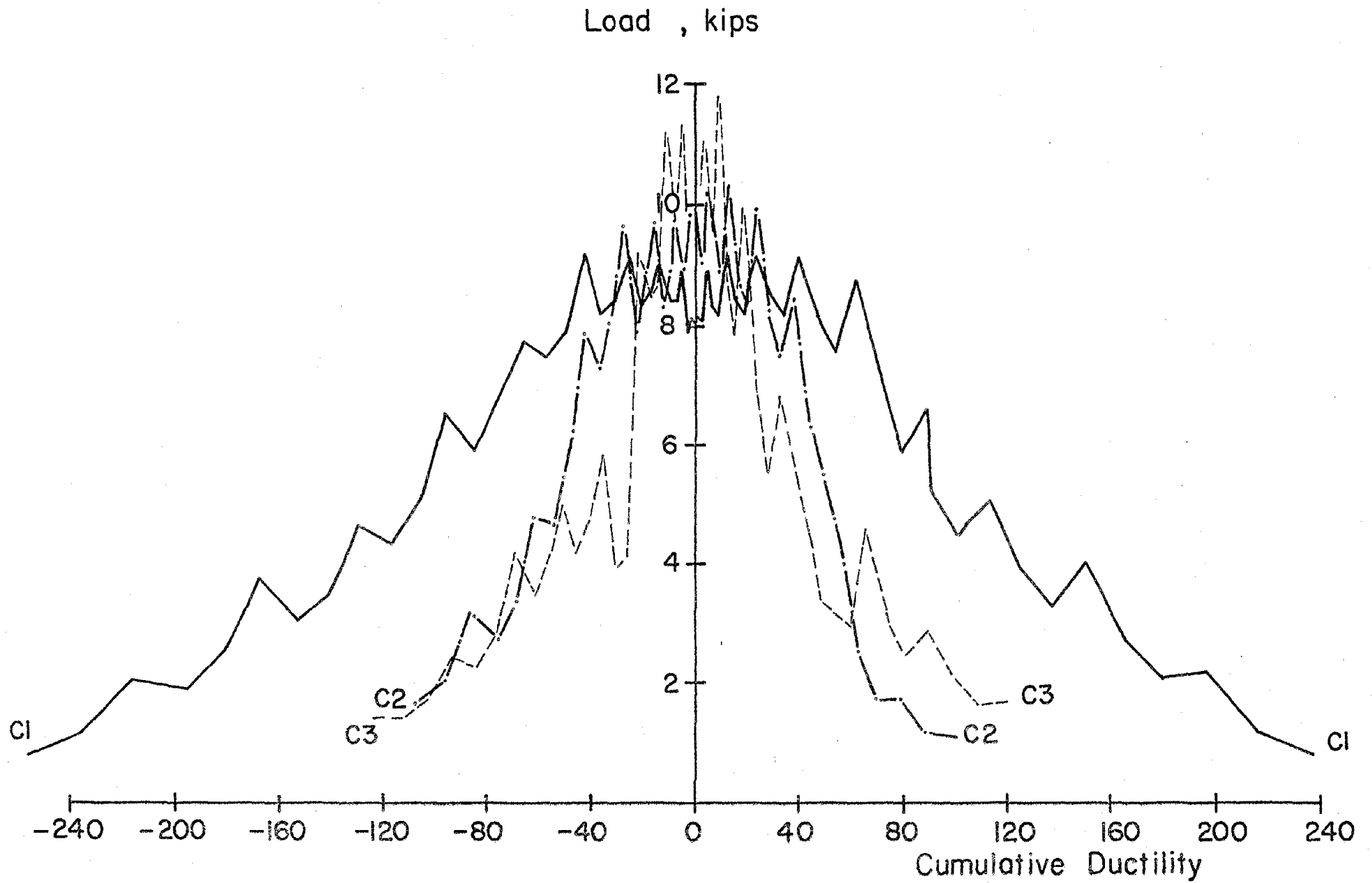
Fig. 41 Cumulative Deflection Ductility for Specimens Cl to C3

Specimen C2 with straight bars exhibited the least ductility and greatest drop in load capacity. Specimen C3 with double diagonal bars in the hinging regions showed properties similar to Specimen C2. However, one of the two beams in this specimen deteriorated rapidly after yielding.

The load versus cumulative deflection ductility relationship for specimens with diagonal reinforcement is shown in Fig. 42. Specimen C6 with the cross-beam diagonal reinforcement showed the greatest strength for increasing values of cumulative ductility. Specimen C3 exhibited the greatest loss of strength and the least cumulative ductility. Specimen C1 and C4 showed the greatest cumulative ductilities but also had significant losses of strength.

A comparison of load versus cumulative ductility for Specimens C2 and C5 is shown in Fig. 43. These specimens had straight bars and differed only in the size of the confined concrete core. Specimen C5, with the larger core size, showed better load retention and greater cumulative ductility.

Summary and Conclusions

Preliminary results of tests on six coupling beam specimens subjected to reversing in-plane loads have been reported. The beams tested had spans of 16.67 in. (423 mm.) and depths of 6.67 in. (169 mm.) Fixed end conditions were imposed by anchoring the ends of the beams in rigid abutment walls. Nominal maximum shear stresses between $7.0 \sqrt{f'_c}$

Load , kips

15

10

5

-270 -240 -210 -180 -150 -120 -90 -60 -30 0 30 60 90 120 150 180 210 240 270

C4

C1

C6

C3

C6

C3

C4

C1

Cumulative Ductility
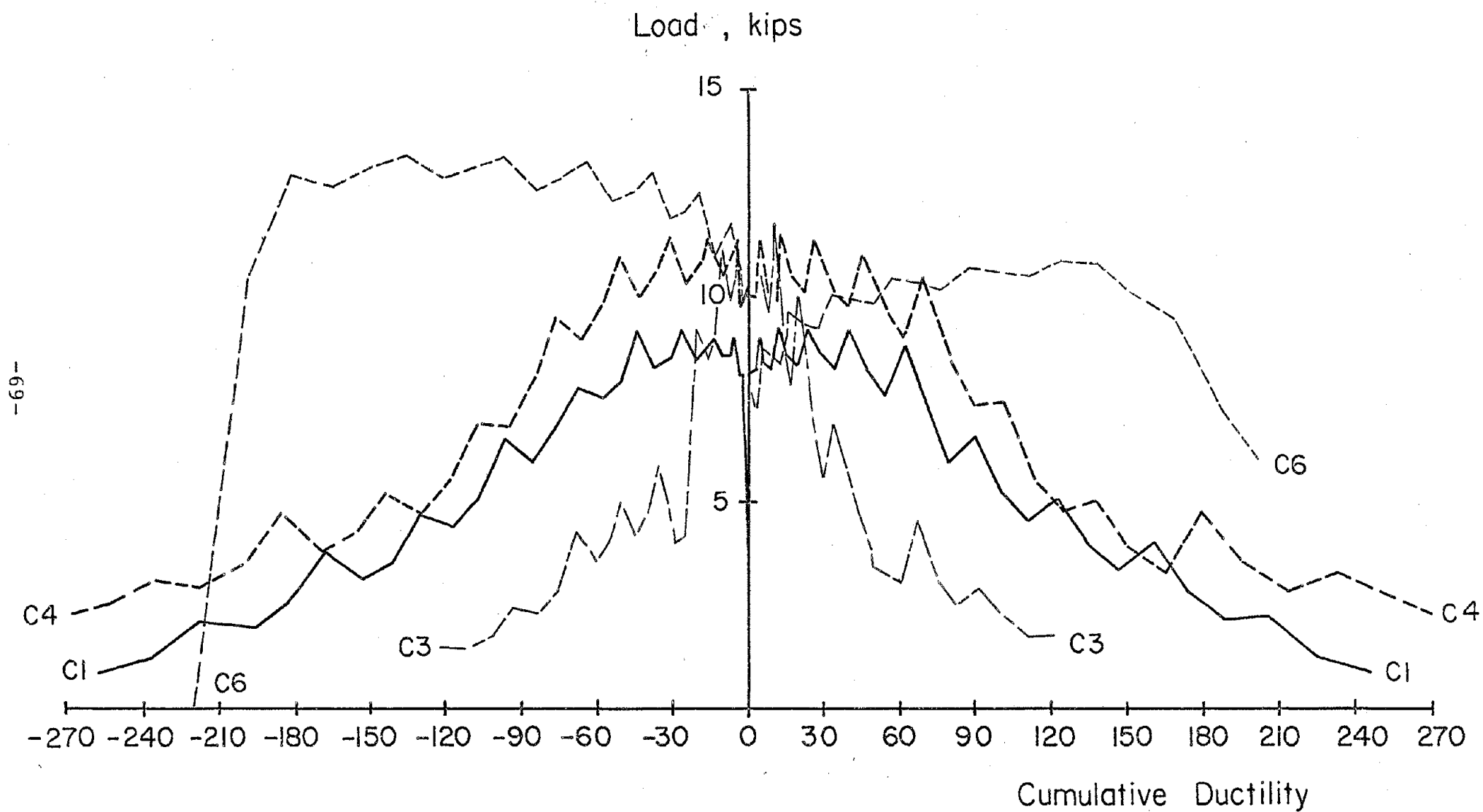
Fig. 42 Cumulative Deflection Ductility for Specimens C1, C3, C4, and C6

-69-
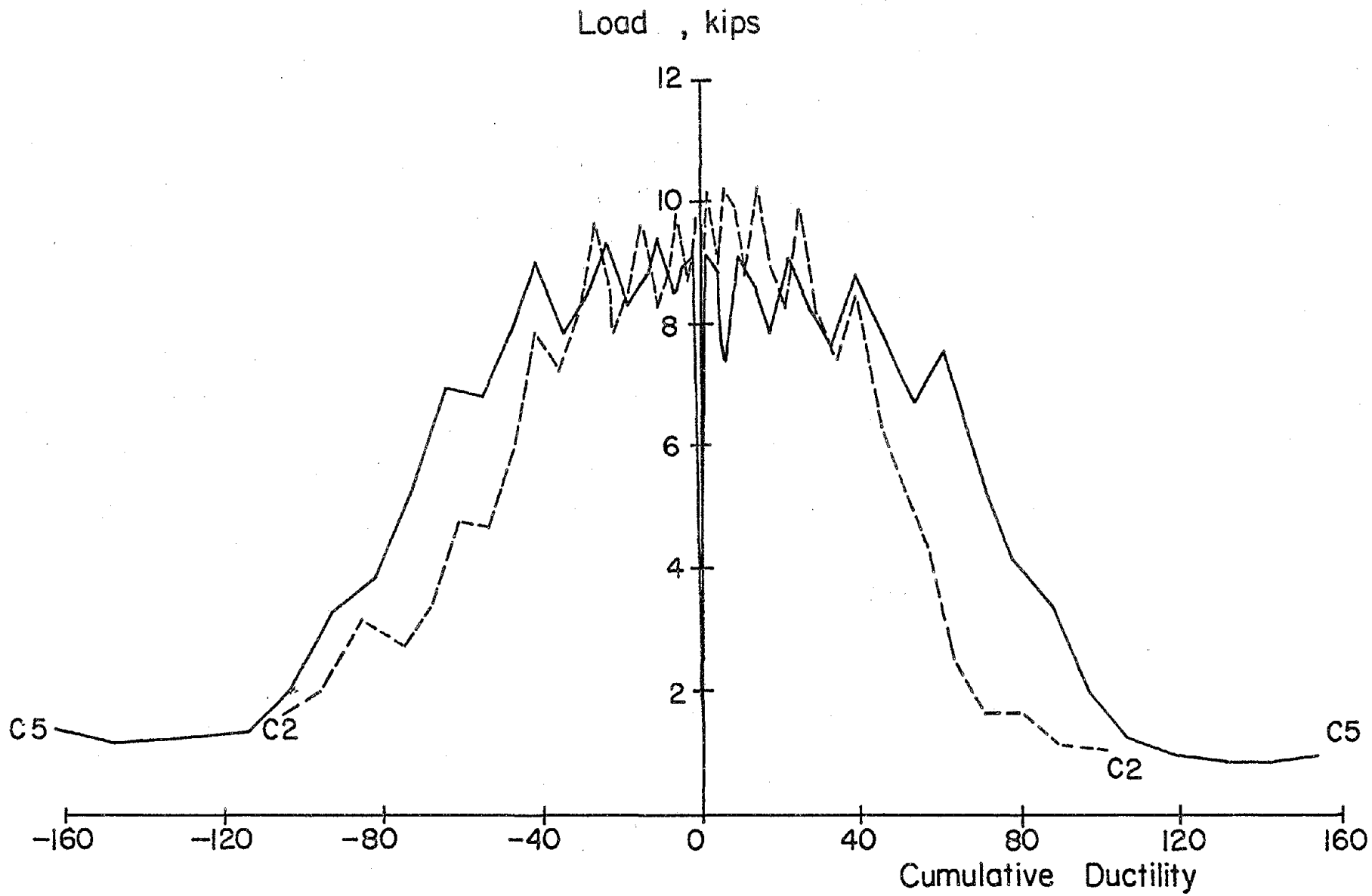
Fig. 43   Cumulative Deflection Ductility for Specimens C2 and C5

$(0.58 \sqrt{f_c'})$ and $10.9 \sqrt{f_c'}$ $(0.91 \sqrt{f_c'})$ were recorded.

The objective of the investigation was to determine the effect of reinforcement details on strength and ductility. Details from one of the beams showing suitable behavior will subsequently be used in connecting elements for an investigation of coupled wall systems. Variables were the type and amount of diagonal reinforcement and size of the confined concrete core.

The specimens were constructed of 3000 psi (20.7 MPa) concrete. Deformed, hot rolled reinforcement of Grade 60 steel was used.

Each specimen was instrumented to measure loads and deflections. Rotations and shear deformations in the hinging regions were measured. Steel strains were also recorded.

Results indicate that all specimens had considerable ductility. Beams with diagonal reinforcement demonstrated improved behavior as compared to beams with straight bars. Two specimens tested without diagonal reinforcement exhibited rapid loss of strength after the peak load was reached. Cumulative ductility was also lower. Slip in these specimens occurred along a flexural crack that formed at the junction of the beams and the fixed supports.

Specimens with diagonal reinforcement in the hinging regions did not exhibit the slip observed in specimens with straight bars. However, these specimens did show significant losses of capacity after the peak load was reached.

The hysteresis loops for specimens with straight bars

and specimens with diagonal bars in the hinging regions showed severe pinching. This indicates that the shear resisting mechanisms in these beams deteriorated under repeated cycles of reversing loads.

A specimen having straight cross-beam diagonals as primary reinforcement exhibited the least strength loss under repeated cycles of inelastic loading. This detail was first suggested by Paulay[3] in an experimental program conducted at the University of Canterbury. The capacity of this specimen continued to increase as imposed deflection was increased during repeated cycles of inelastic loading. Furthermore, the hysteresis loops for this specimen did not show the pinching that was evident in the other specimens. Therefore the energy absorbed by this specimen was greater.

Two specimens tested with straight bars differed only in the size of the confined concrete core. The specimen with the larger core area exhibited a reduced rate of decay after the peak load was reached. However, the increased core area did not affect the magnitude of the peak load.

REFERENCES

1. Bertero, V. V. and Popov, E. P., "Hysteretic Behavior of Reinforced Concrete Flexural Members with Special Web Reinforcement," _Proceedings_, U. S. National Conference on Earthquake Engineering, Ann Arbor, June 1975 (EERI).

2. ACI Committee 318, "Building Code Requirements for Reinforced Concrete, (ACI 318-71)," American Concrete Institute, Detroit, 1971.

3. Paulay, T., "Simulated Seismic Loading of Spandrel Beams," _Journal of the Structural Division_, ASCE, Vol. 97, No.ST9, Proc. Paper 8365, September 1971, pp. 2407-2419.

ACKNOWLEDGMENTS

APPENDIX A - DATA PRESENTATION

Reduced data from each test specimen are presented in this Appendix. The location of external gages is shown in Fig. A1. Data consists of plots showing load and deflection history, load versus deflection relationships, moment versus rotation relationships, shear versus shear distortion relationships, and load versus steel strain relationships. Pertinent information relating to each of these groups of data is also presented.

Rotation and shear deformation data determined for the internal region of each beam indicated that relatively small deformations occurred in this region. Therefore, only data from the base regions of the beams is presented.

Load and Deflection Histories

Plots of load versus load cycle and deflection versus load cycle are shown for each specimen. Yield loads and yield deflections recorded during the tests are indicated on these figures. Yield was defined with respect to measured strains in the main flexural reinforcement.

Load versus Deflection Relationships

Load versus deflection relationships for each of the specimens are shown for the first load cycle of each load increment. These plots were obtained from readings taken at each load stage within the cycles. The numbers on these plots indicate the number of the load cycle and correspond

to the load and deflection history plots. This same format
is used for other figures.

Also shown are the load versus deflection envelopes for
each specimen.

Moment versus Rotation Relationships

Moment versus rotation relationships for each beam
except Specimen C1 are shown for the first cycle of loading
at each load increment. Moments were calculated for the
section at the base of the beams. Rotations were calculated
from instrumentation in the base region. The method of
calculation is shown in Fig. A1.

Shear versus Shear Distortion Relationships

Average applied shear versus shear distortions in the
base region are presented for each specimen. The method for
calculating shear distortions is shown in Fig. A2.

Load versus Steel Strain Relationships

Load versus strain relationships are shown for flexural
reinforcement, diagonal reinforcement, and stirrup-ties.
The relationships shown are for the first load cycle at each
new load increment.

N

West-Beam   East-Beam

Deflection gages

Internal Section

Base Section

4"
4"

4½"
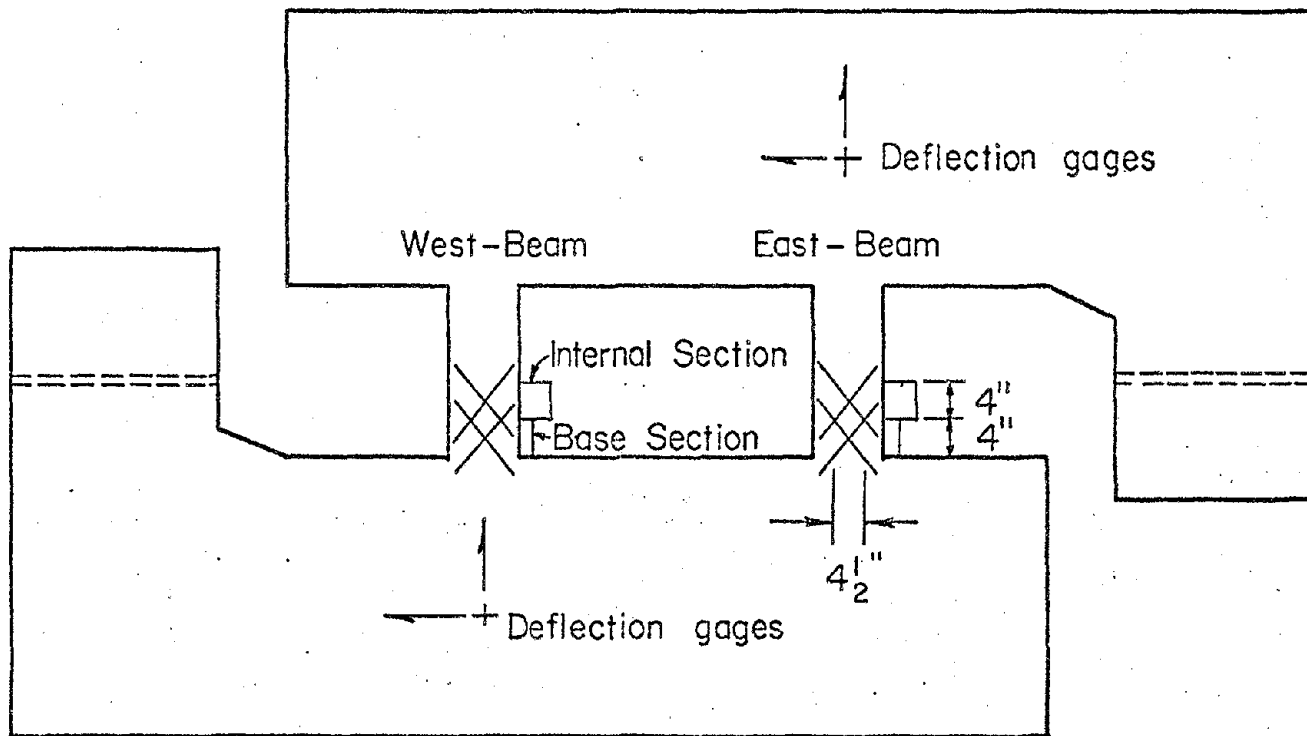
Deflection gages

Fig. A-1   Location of External Gages
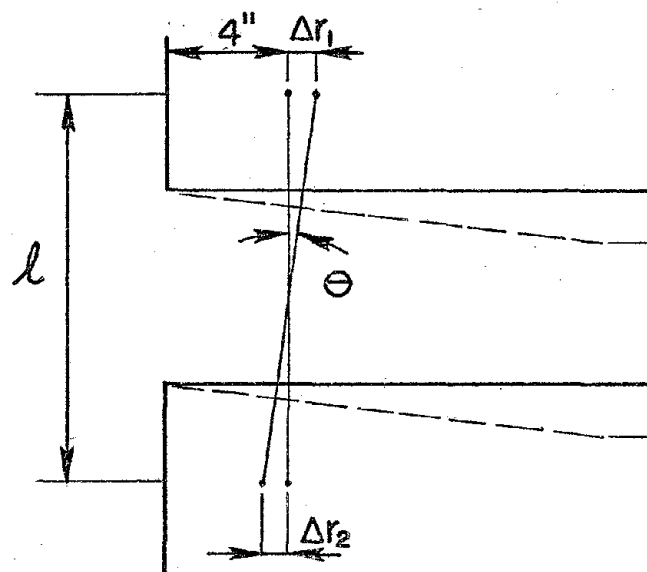
Fig. A-2 Calculation for Rotation
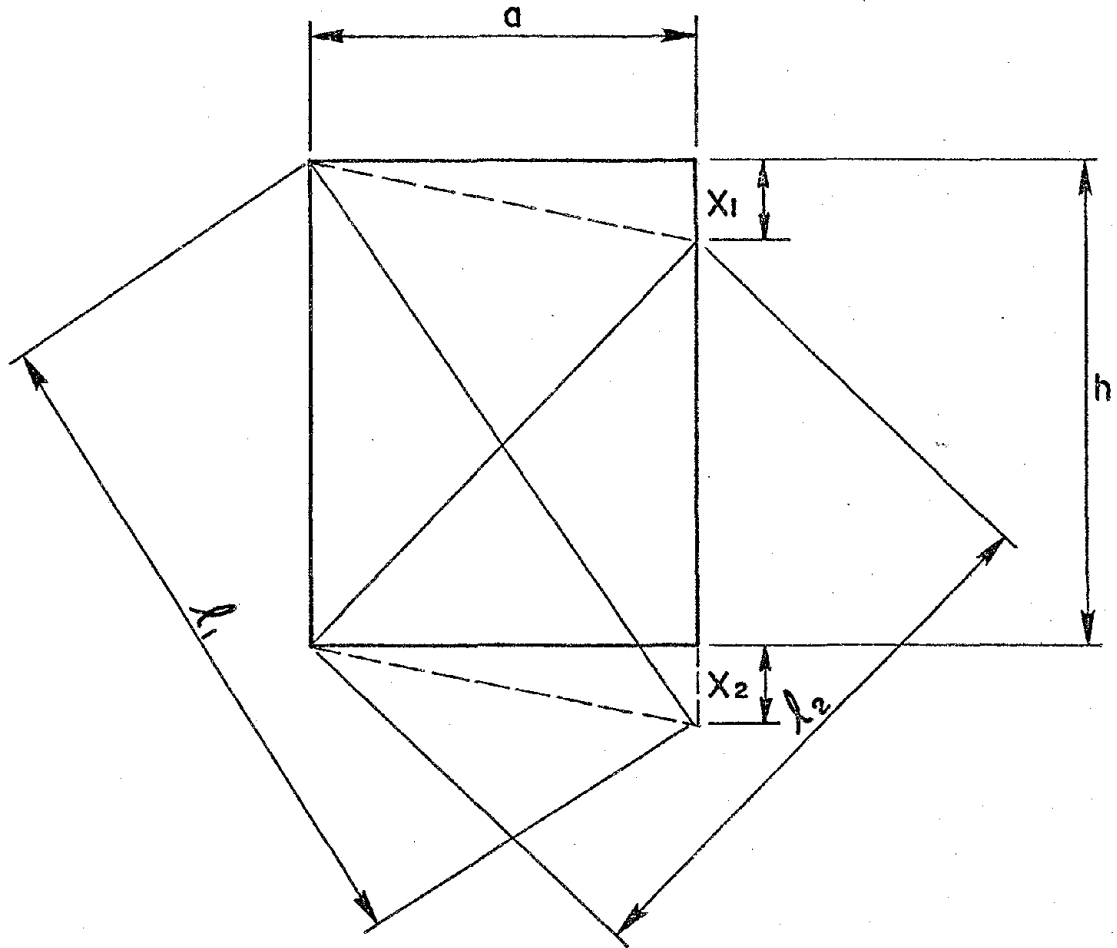
$$\gamma_{av} = \frac{X_1 + X_2}{2a} = \frac{\sqrt{\ell_1^2 - a^2} - \sqrt{\ell_2^2 - a^2}}{2a}$$

Fig. A-3   Calculation for Shear Distortion

A-5
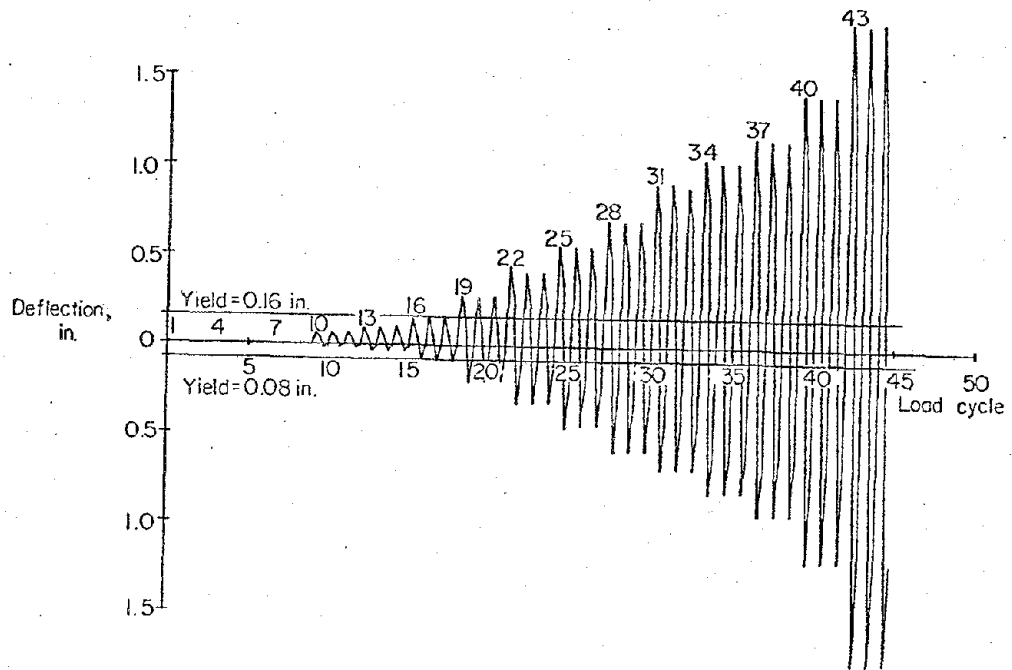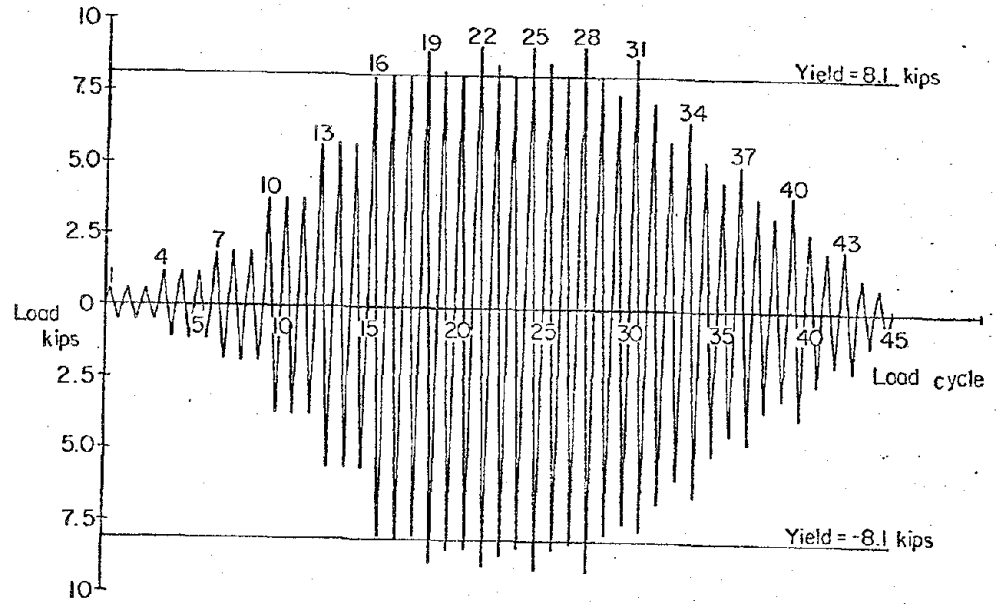
Fig. A-4 Load and Deflection Histories for Specimen C1
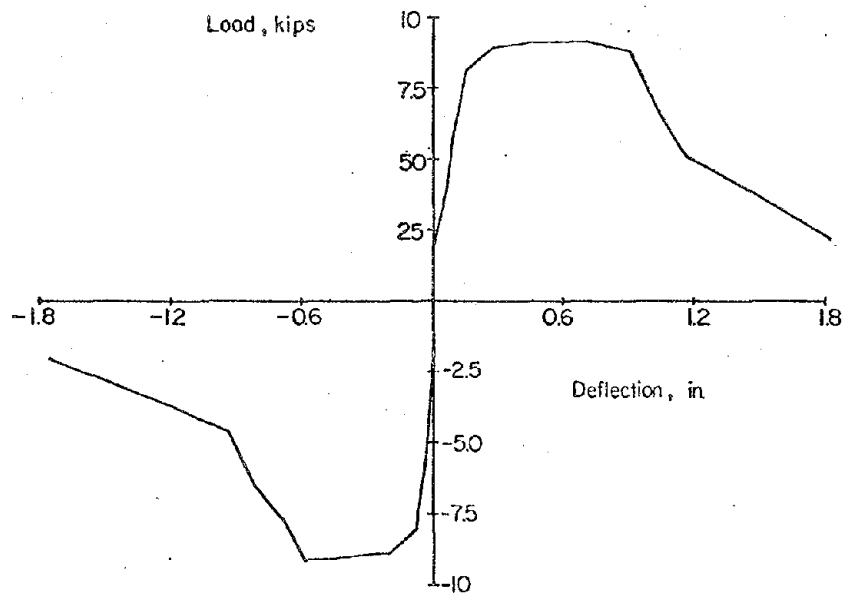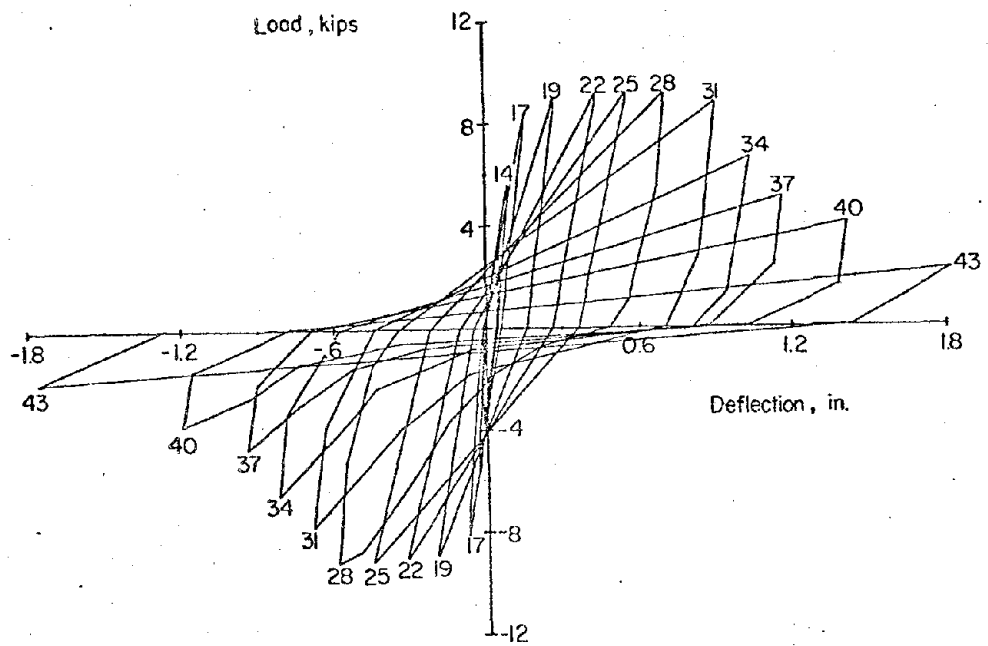
Fig. A-5   Load versus Deflection for Specimen Cl
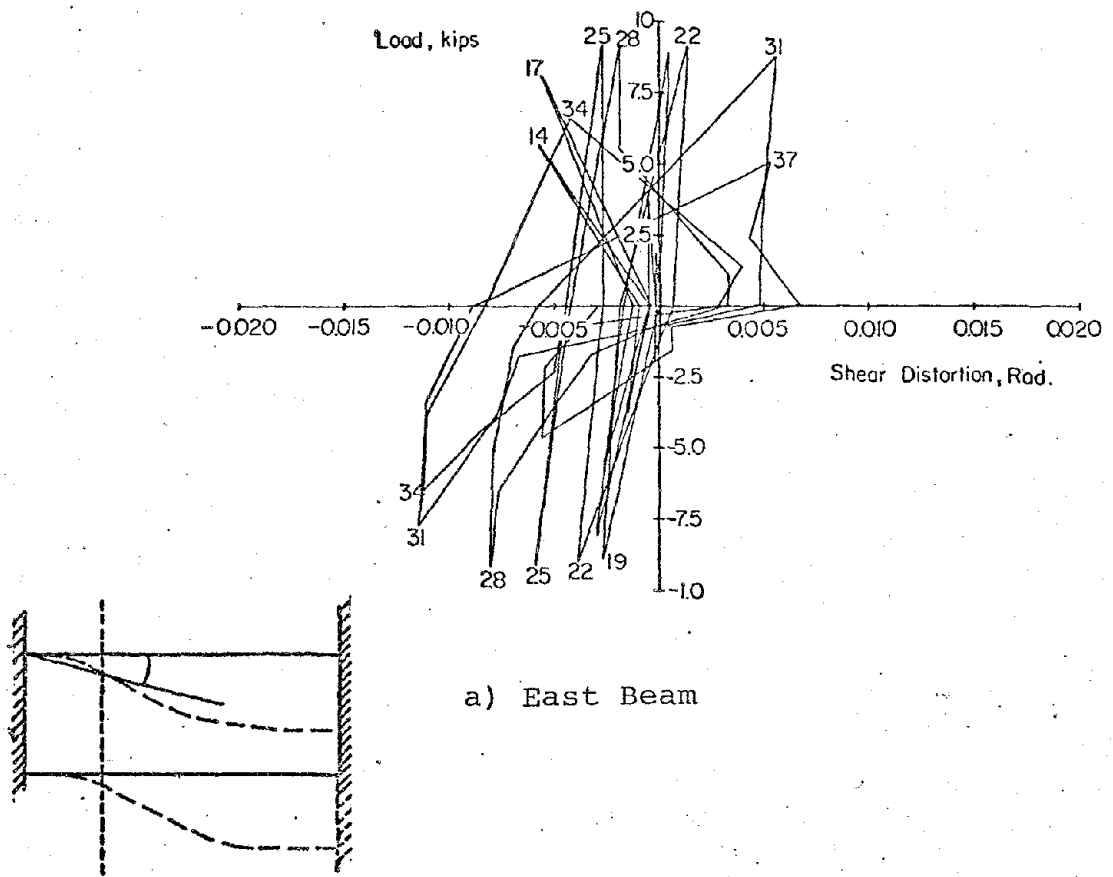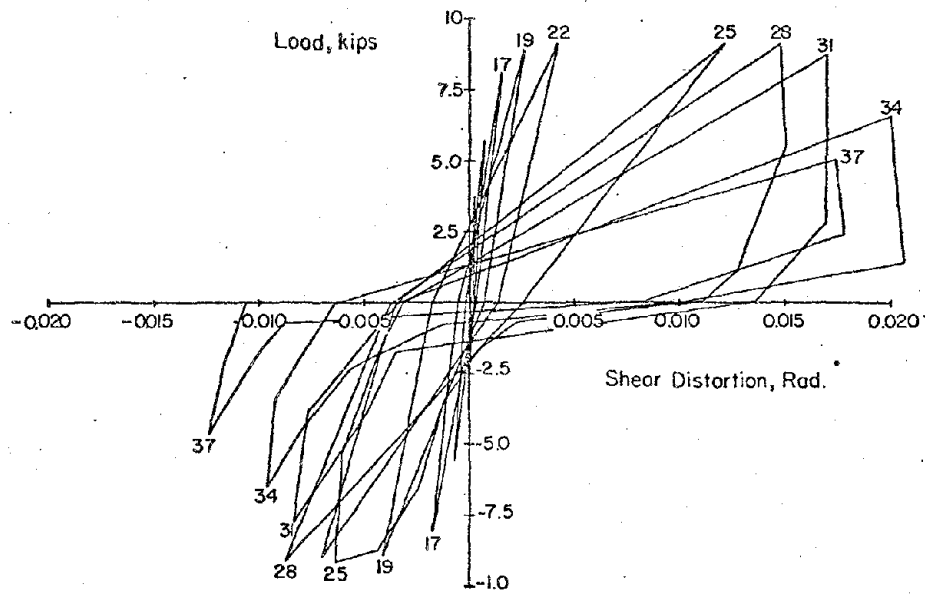
a) East Beam

b) West Beam

Fig A-6   Load versus Shear Distortion for Specimen Cl

A-8

Load, kips

Gage 33

Strain Millionths

Load, kips

Gage 31

Strain Millionths
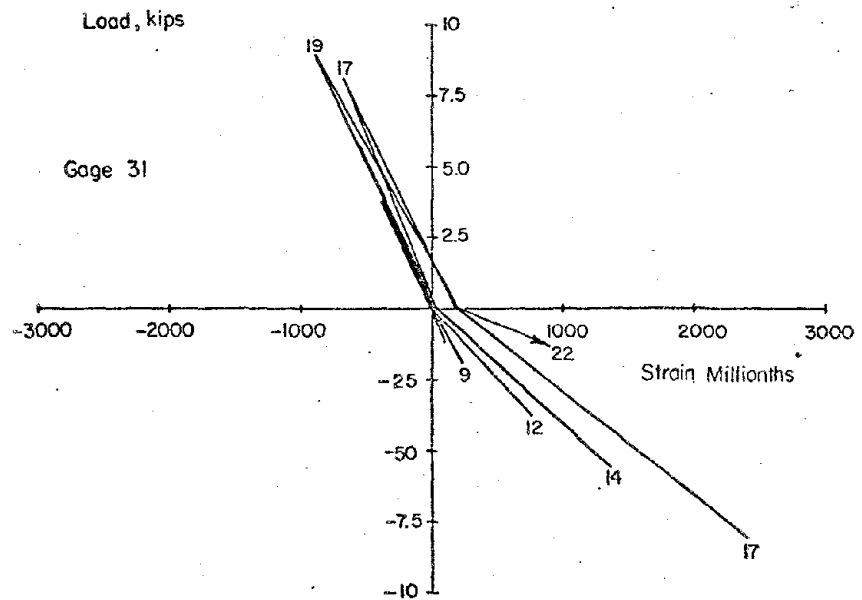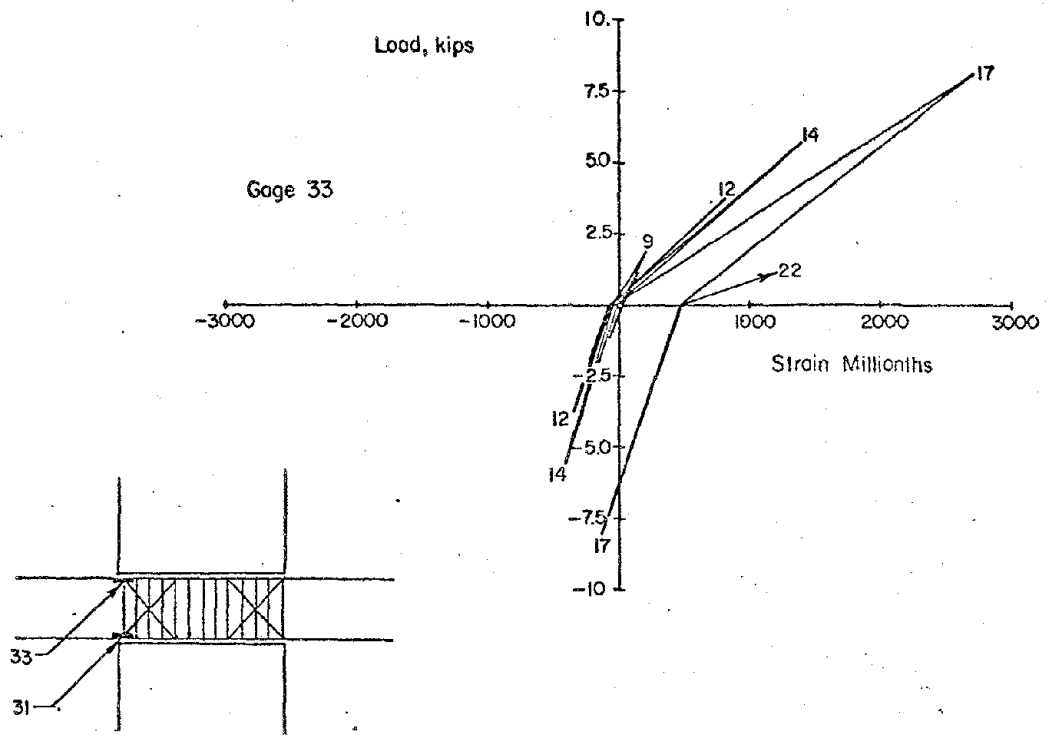
Fig. A-7   Load versus Flexural Steel Strains
for Specimen C1 (East Beam)
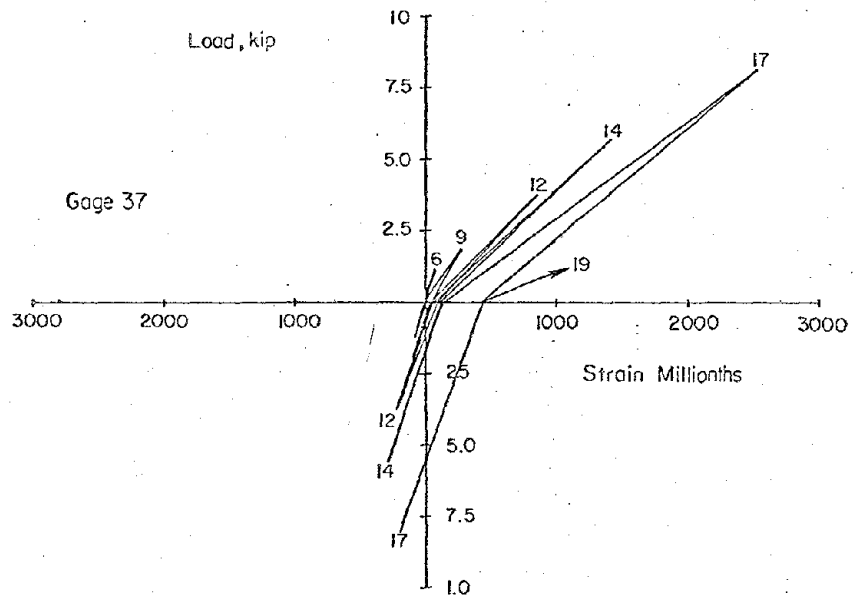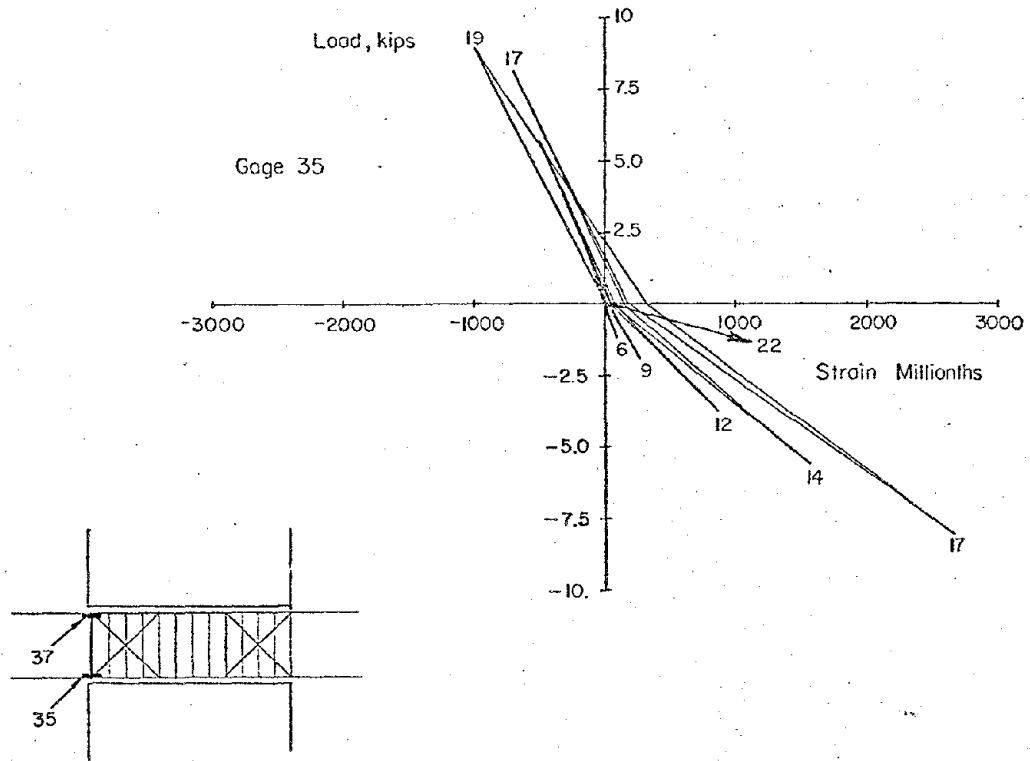
Fig. A-8   Load versus Flexural Steel Strains
for Specimen C1 (West Beam)

A-10

Fig. A-9 Load versus Diagonal Steel Strains
for Specimen C1 (East Beam)

Load, kips

Gage 41

10

7.5

5.0

2.5

-2.5

-5.0

-7.5

-10

-3000   -2000   -1000   1000   2000   3000

Strain Millionths

22

12

14

17

19

41 42

Load, kips

Gage 42

10

7.5

5.0

2.5

-2.5

-5.0

-7.5

-10

-3000   -2000   -1000   1000   2000   3000

Strain Millionths

17   19   22

14

12

25

22   19
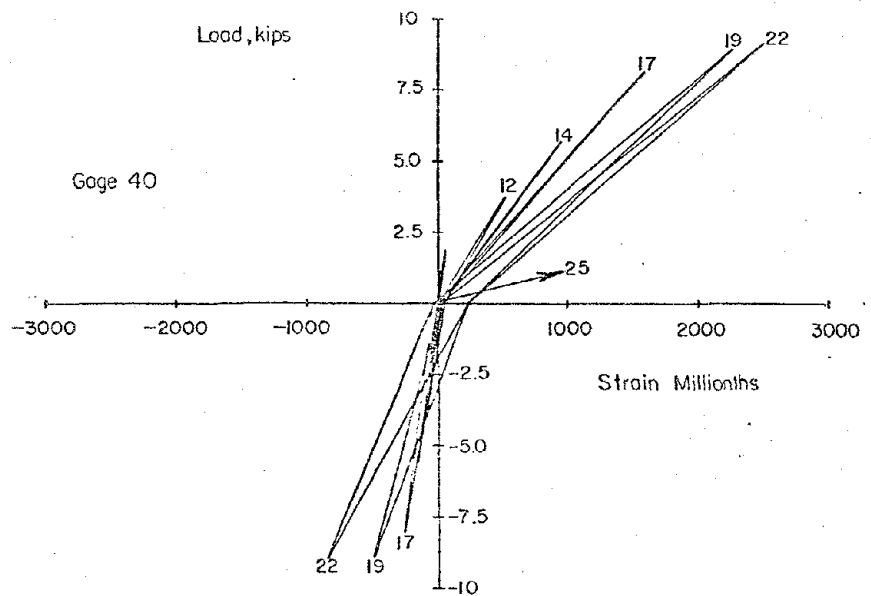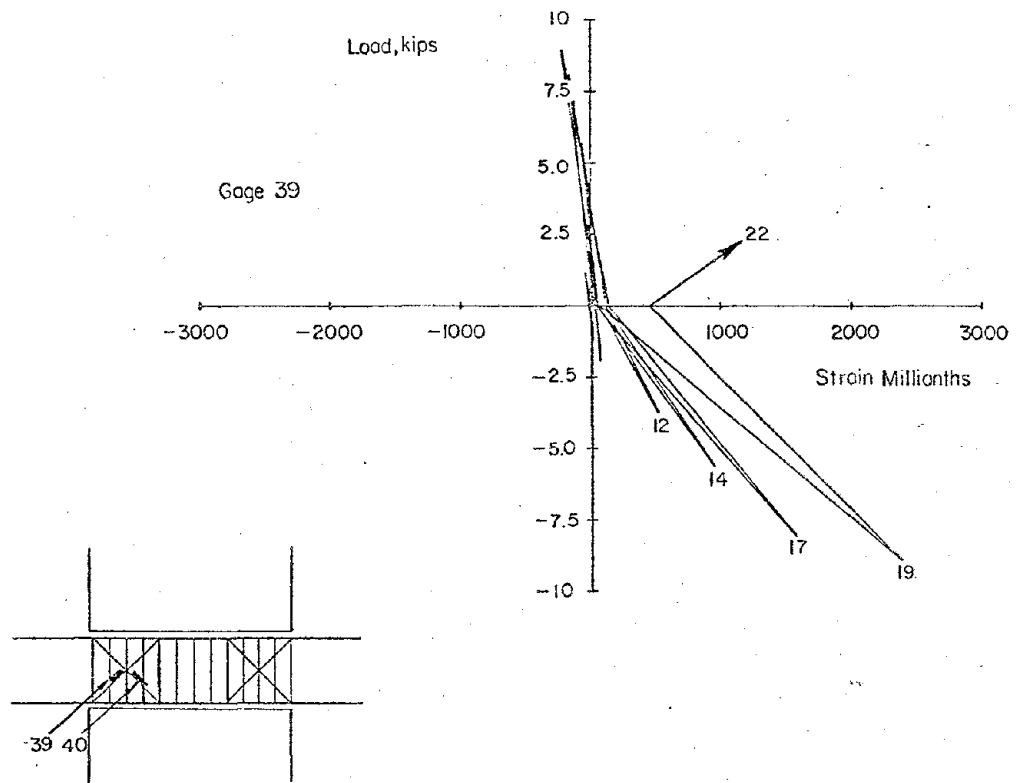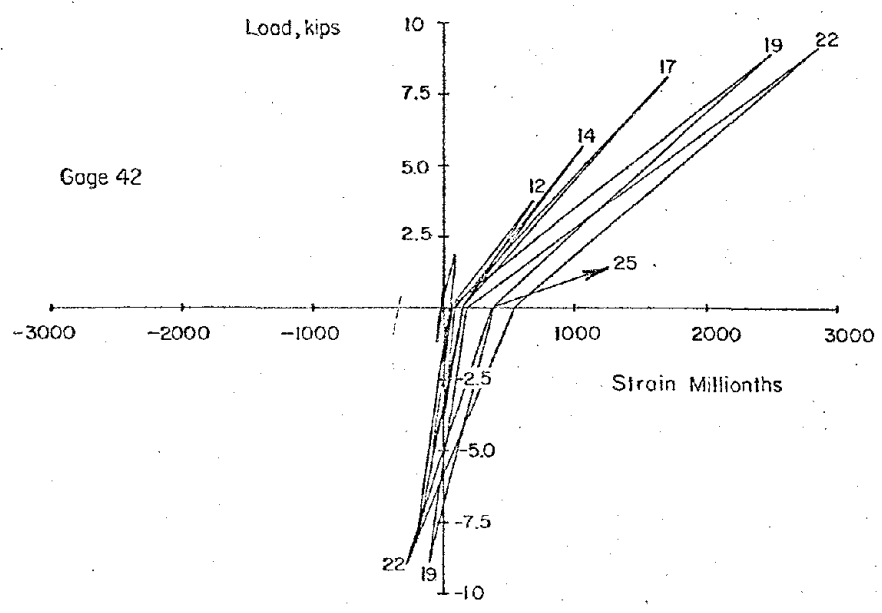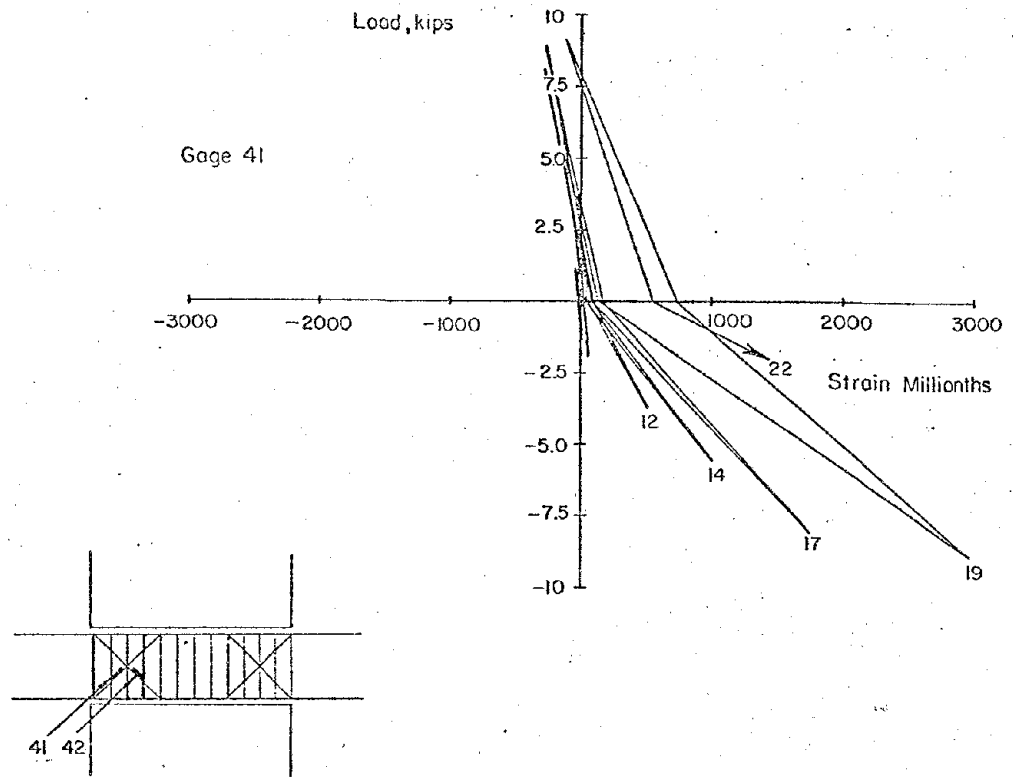
Fig. A-10   Load versus Diagonal Steel Strains
for Specimen C1 (West Beams)

A-12
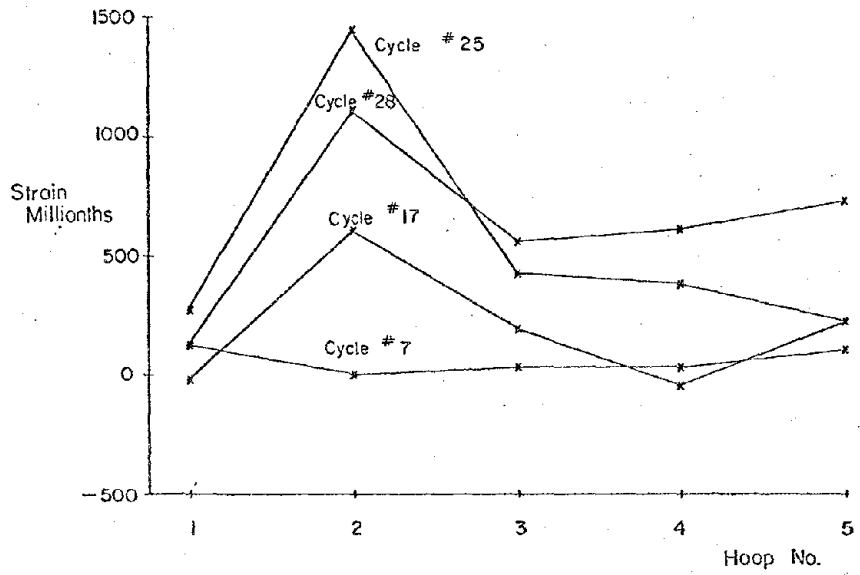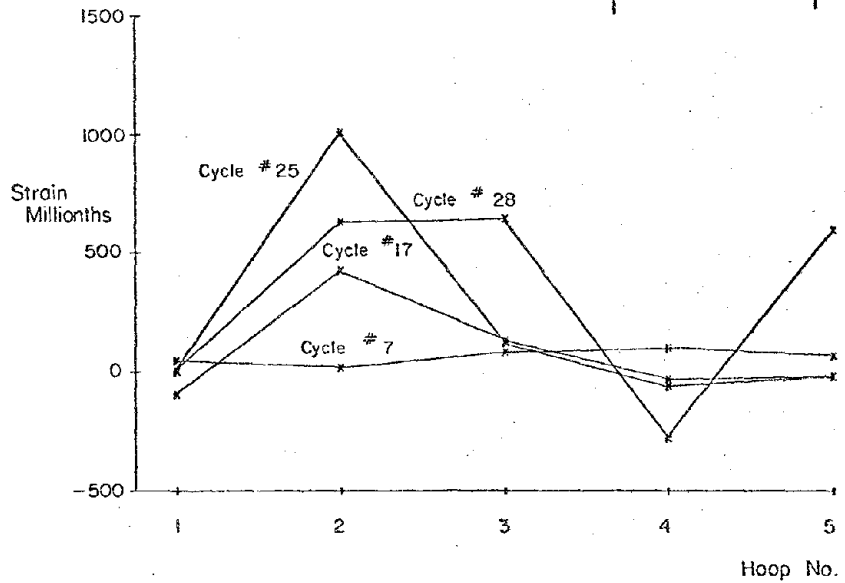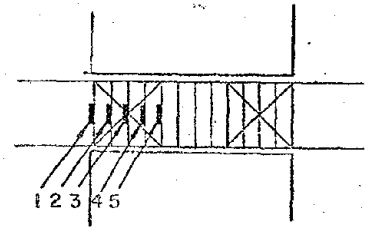
a) East Beam

b) West Beam

Fig. A-11 Stirrup-tie Steel Strains for Specimen Cl

A-13
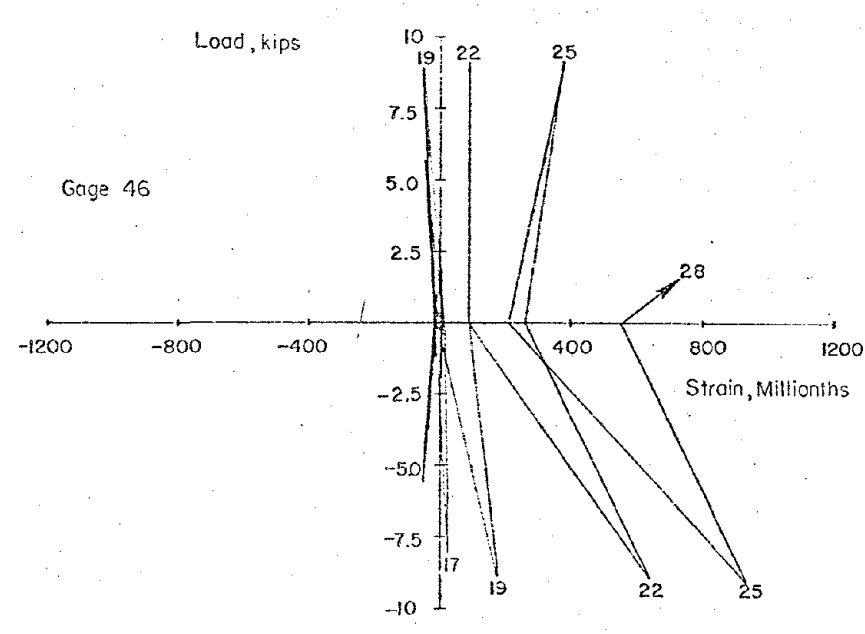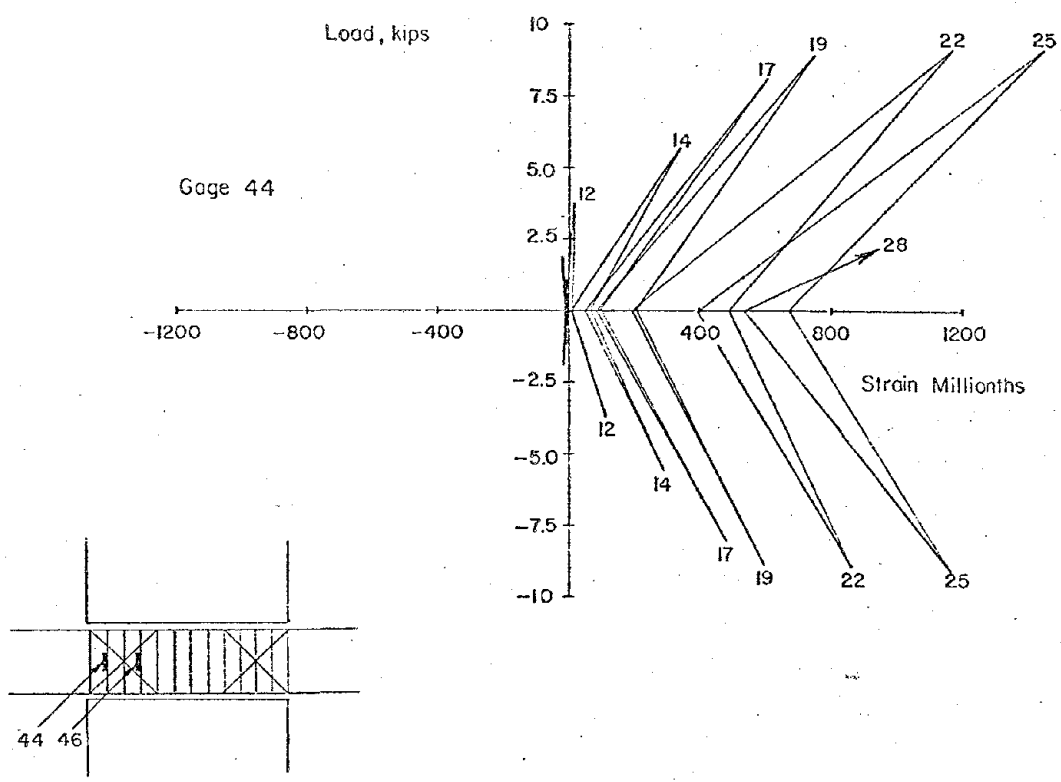
Fig. A-12   Load versus Stirrup-tie Steel Strains
for Specimen Cl (East Beam)

A-14
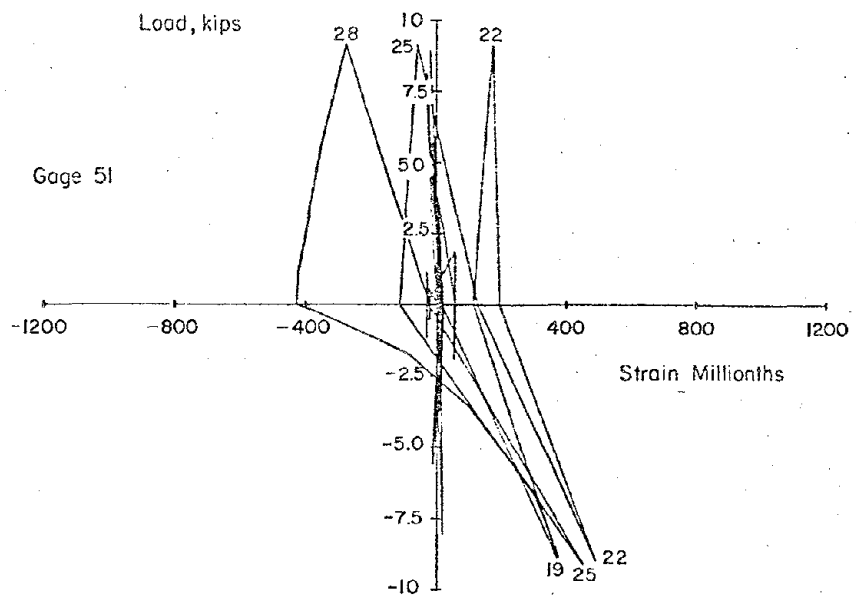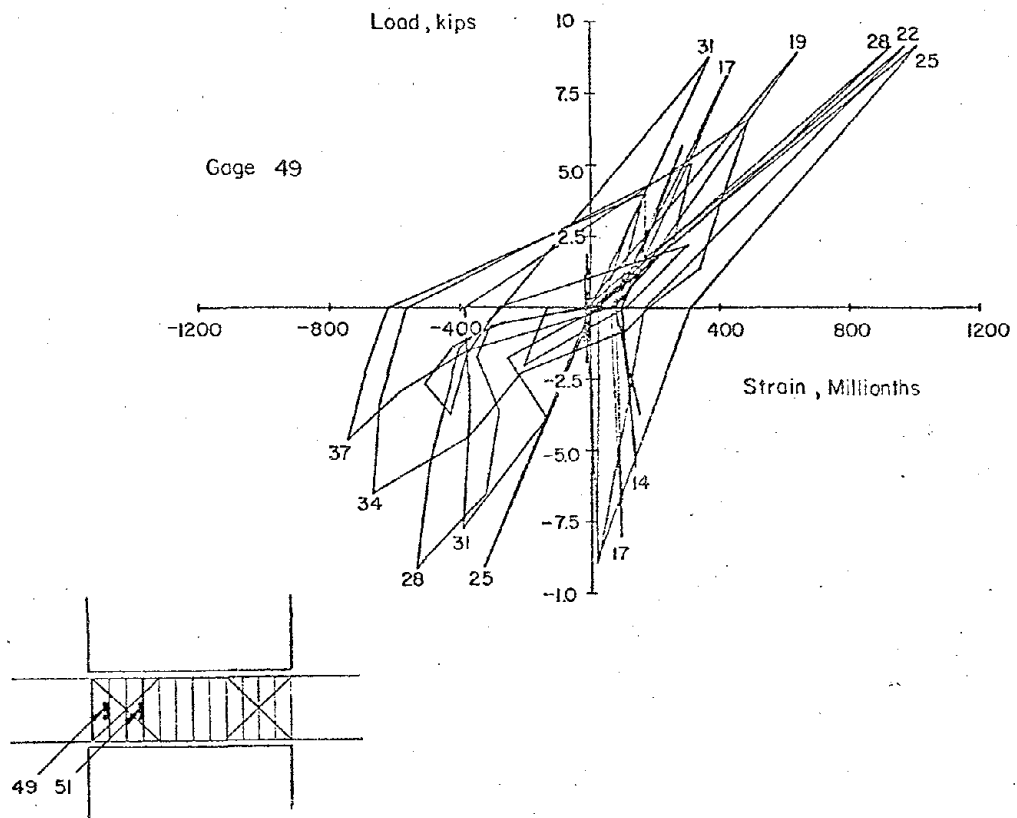
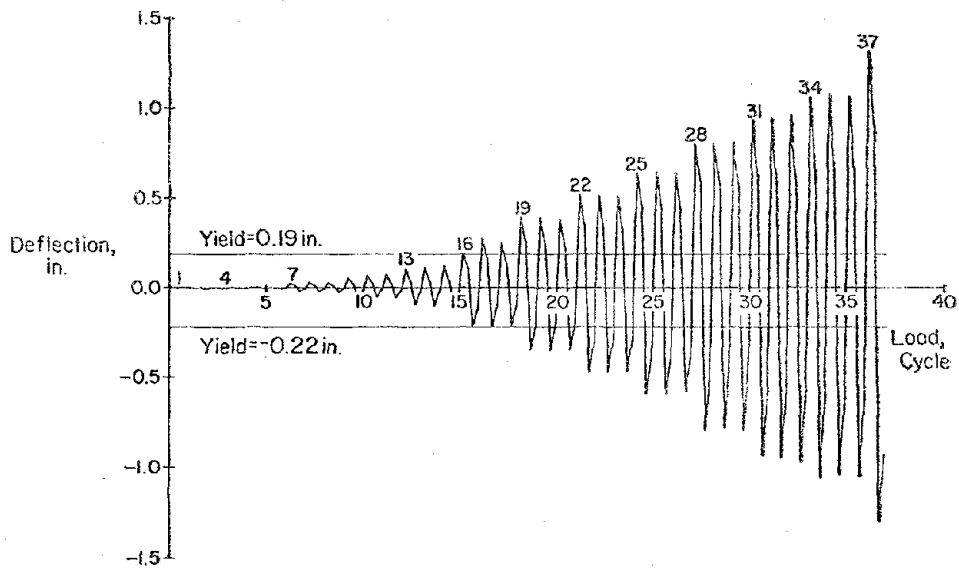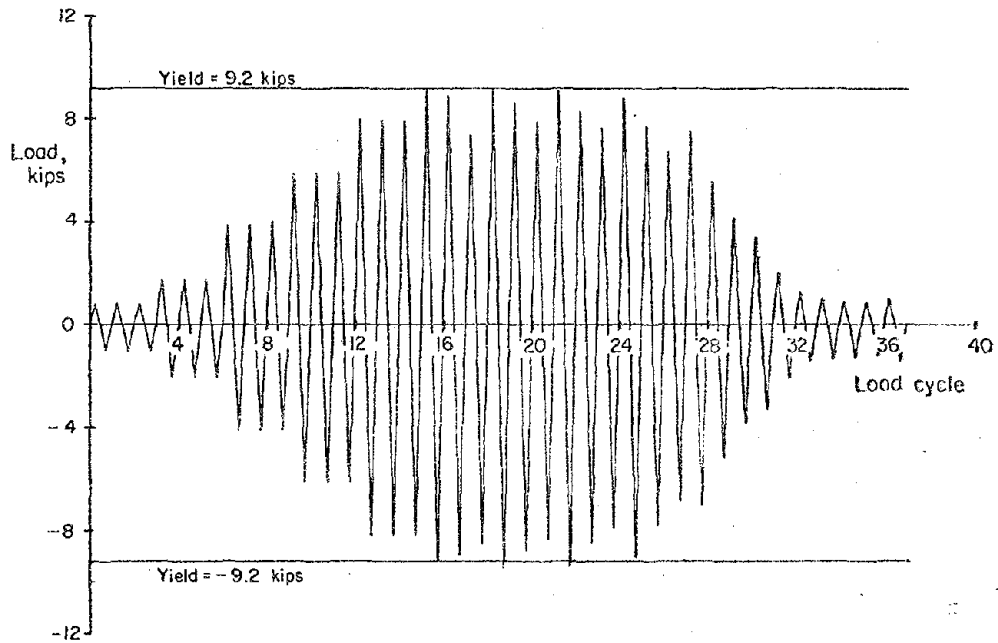Fig. A-13 Load versus Stirrup-tie Steel Strains
for Specimen Cl (West Beam)
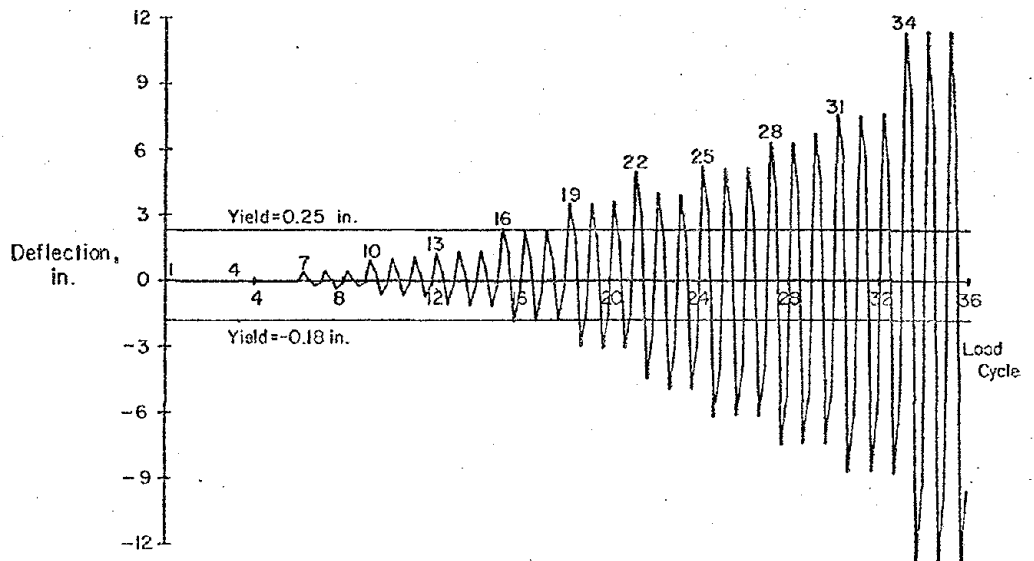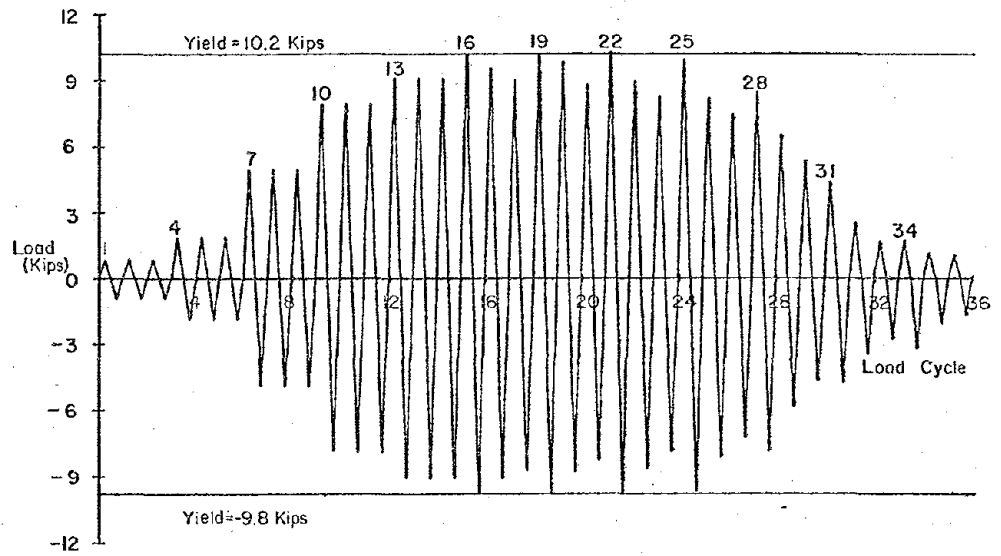
Fig. A-14   Load and Deflection Histories for Specimen C2
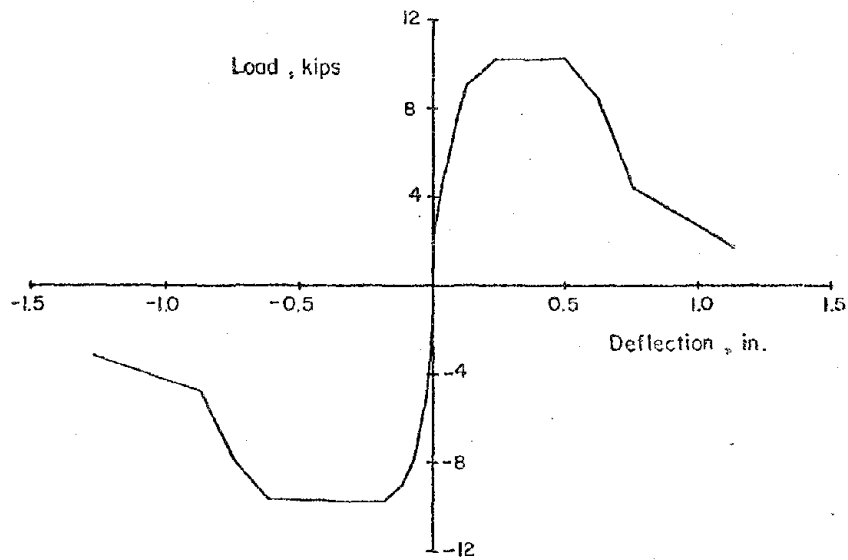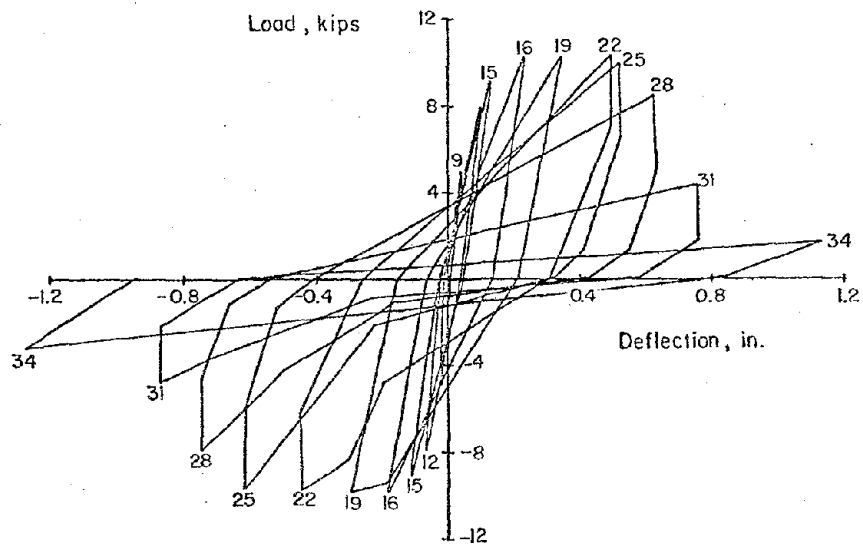
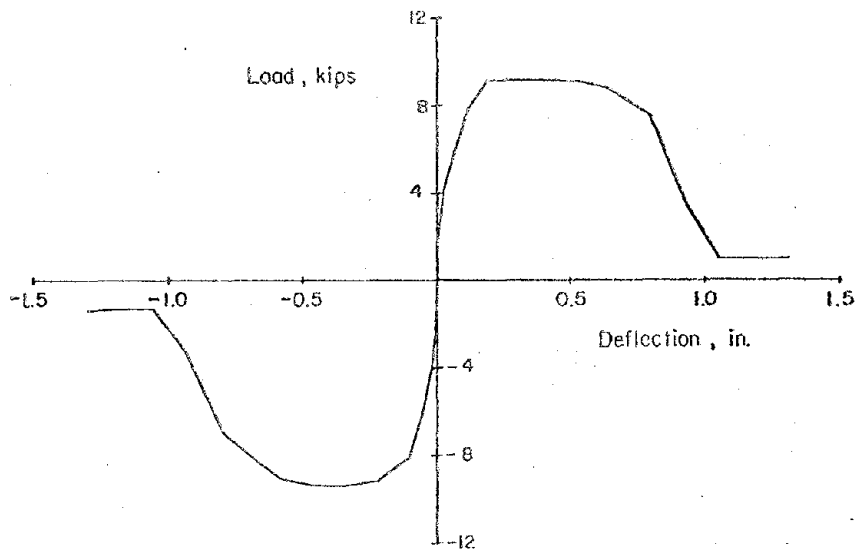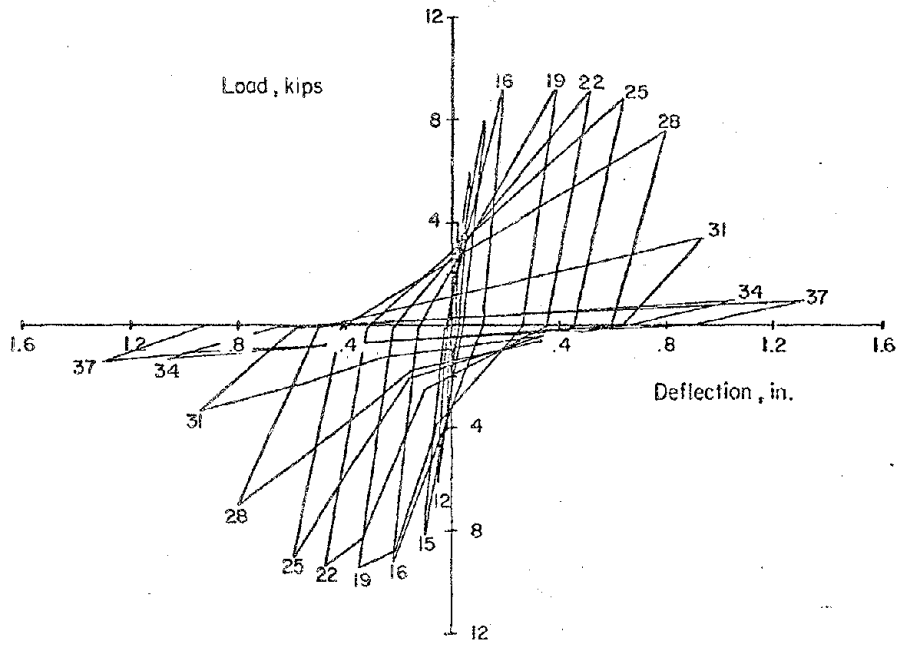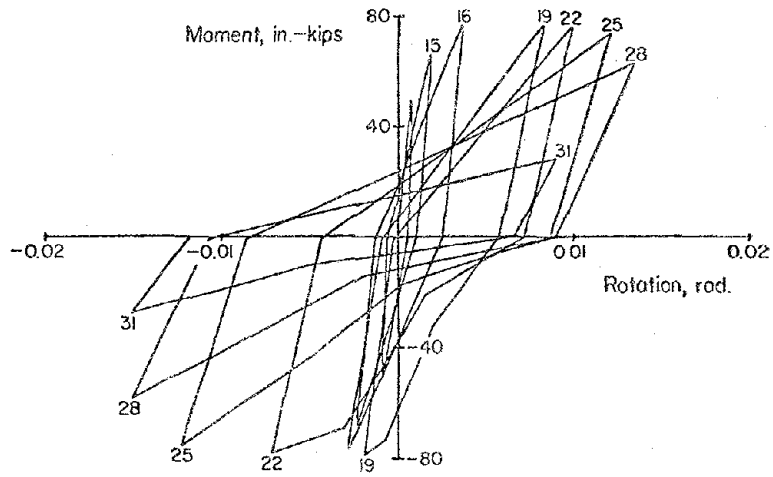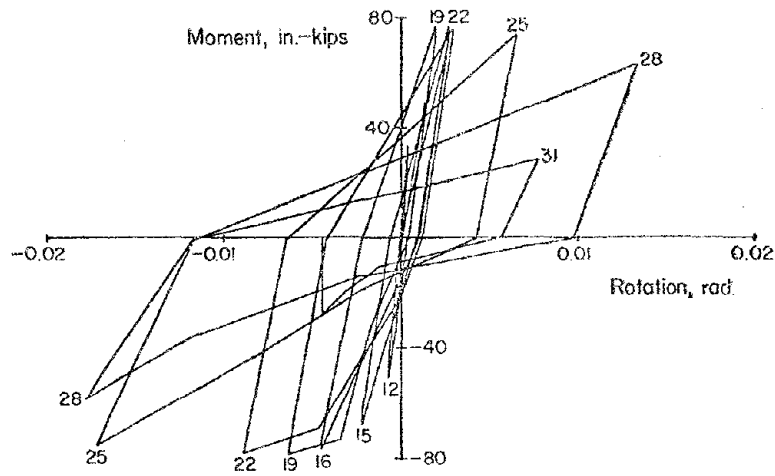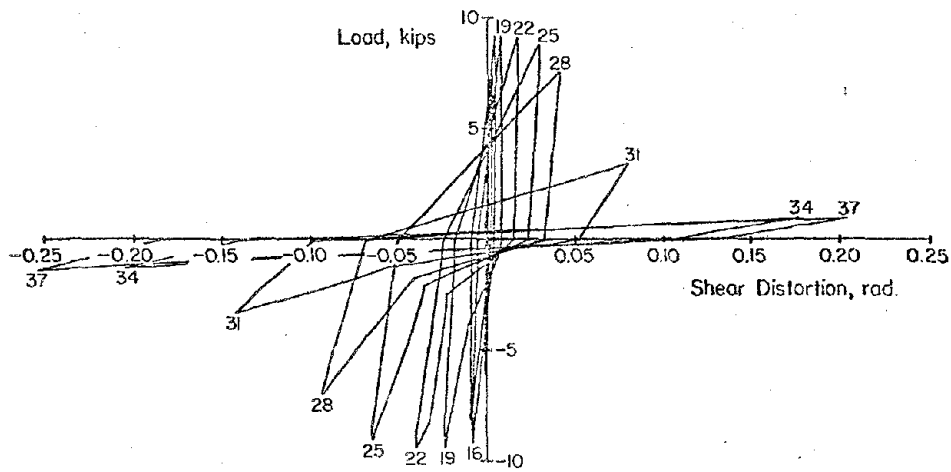Fig. A-15 Load versus Deflection for Specimen C2

A-17
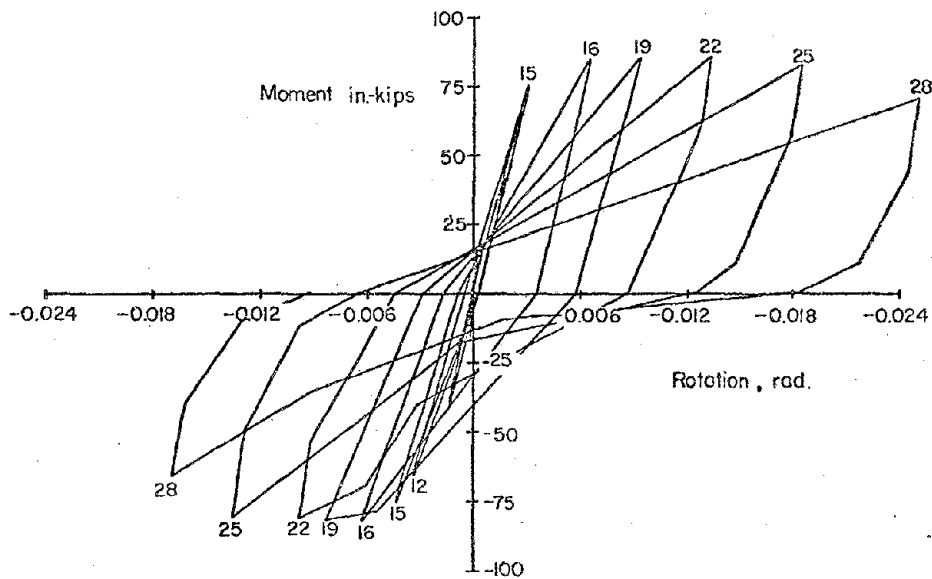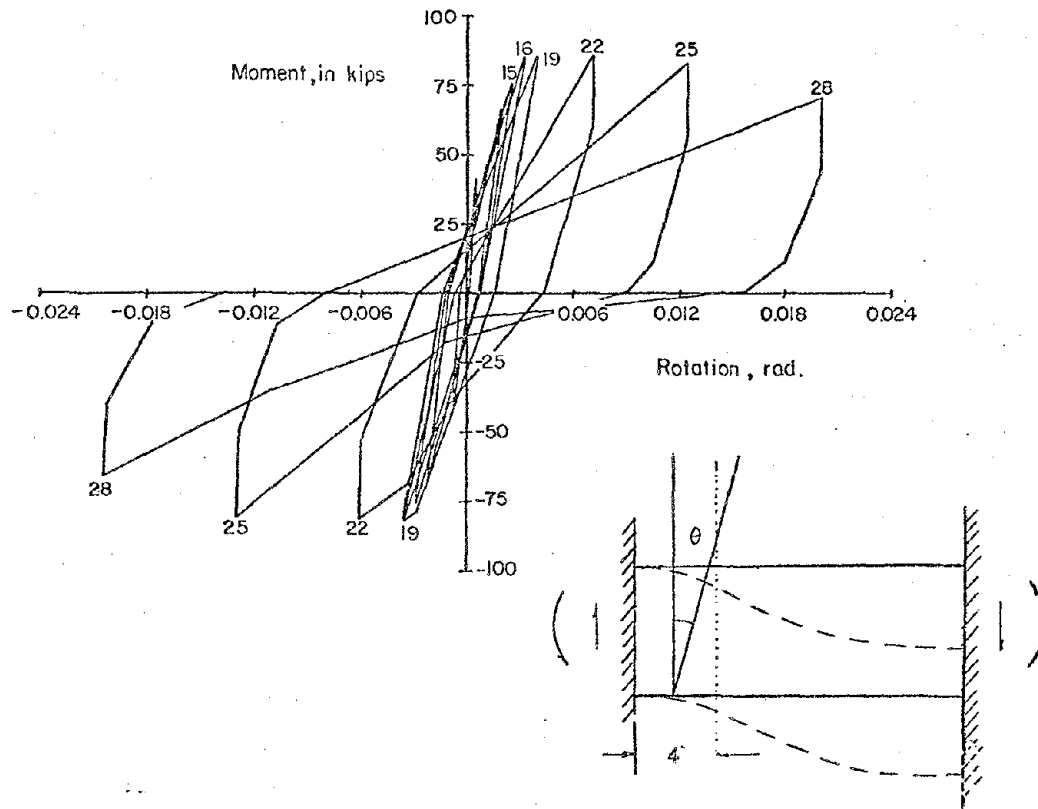
Fig. A-16   Moment versus Rotation for Specimen C2

A-18

Fig. A-17   Load versus Shear Distortion for Specimen C2

A-19

Load , kips

15
12
Gage 31
9
12
8
4
6
9
12
15

-2500 -2000 -1500 -1000 -500 500 1000 1500 2000 2500

Strain , millionths

-4

-8

-12

Load , kips

15
12
Gage 33
9
6
3
16
6
8
4

-2500 -2000 -1500 -1000 -500 500 1000 1500 2000 2500
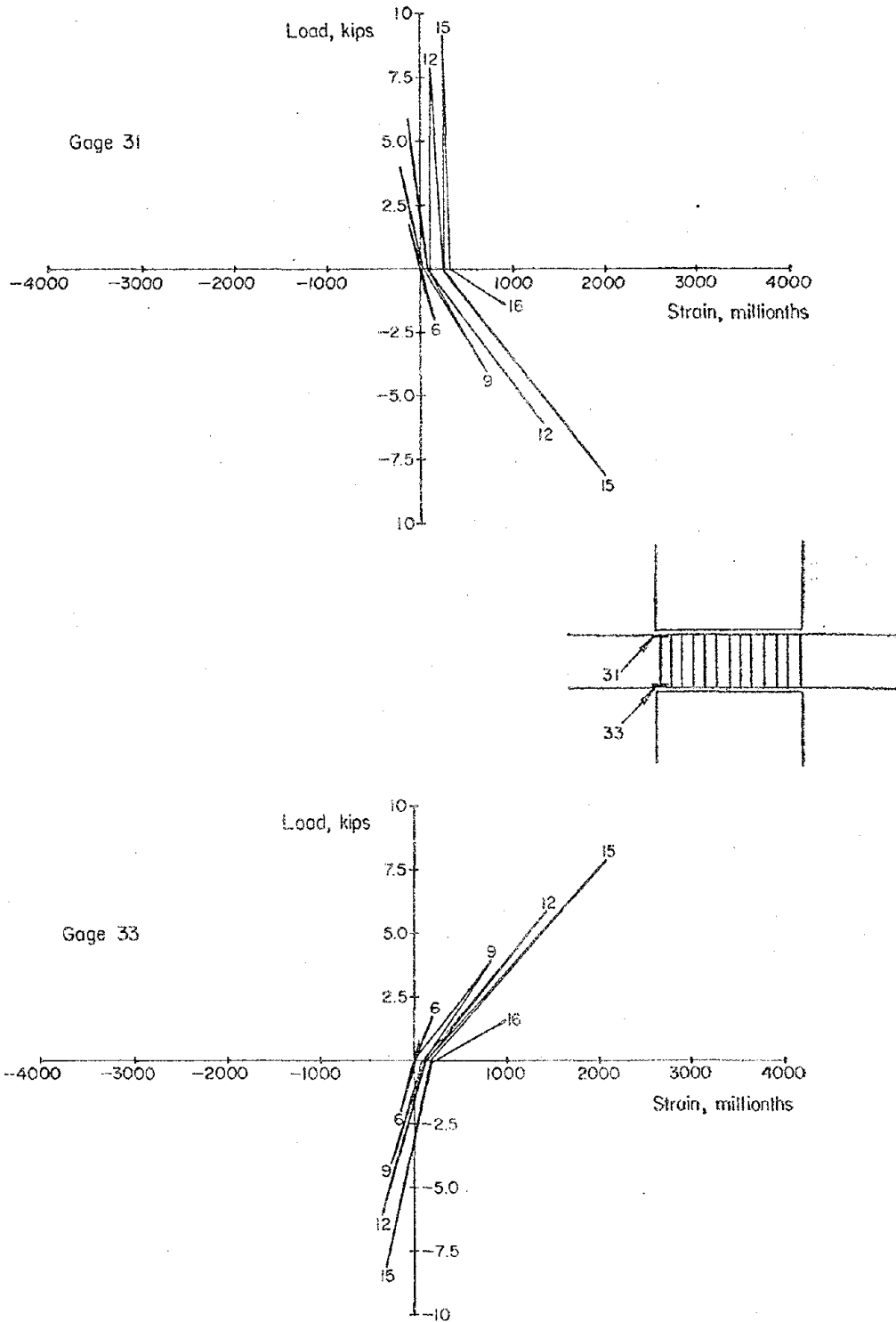
Strain , millionths
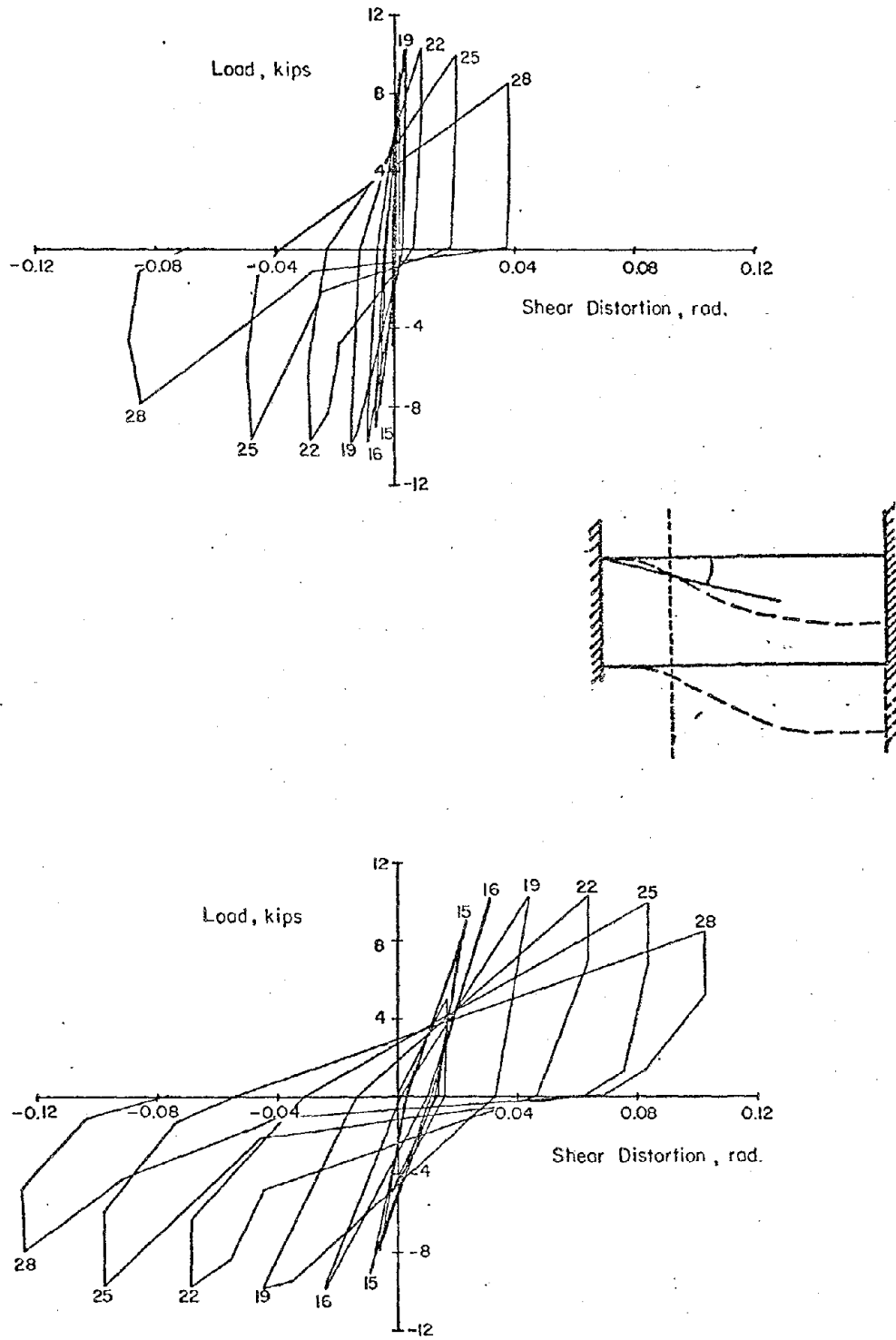
9
-4
12
15
-8
-12
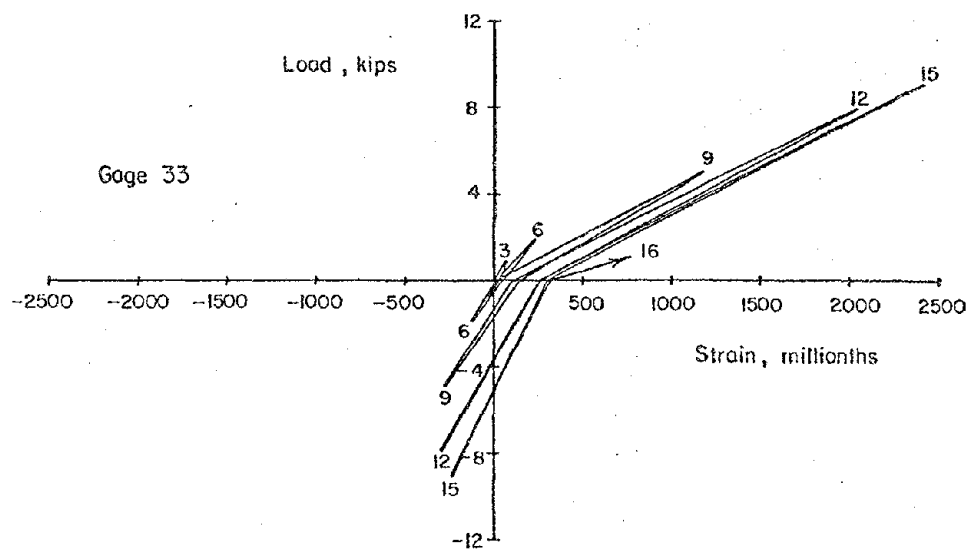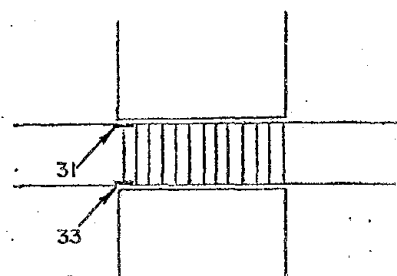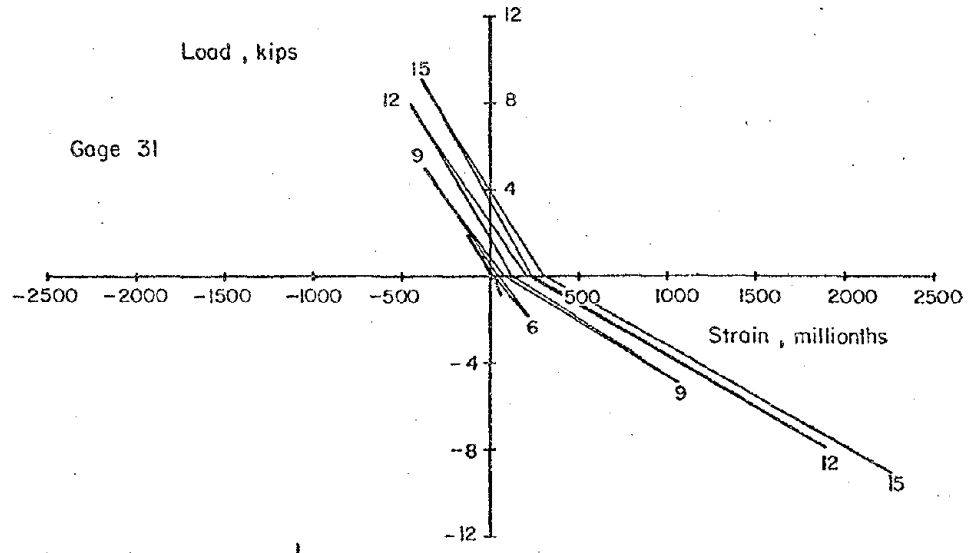
Fig. A-18   Load versus Flexural Steel Strains
for Specimen C2 (East Beam)
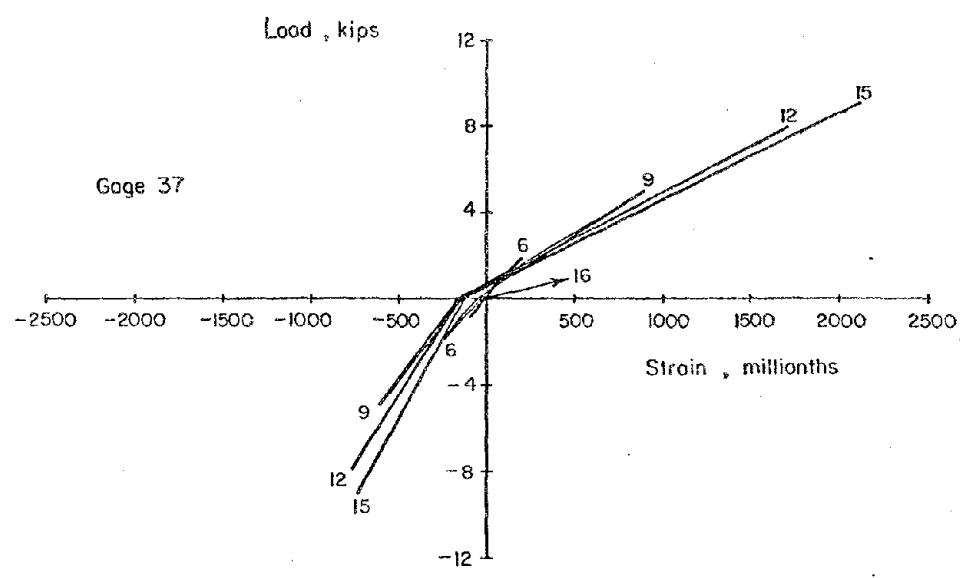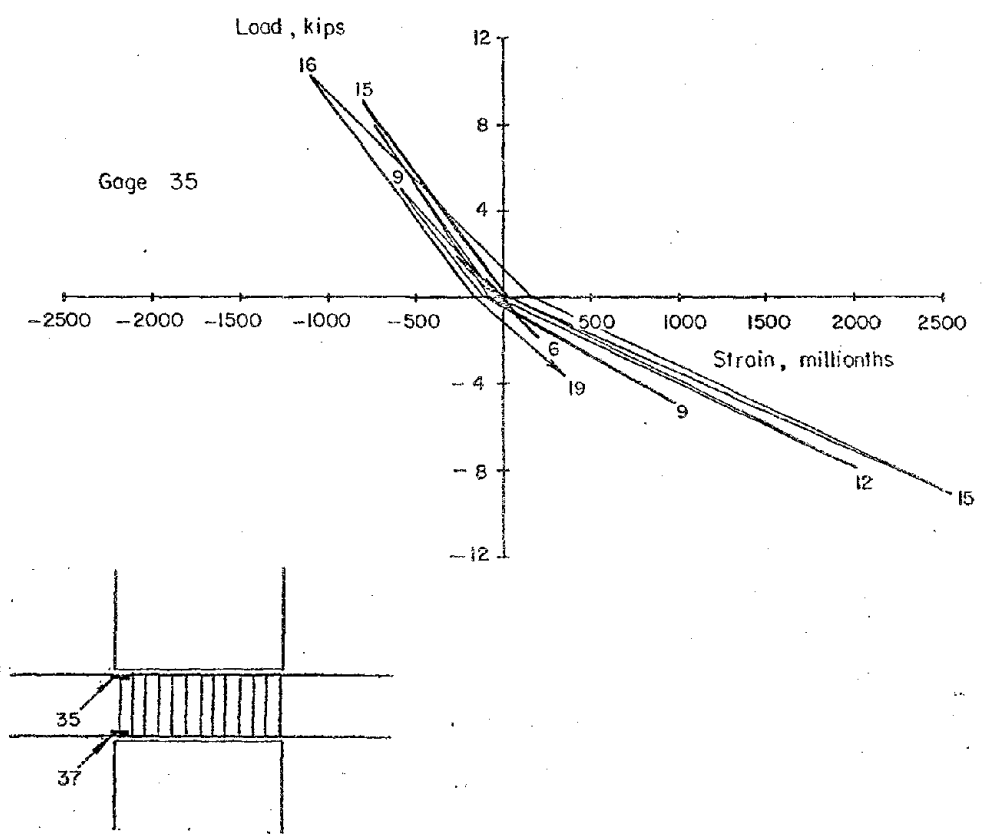
Fig. A-19 Load versus Flexural Steel Strains
for Specimen C2 (West Beam)

Fig. A-20   Stirrup-tie Steel Strains for Specimen C2

Load kips

Gage 40

12
16 19 22 25
15
12
8
9
4

-2000   -1500   -1000   -500   500   1000   1500   2000
                                                    Strain , millionths

-4
9
-8
12
15
16   19   22

-12

40 42

Load , kips

Gage 42

12
19 22
12   28
8

4

31

-2000   -1500   -1000   -500   500   1000   1500   2000
                                                    Strain , millionths

-4

-8
12
15   28
16 19 22
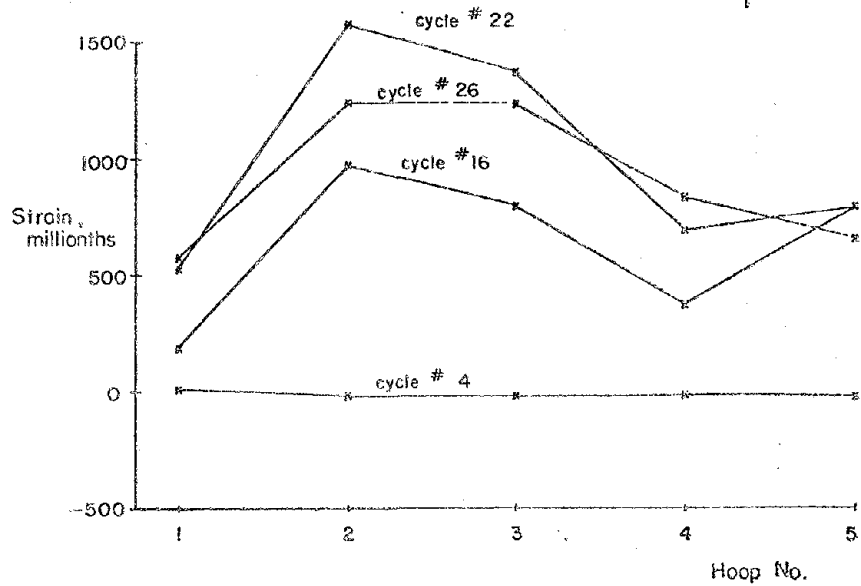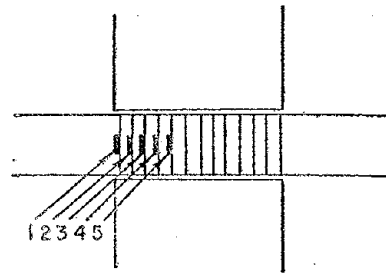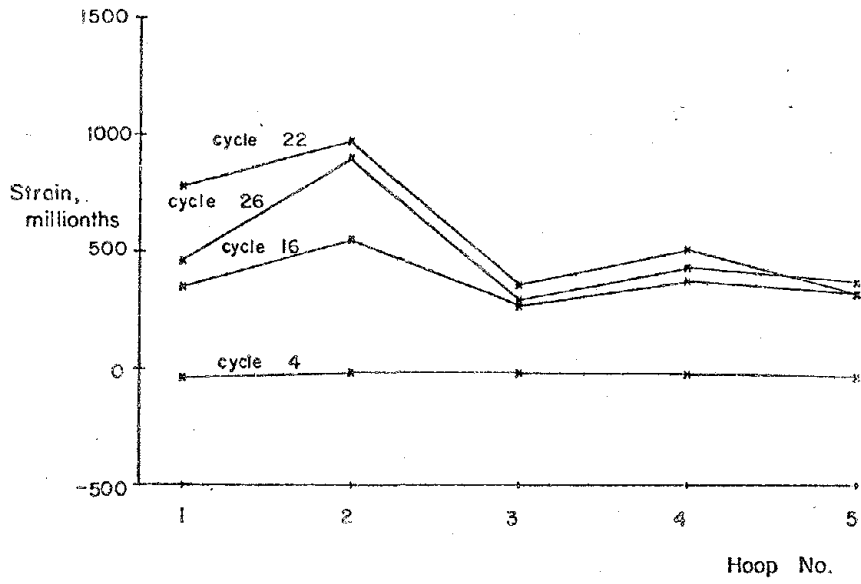
-12
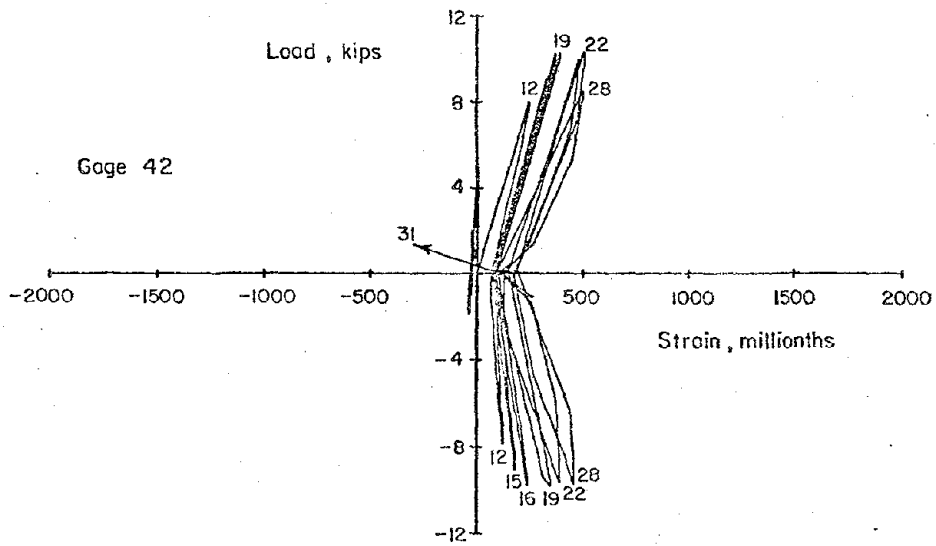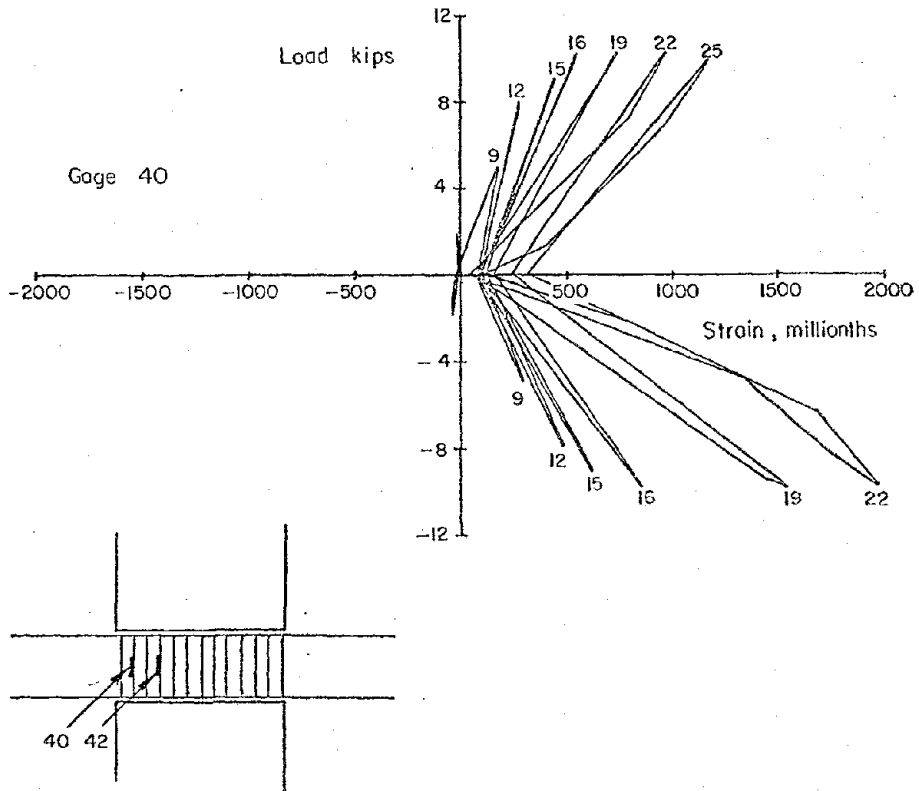
Fig. A-21   Load versus Stirrup-tie Steel Strains
            for Specimen C2 (East Beam)

A-23
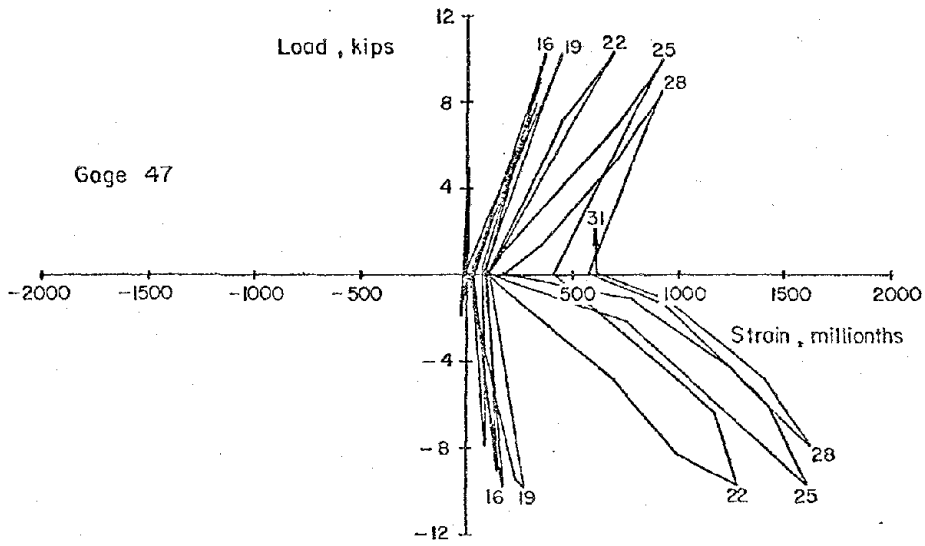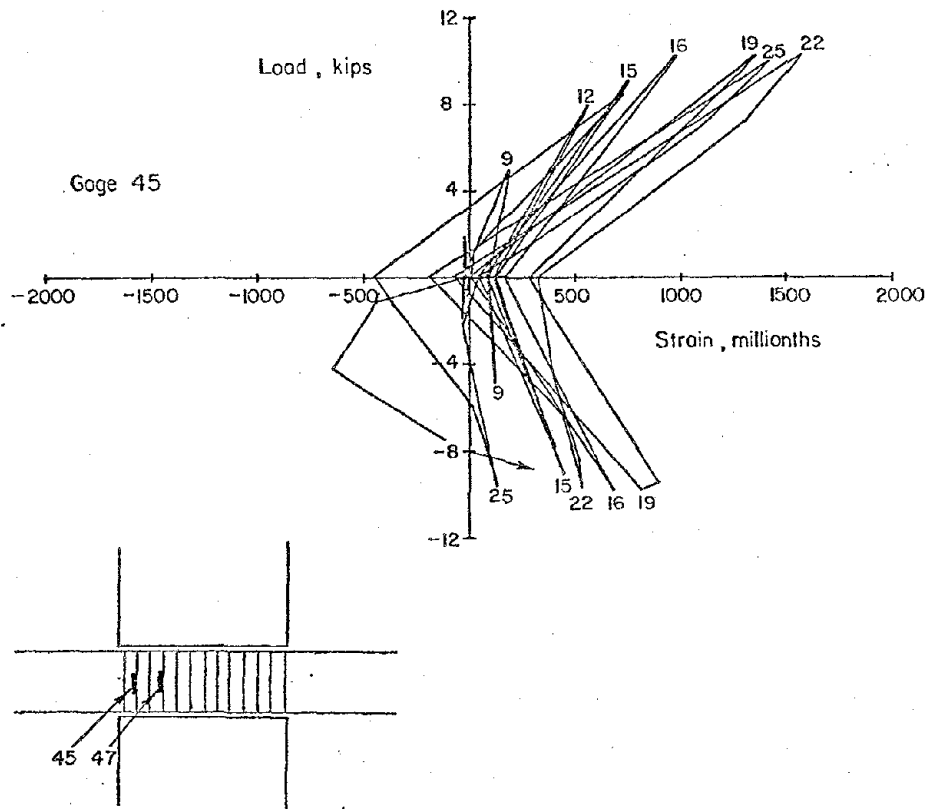
Fig. A-22   Load versus Stirrup-tie Steel Strains
            for Specimen C2 (West Beam)
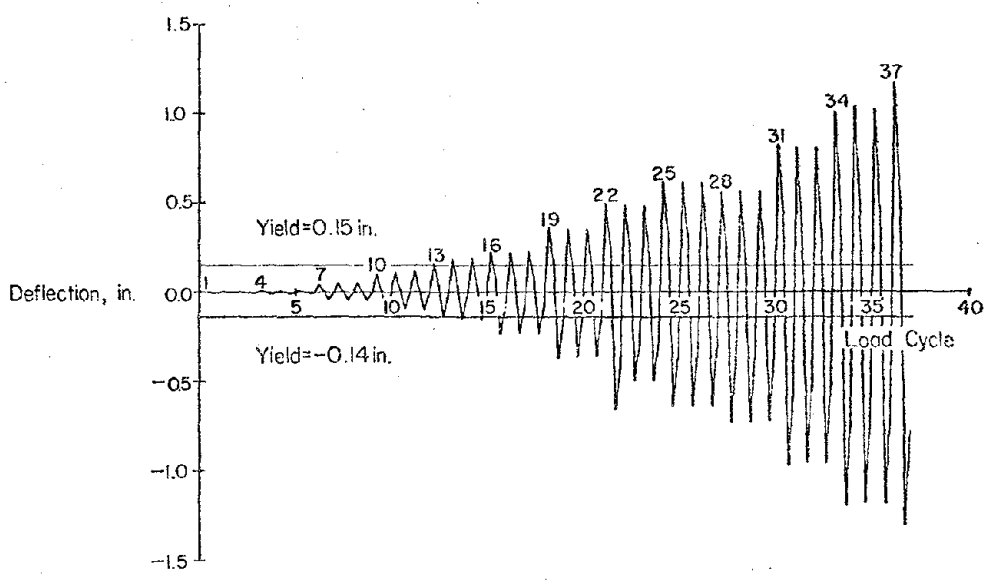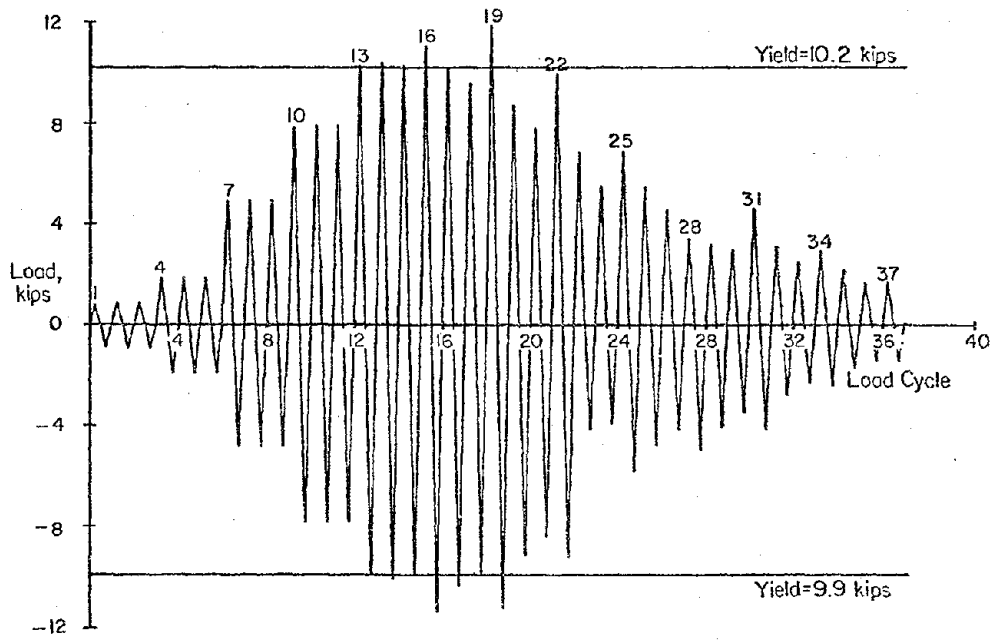
Fig. A-23 Load and Deflection Histories for Specimen C3
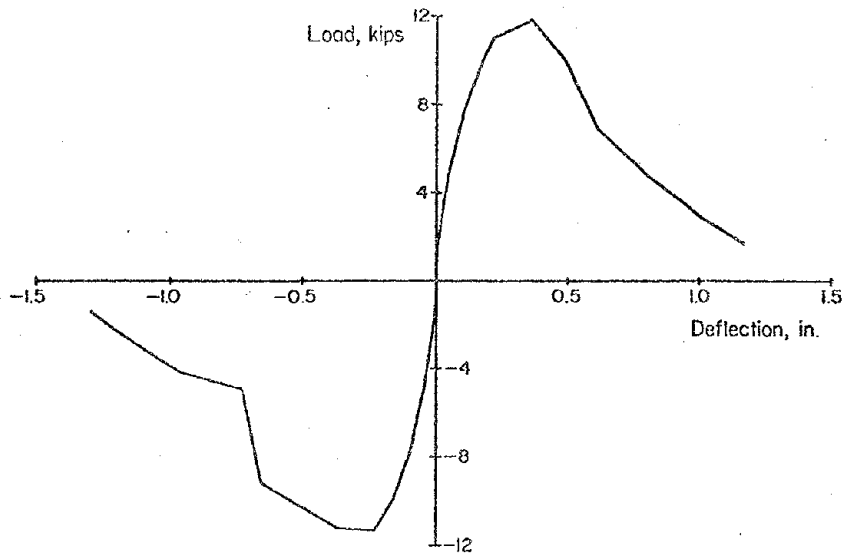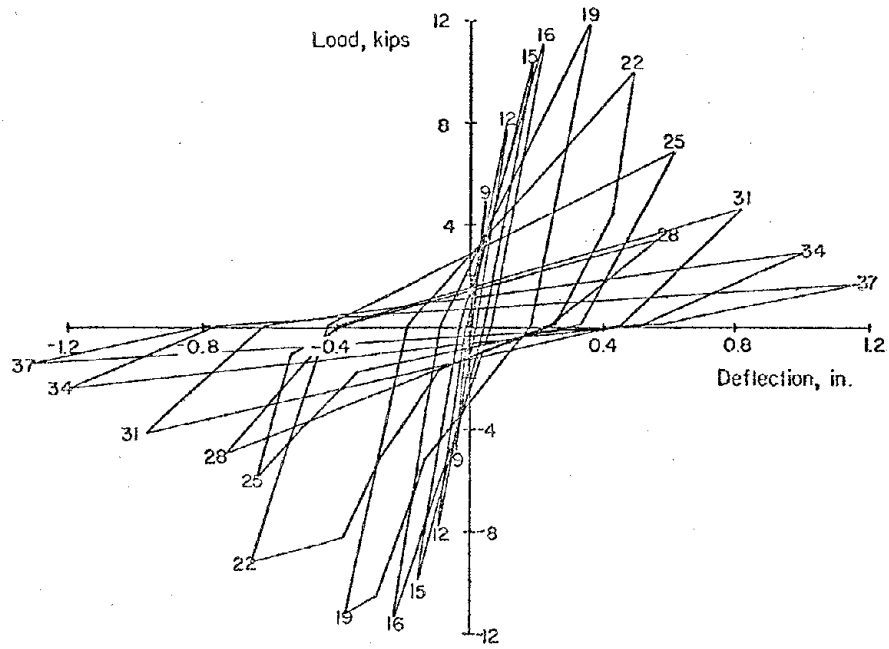
Fig. A-24   Load versus Deflection for Specimen C3
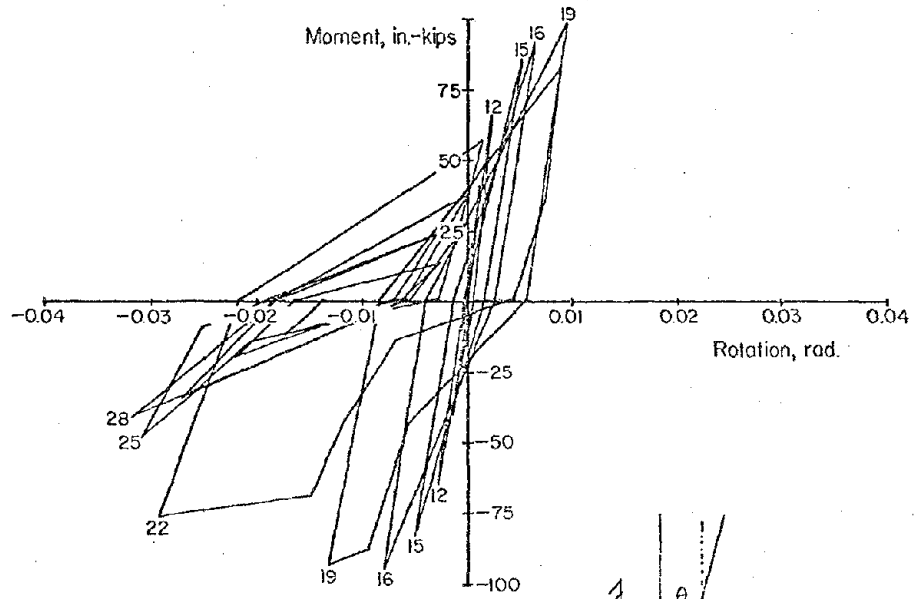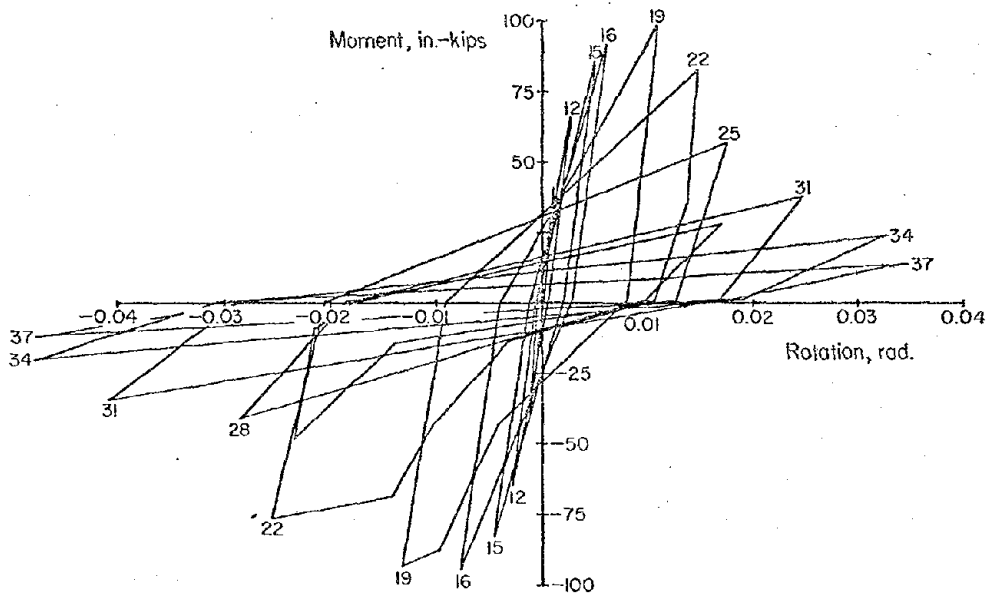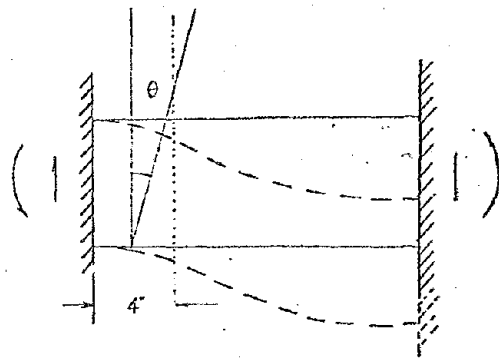
a) East Beam

b) West Beam

Fig. A-25   Moment versus Rotation for Specimen C3
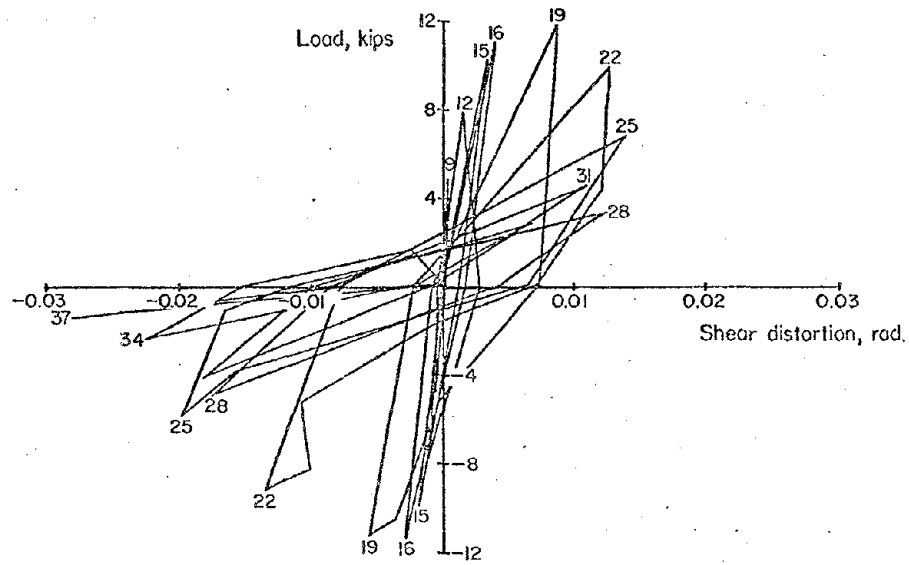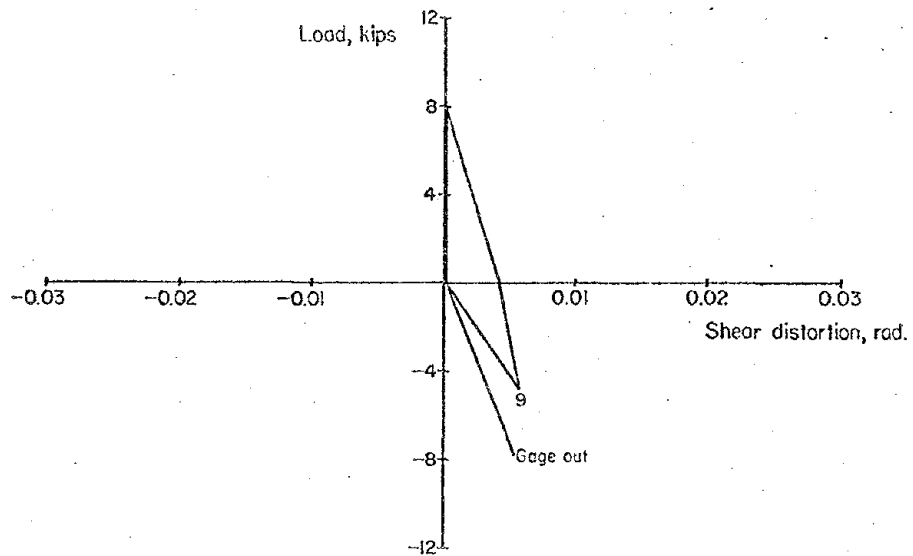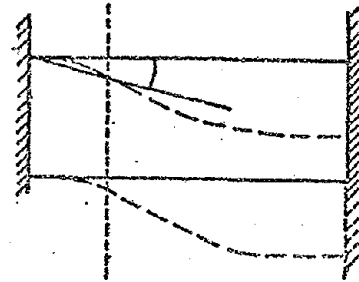
a) East Beam

b) West Beam

Fig. A-26 Load versus Shear Distortion for Specimen C3
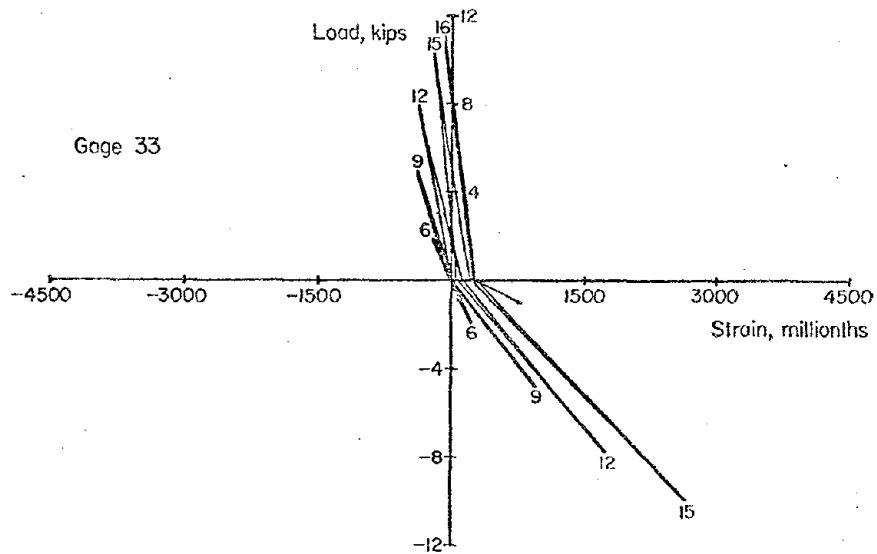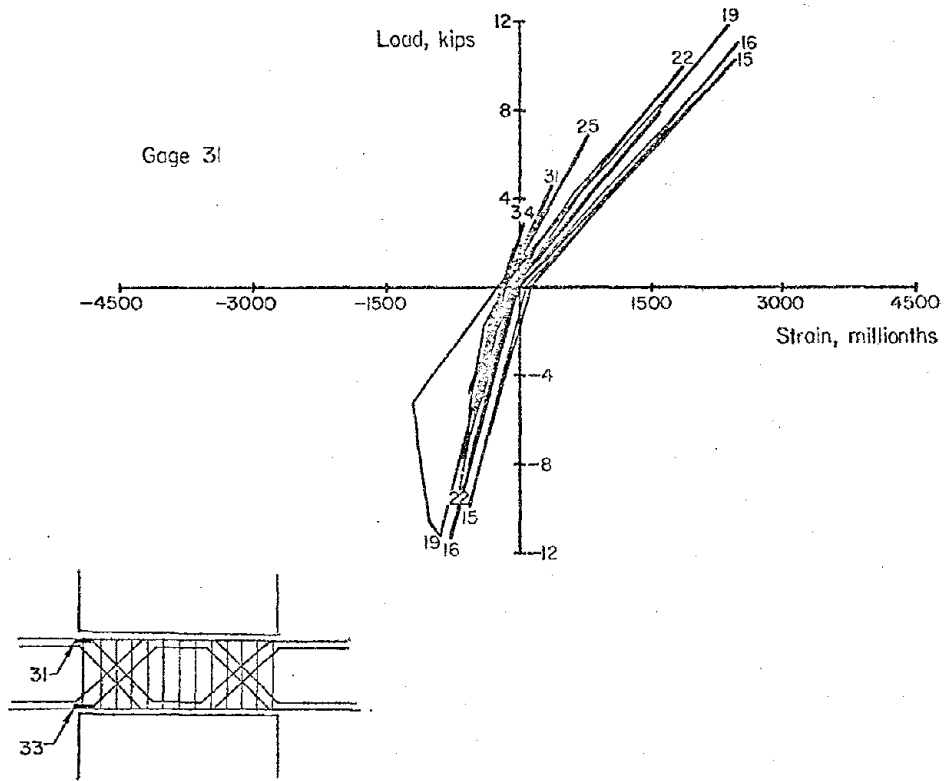
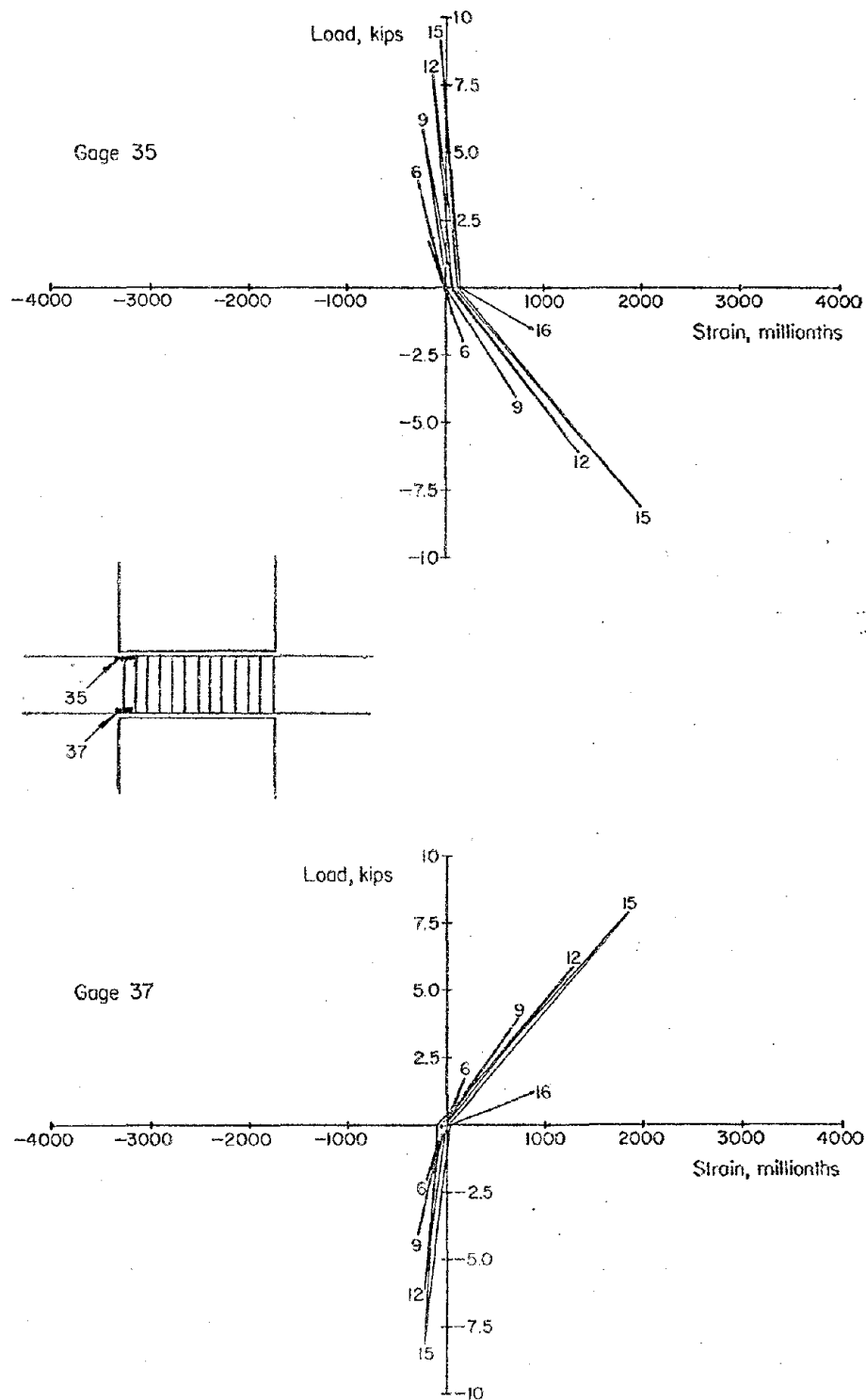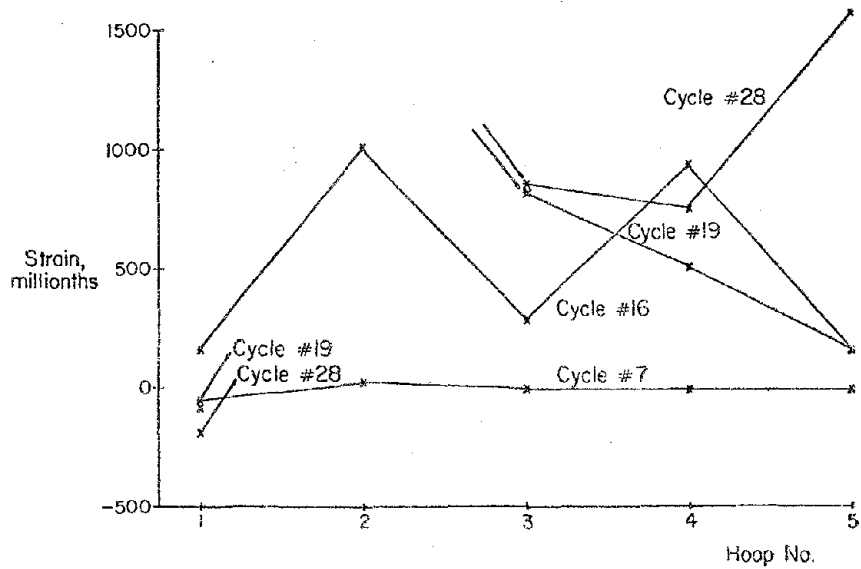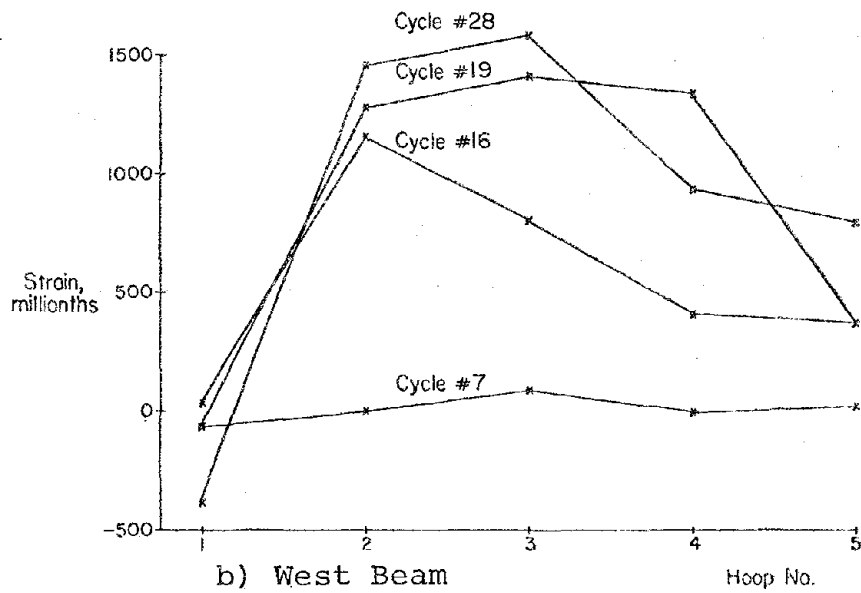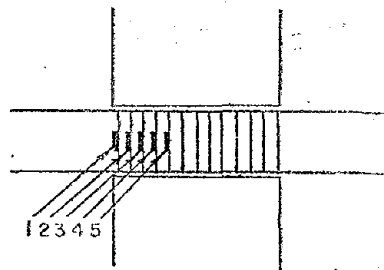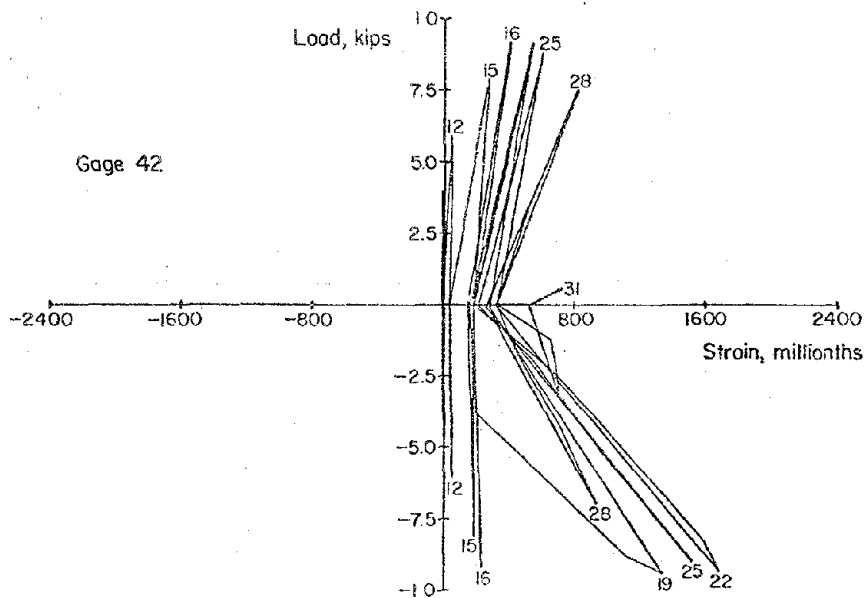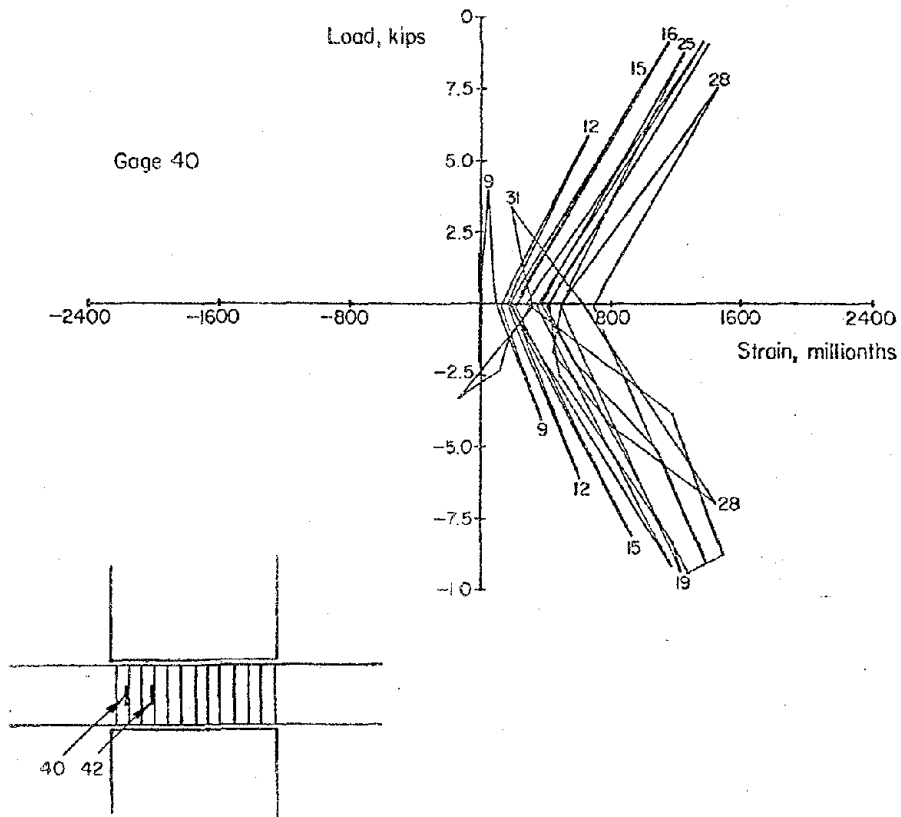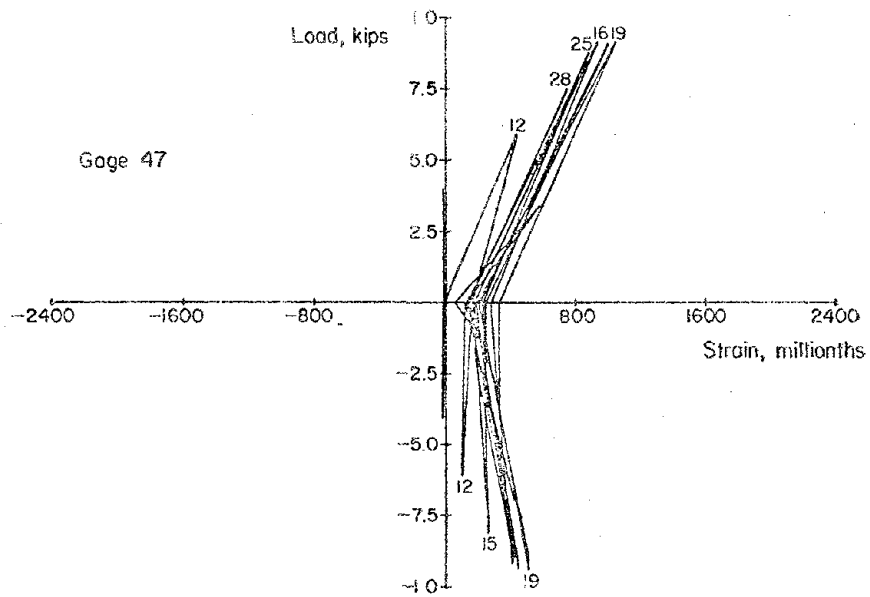Fig. A-27   Load versus Flexural Steel Strains
for Specimen C3 (East Beam)
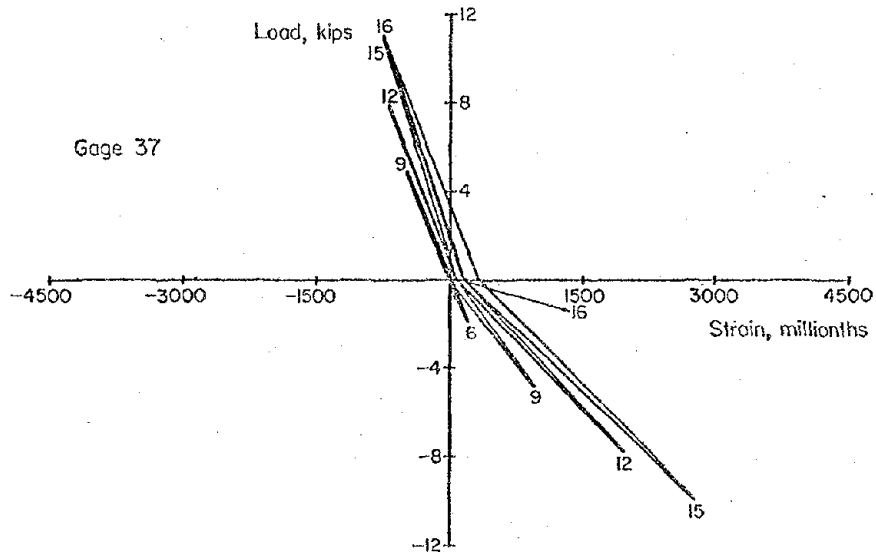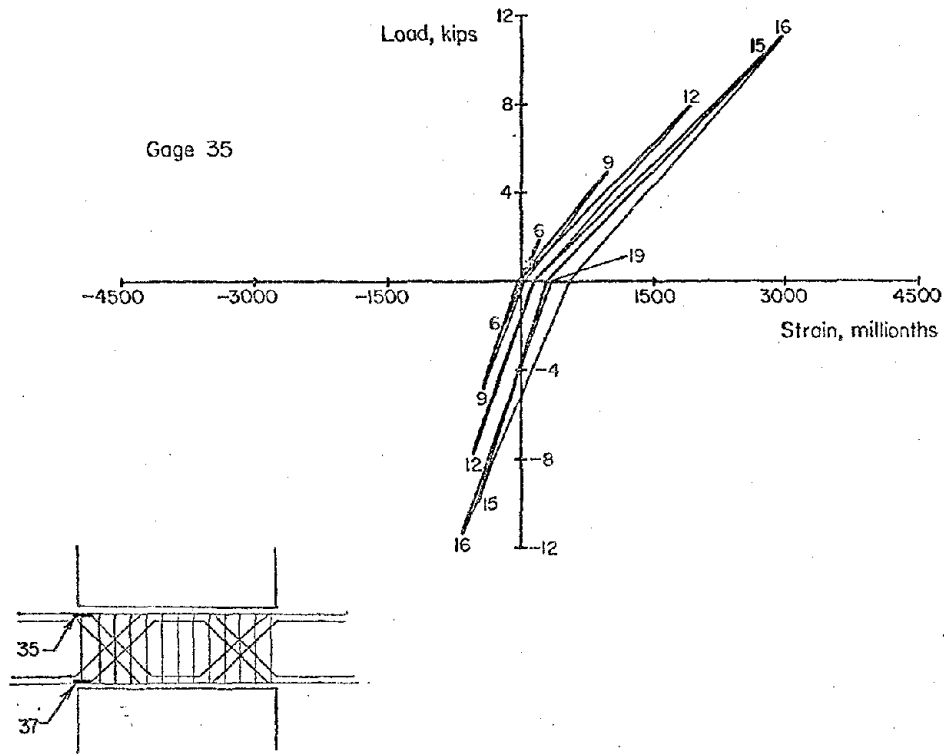
Fig. A-28   Load versus Flexural Steel Strains
for Specimen C3 (West Beam)

Fig. A-29 Load versus Diagonal Steel Strains
for Specimen C3 (East Beam)

Load, kips

Gage 43

12
8
4
6
-4
-8
-12

15 16 19
12 22
25
9

-2700   -1800   -900   900   1800   2700
Strain, millionths

57
34

19 16

43
45

Load, kips

Gage 45

12 19
16
22
8
4
34
-4
-8
-12

-2700   -1800   -900   1800   2700
Strain, millionths

9
25
12
15
16 19
22
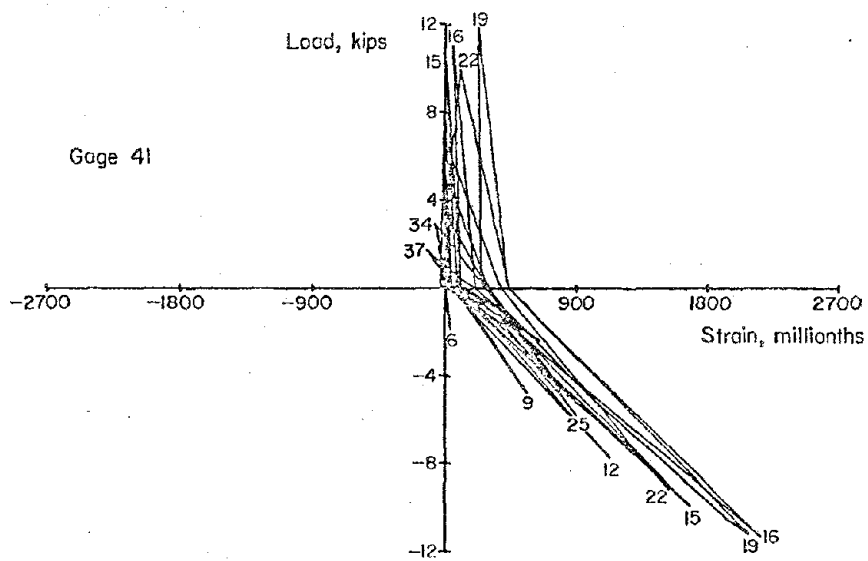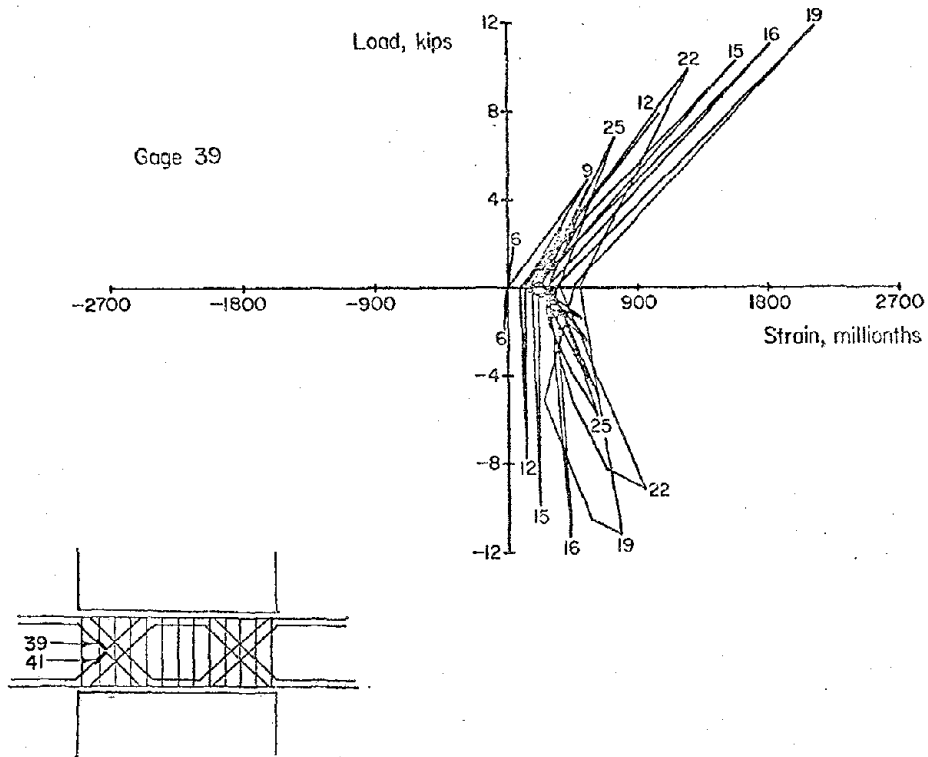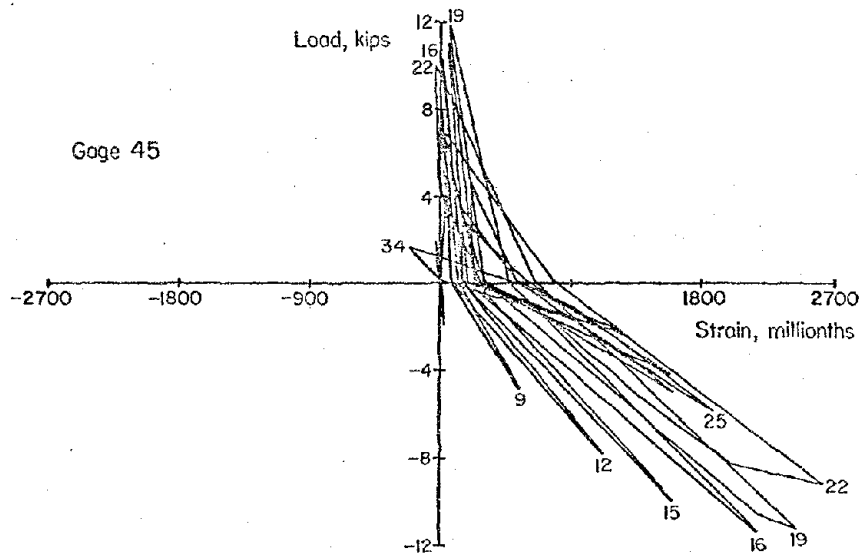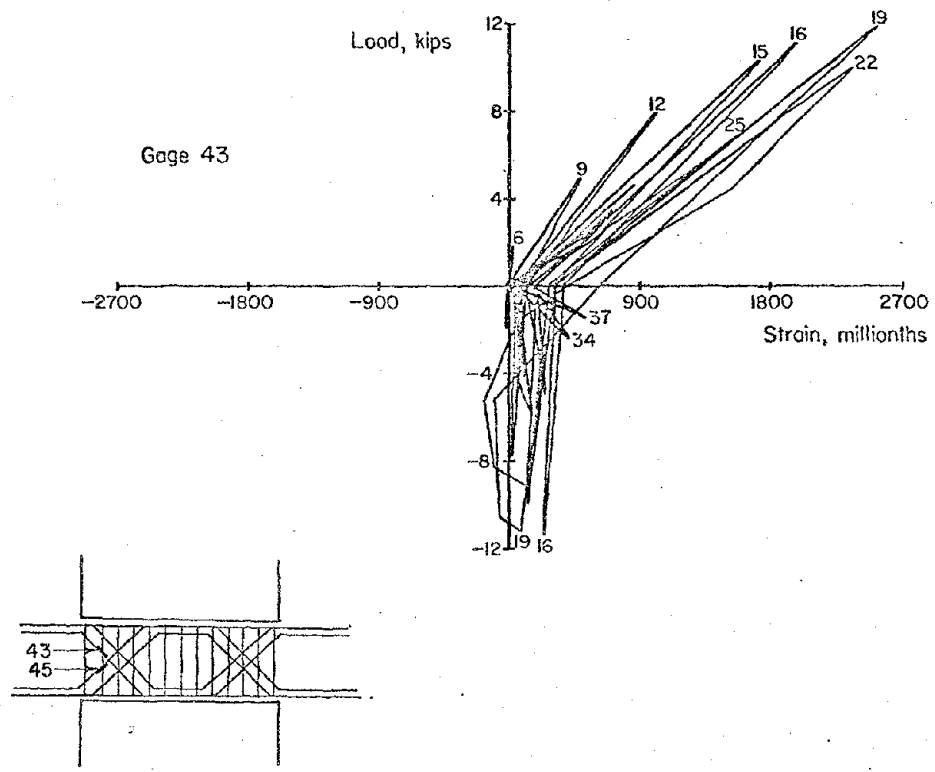
Fig. A-30   Load versus Diagonal Steel Strains
for Specimen C3 (West Beam)
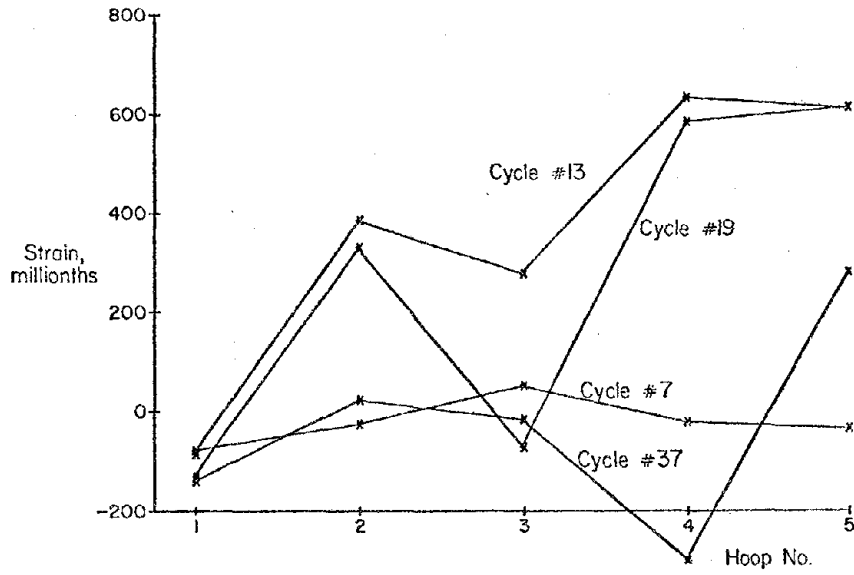
a) East Beam
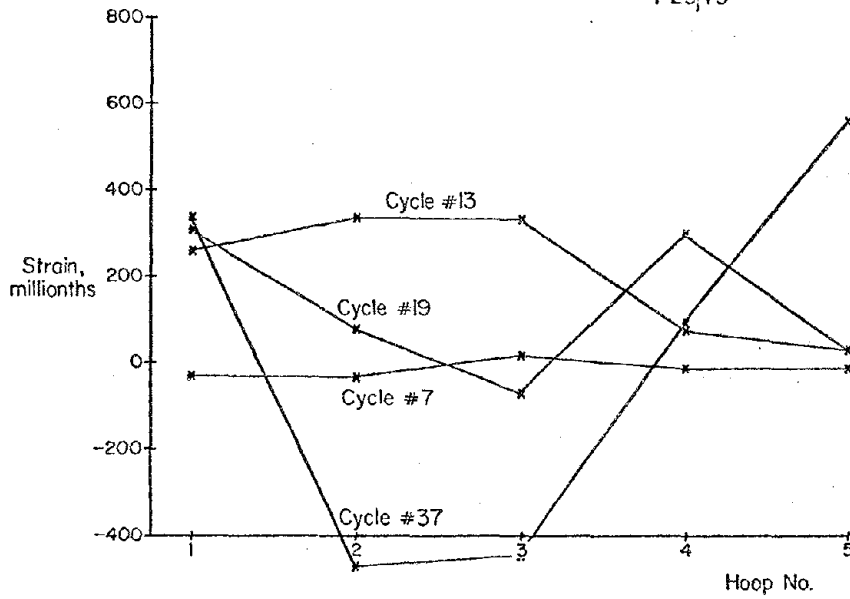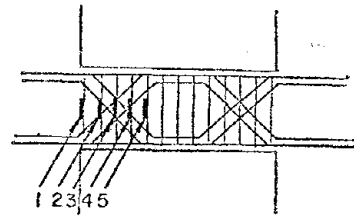
b) West Beam

Fig. A-31   Stirrup-tie Steel Strains for Specimen C3
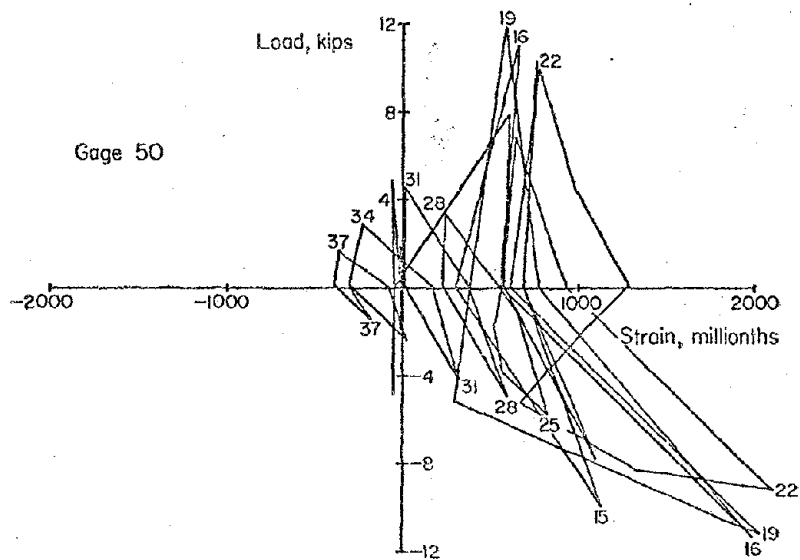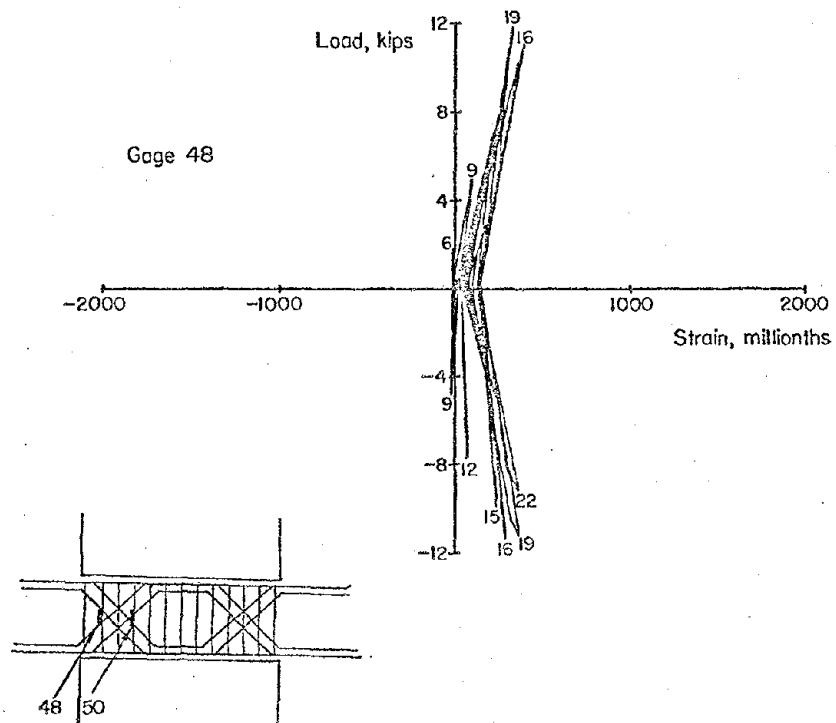
Fig. A-32   Load versus Stirrup-tie Steel Strains
for Specimen C3 (East Beam)
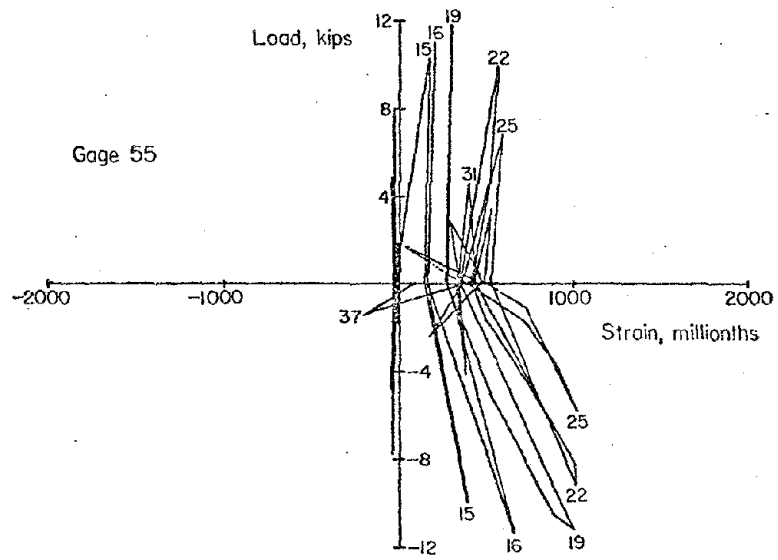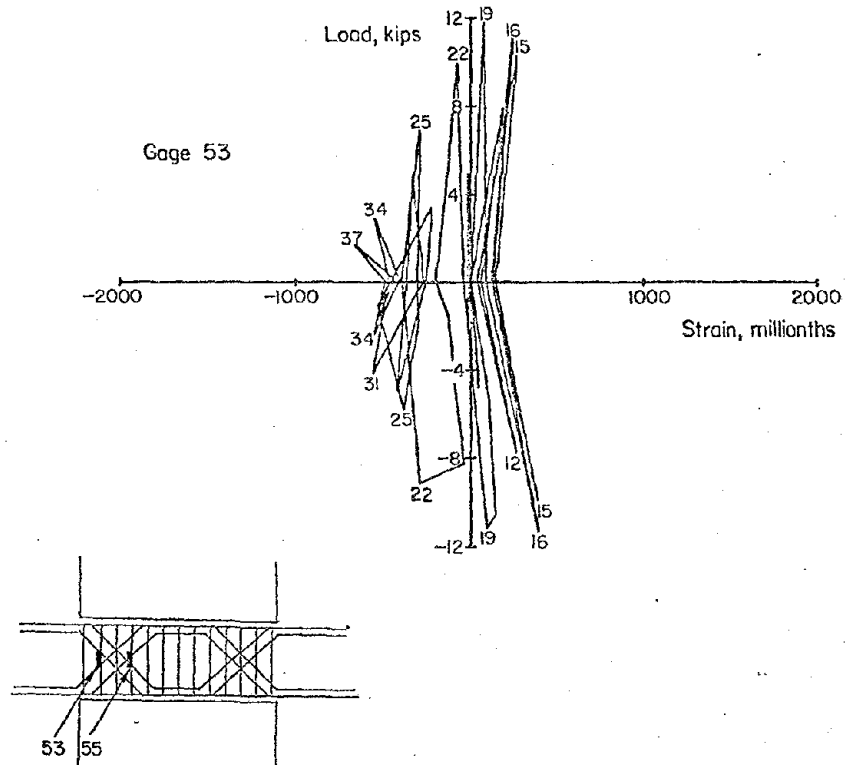
Fig. A-33   Load versus Stirrup-tie Steel Strains
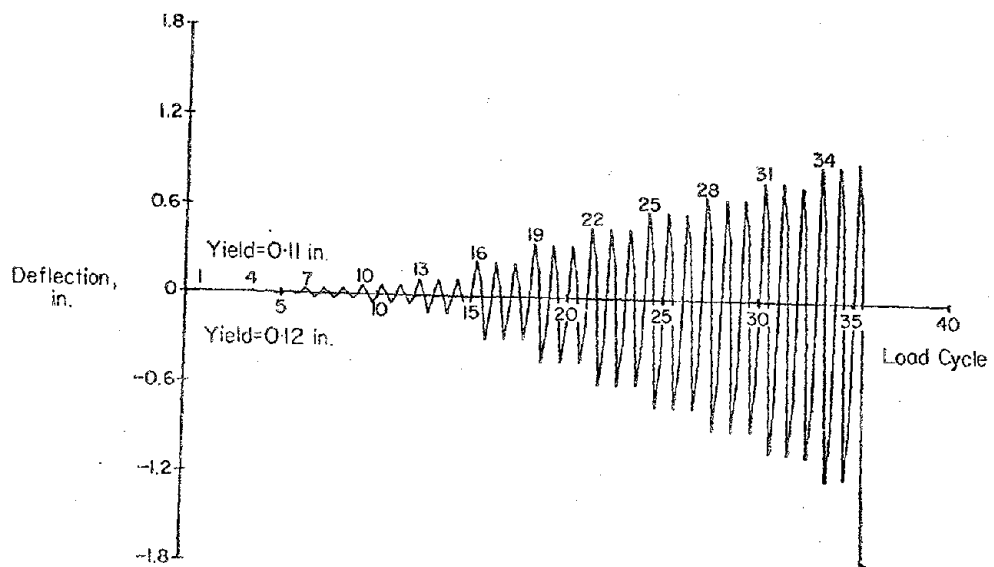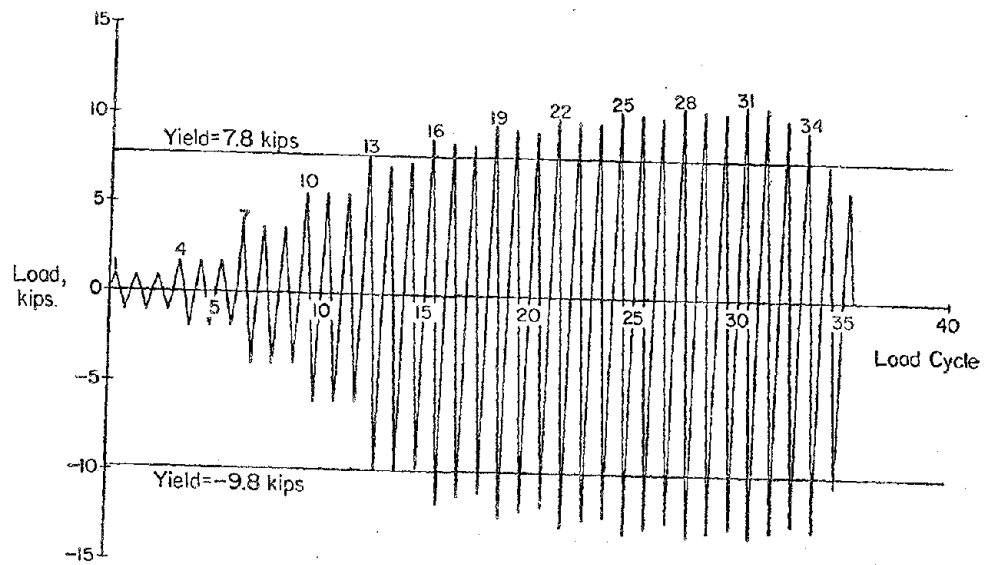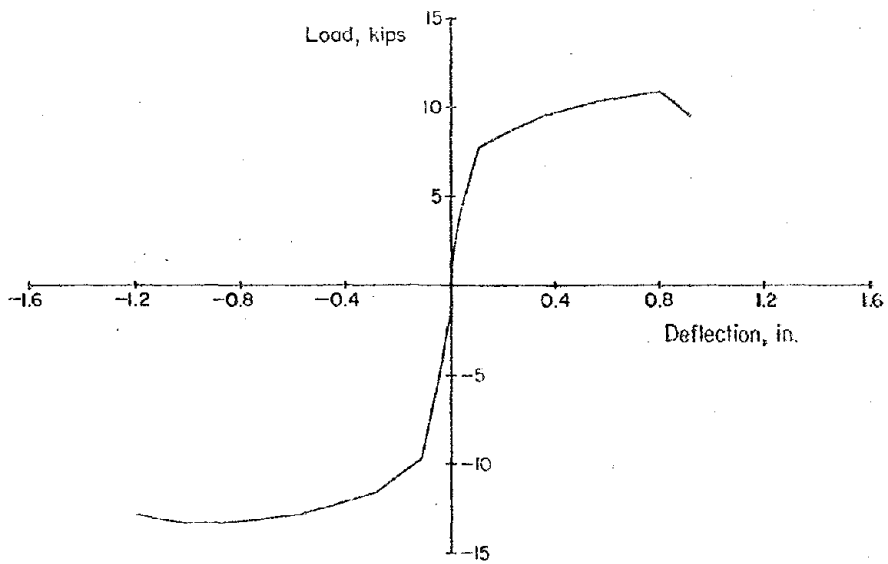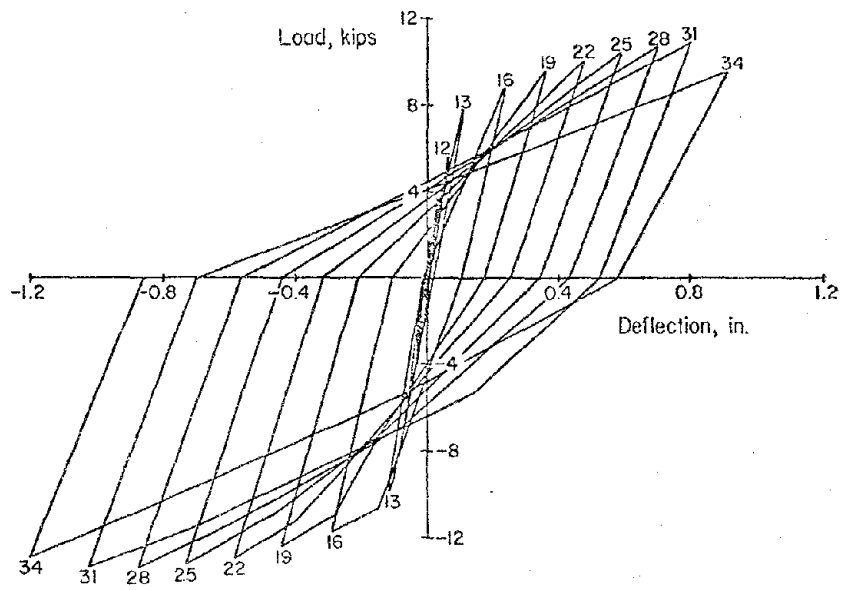for Specimen C3 (West Beam)
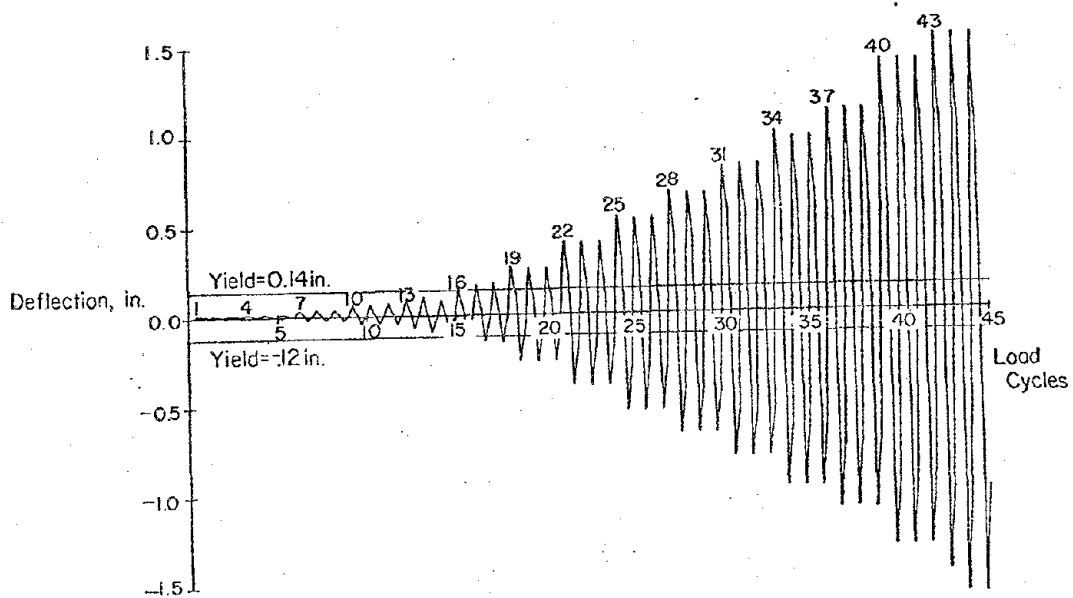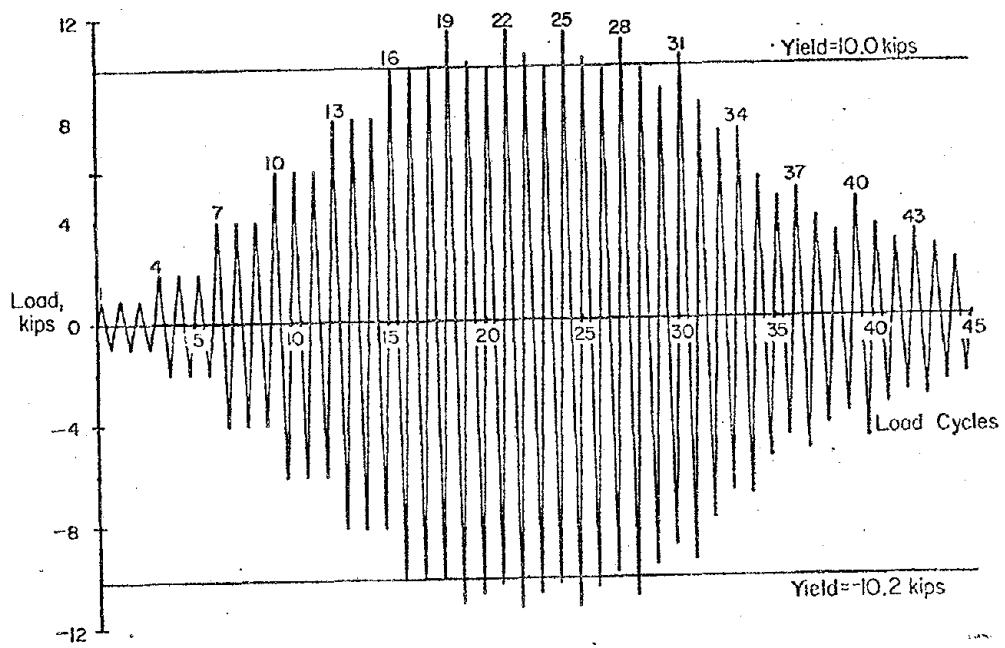
Fig. A-34 Load and Deflection Histories for Specimen C4

A-36
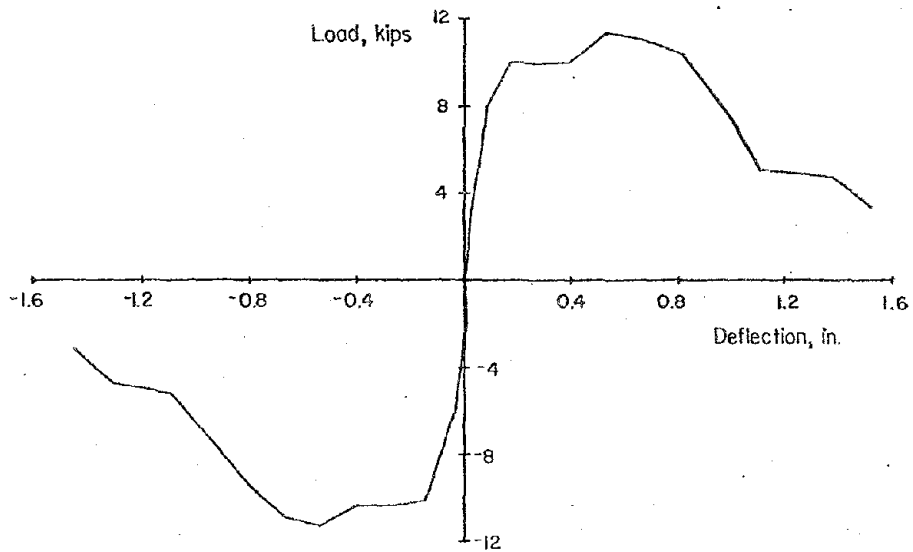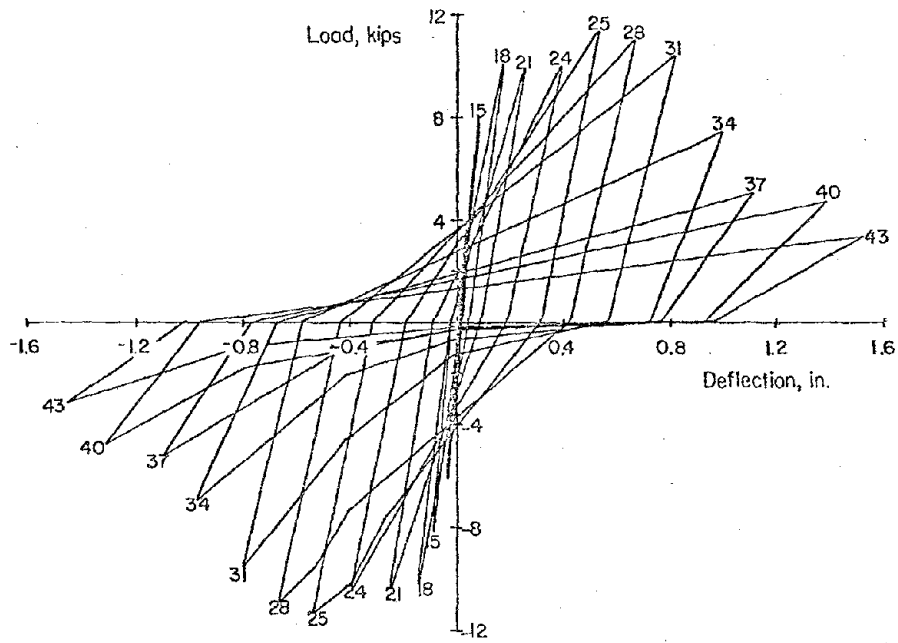
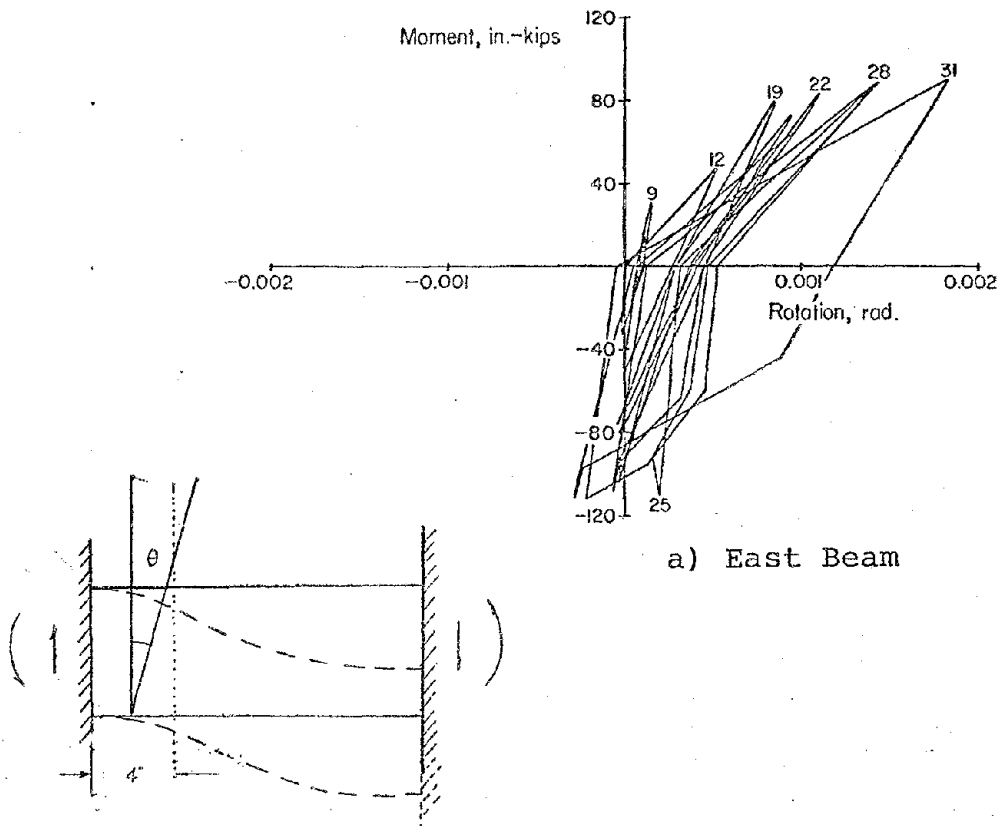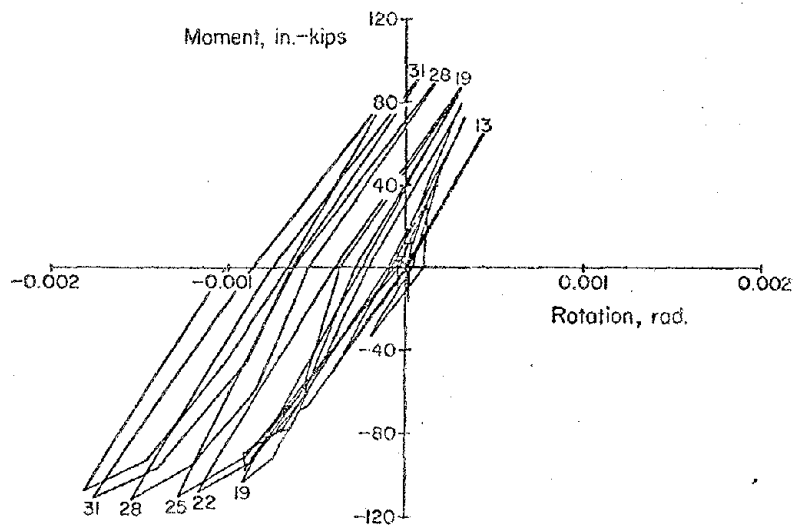Fig. A-35 Load versus Deflection for Specimen C4
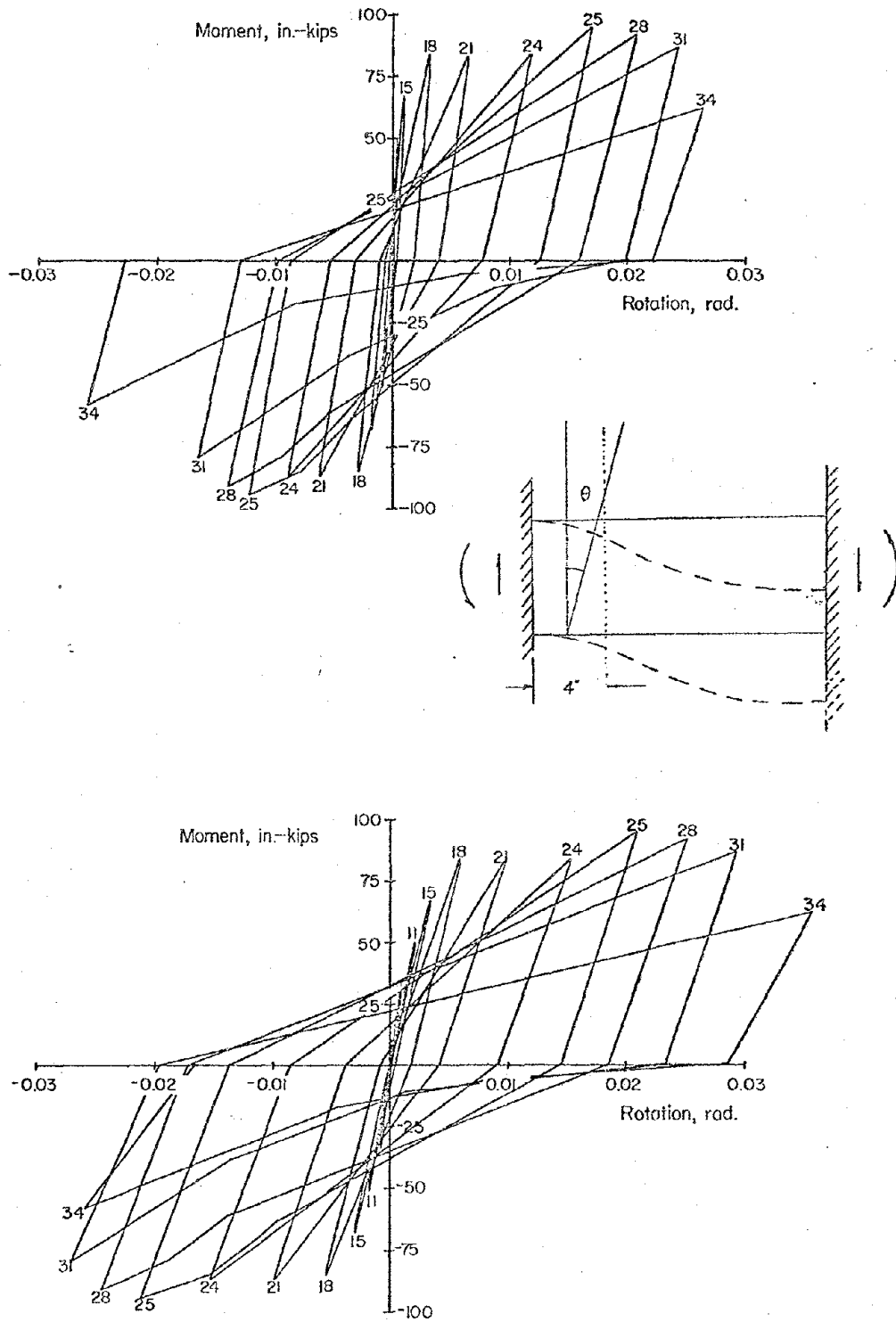
Fig. A-36   Moment versus Rotation for Specimen C4
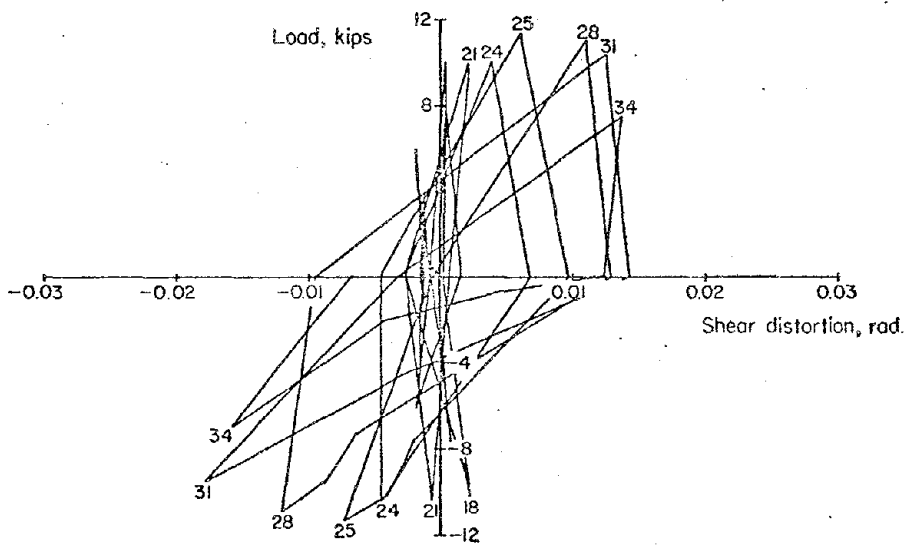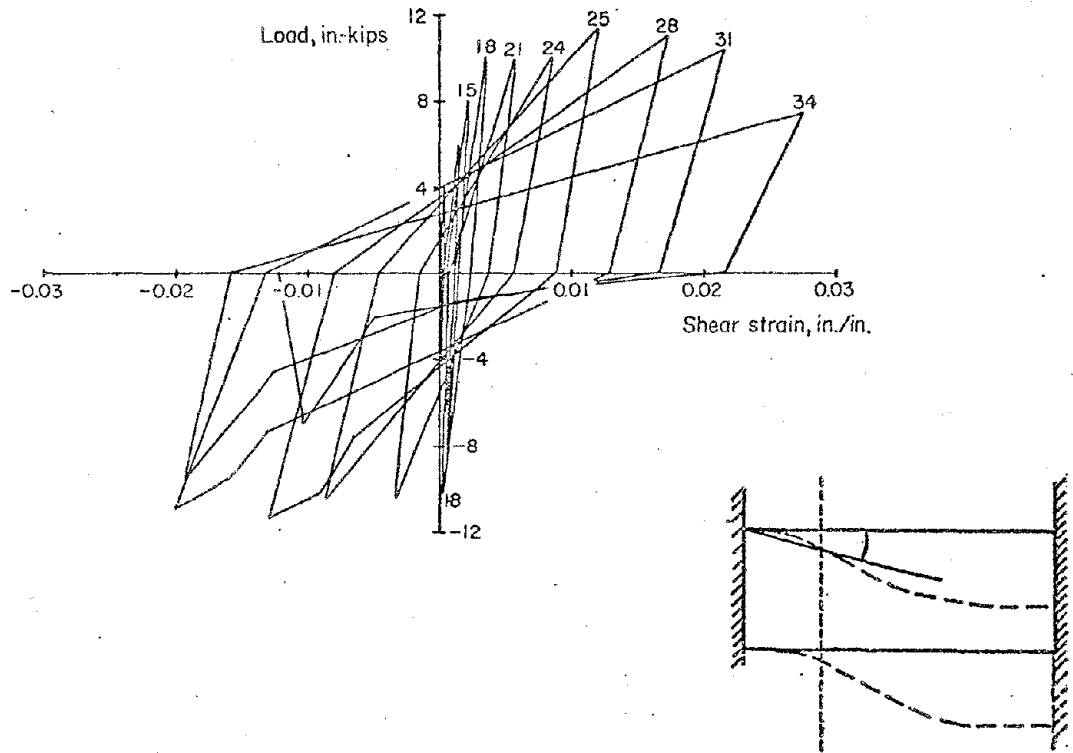
Fig. A-37 Load versus Shear Distortion for Specimen C4

Fig. A-38 Load versus Flexural Steel Strains
for Specimen C4 (East Beam)

Load, kips

Gage 35

Strain, millionths

Load, kips

Gage 37

Strain, millionths
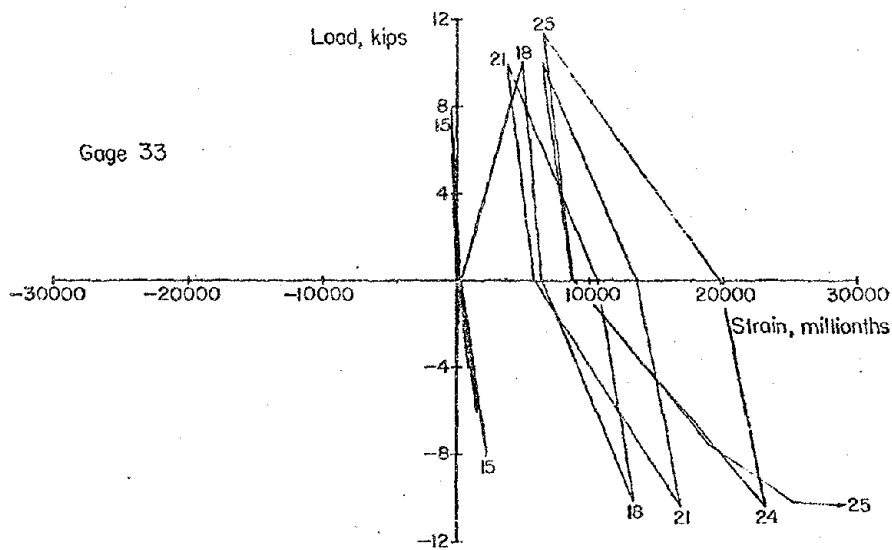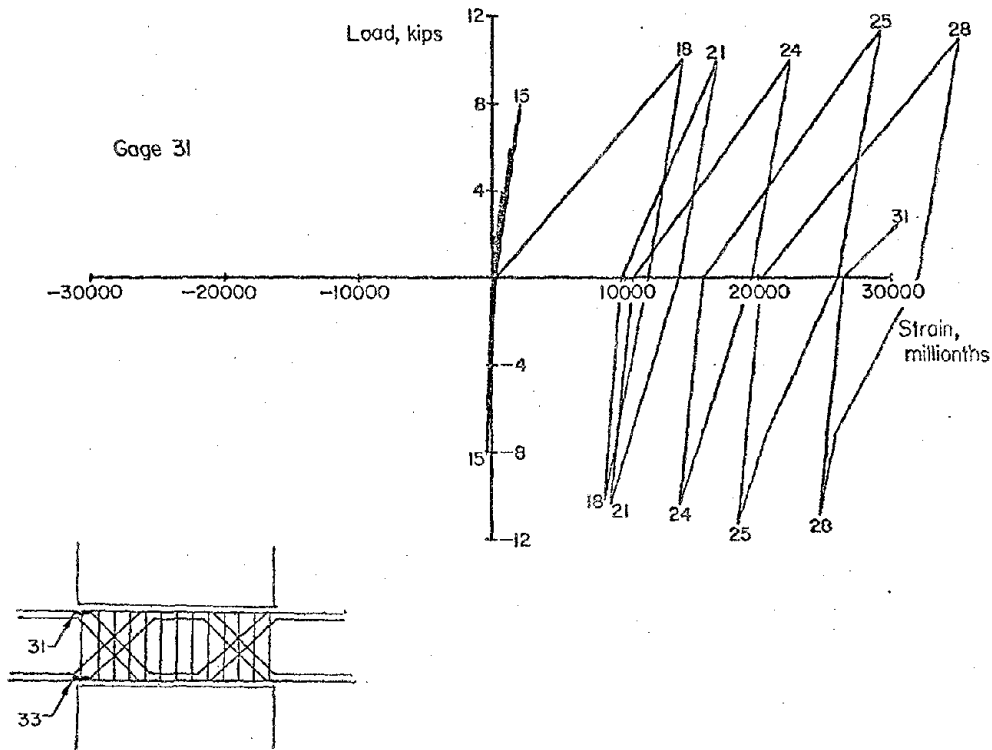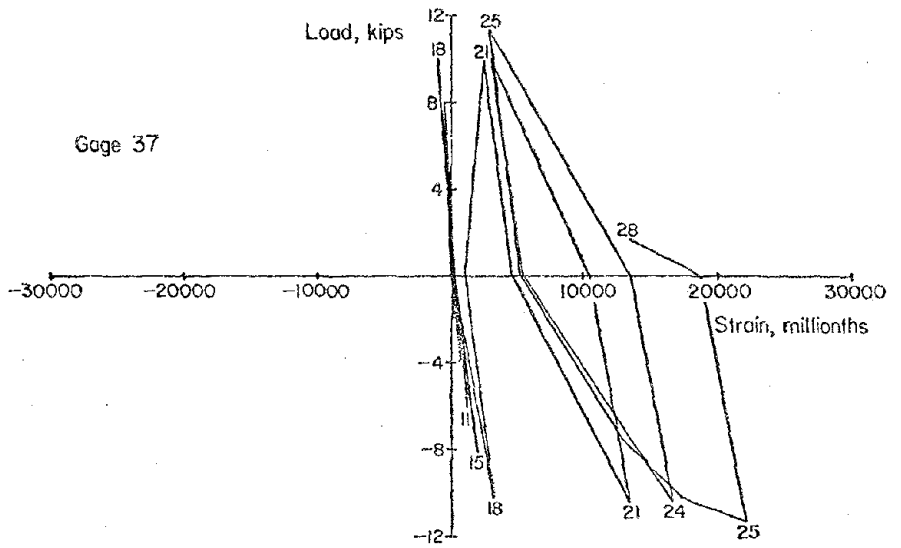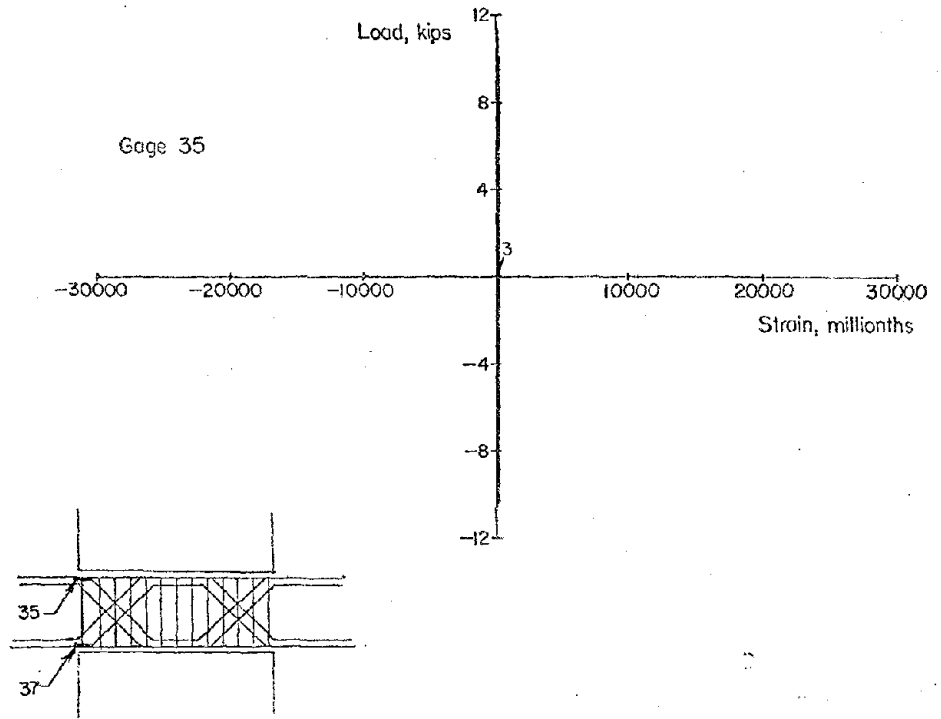
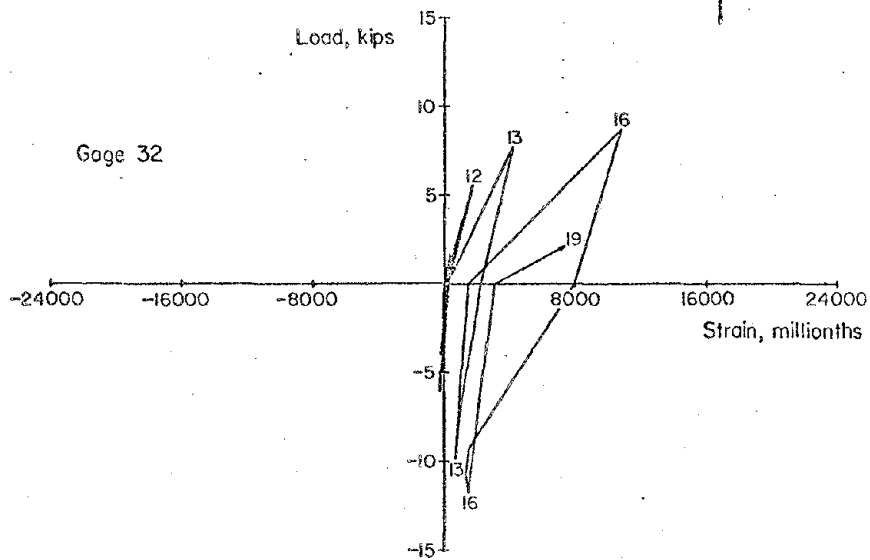Fig. A-39   Load versus Flexural Steel Strains
for Specimen C4 (West Beam)

A-41
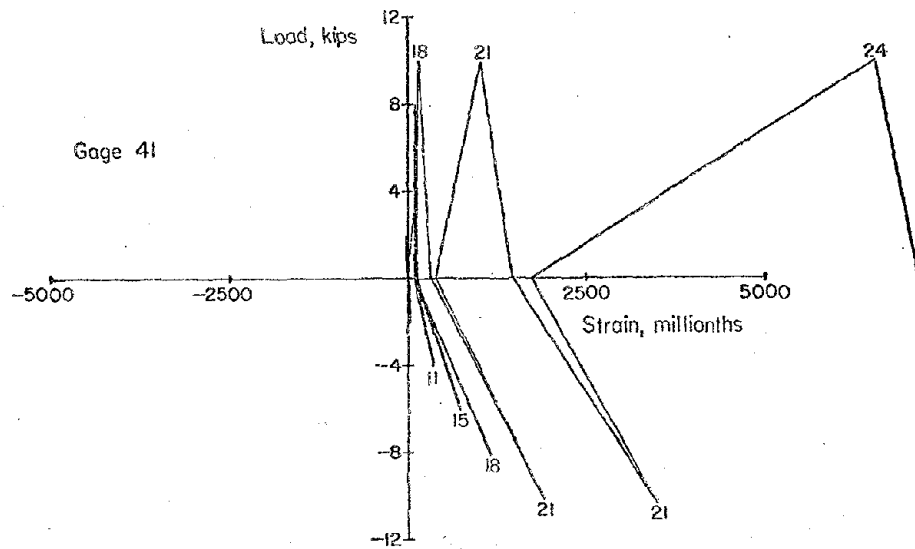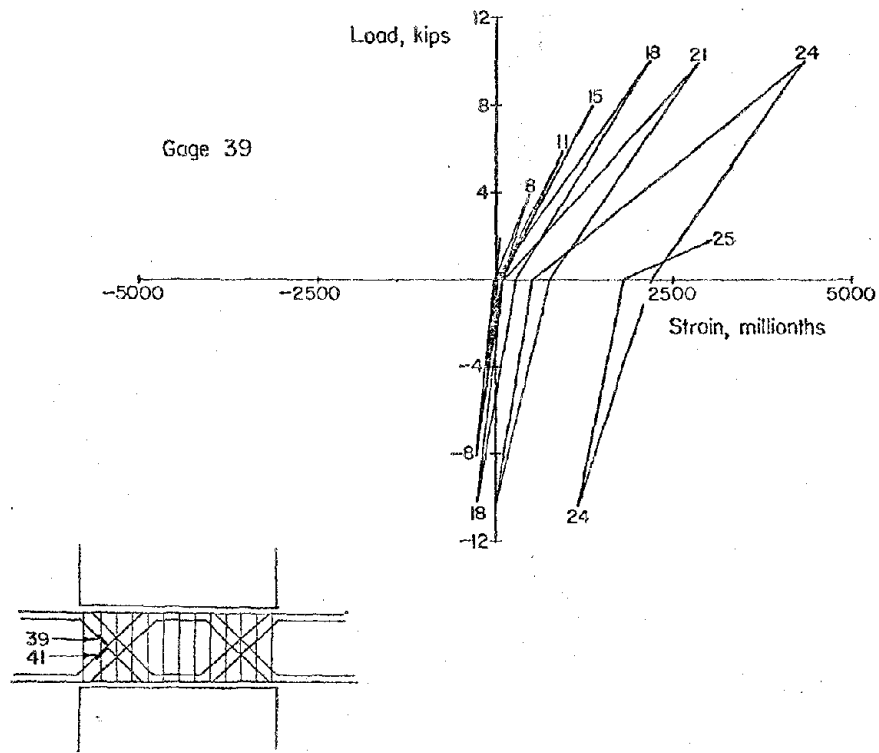
Fig. A-40   Load versus Diagonal Steel Strains
for Specimen C4 (East Beam)

A-42
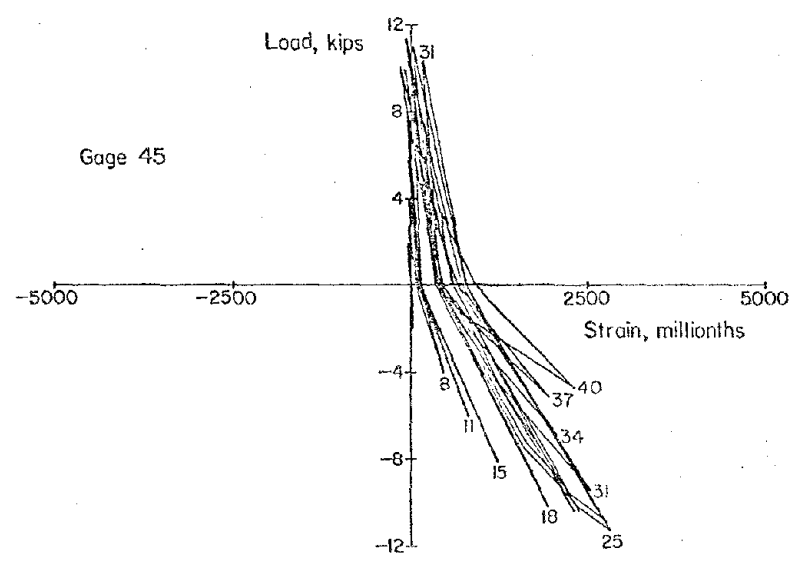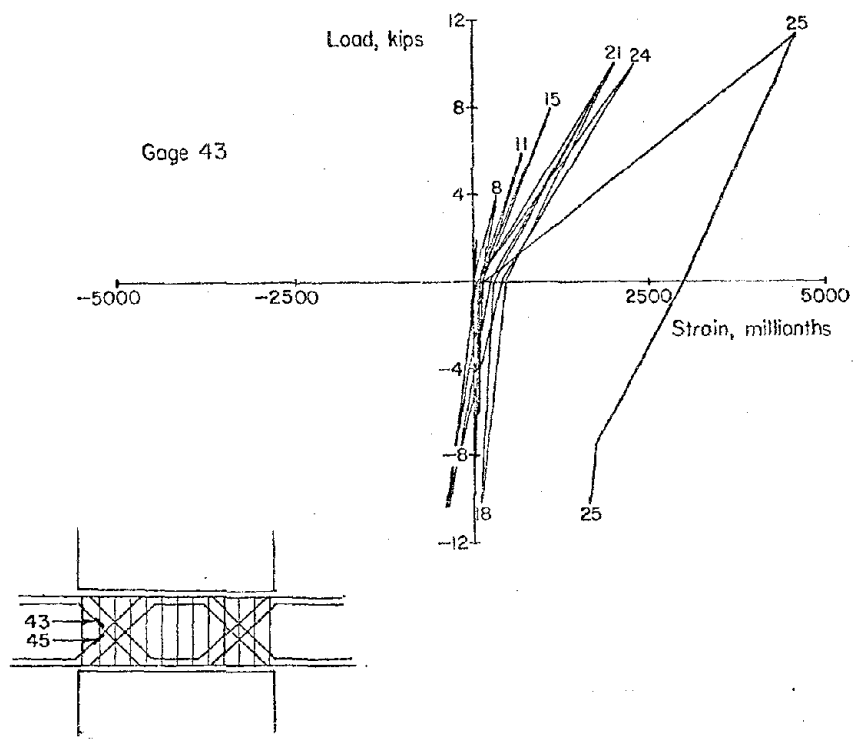
Fig. A-41   Load versus Diagonal Steel Strains
            for Specimen C4 (West Beam)
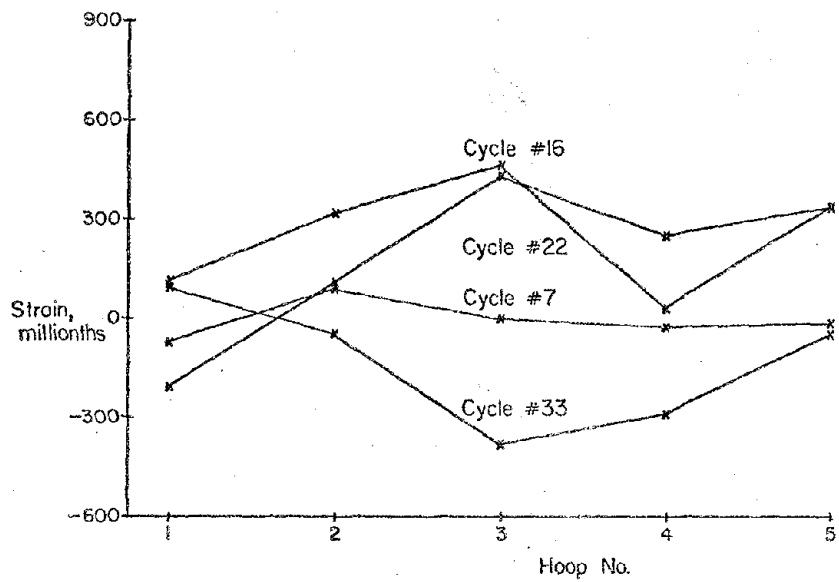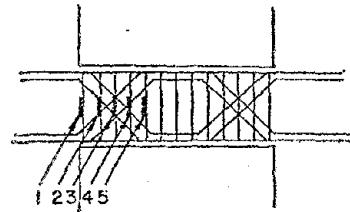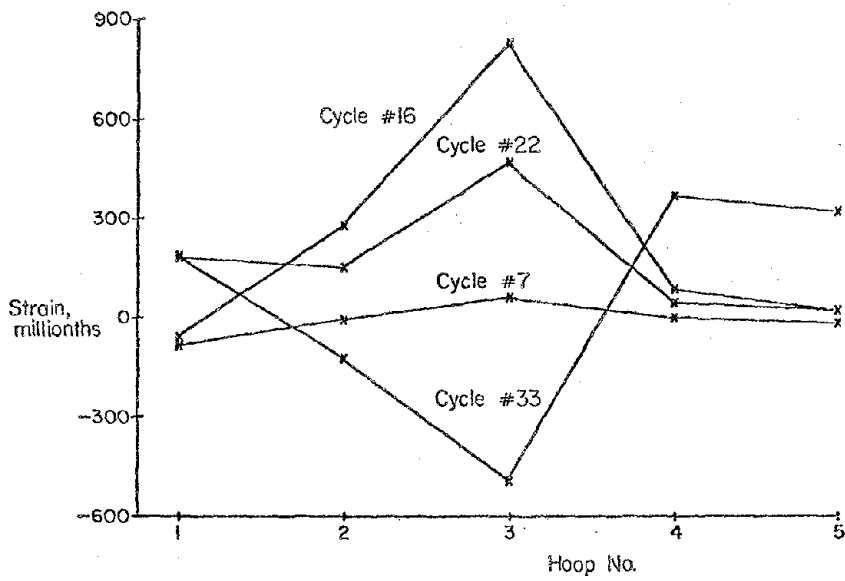
Fig. A-42   Stirrup-tie Steel Strains for Specimen C4
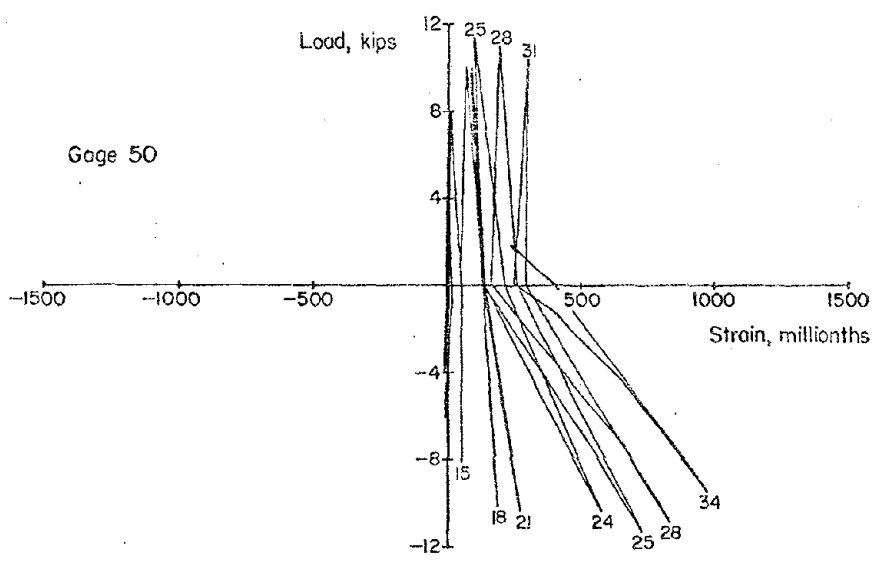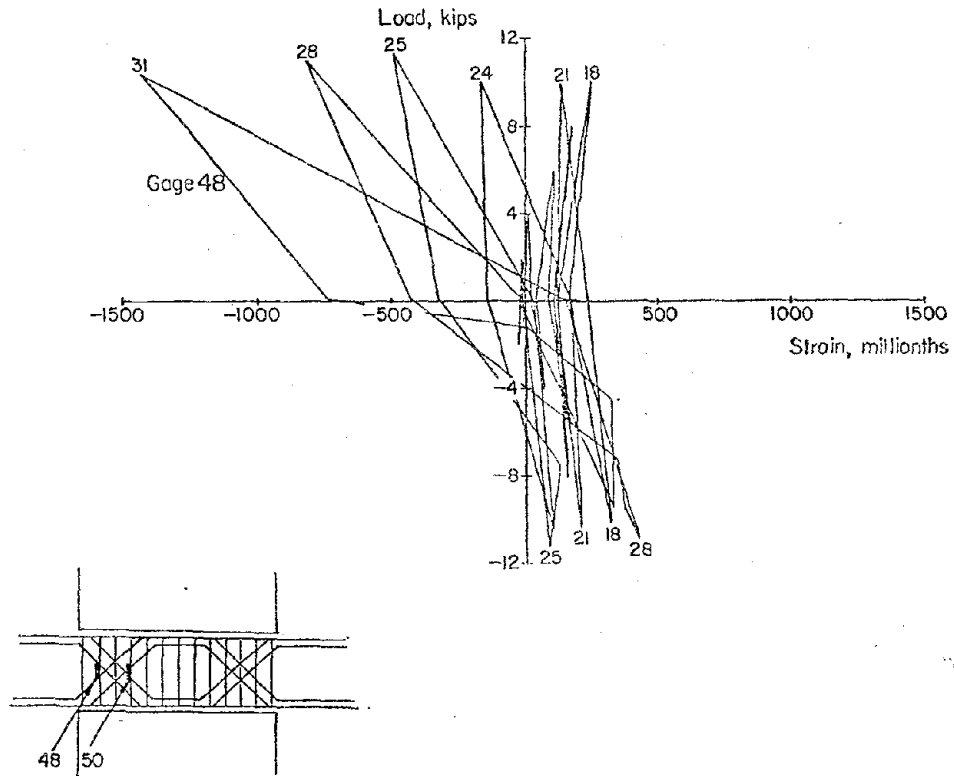
Fig. A-43 Load versus Stirrup-tie Steel Strains
for Specimen C4 (East Beam)
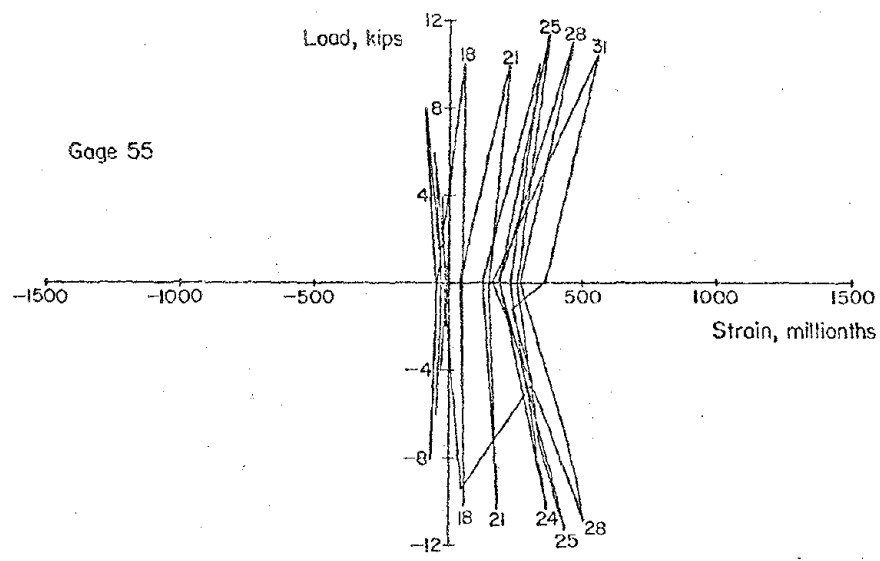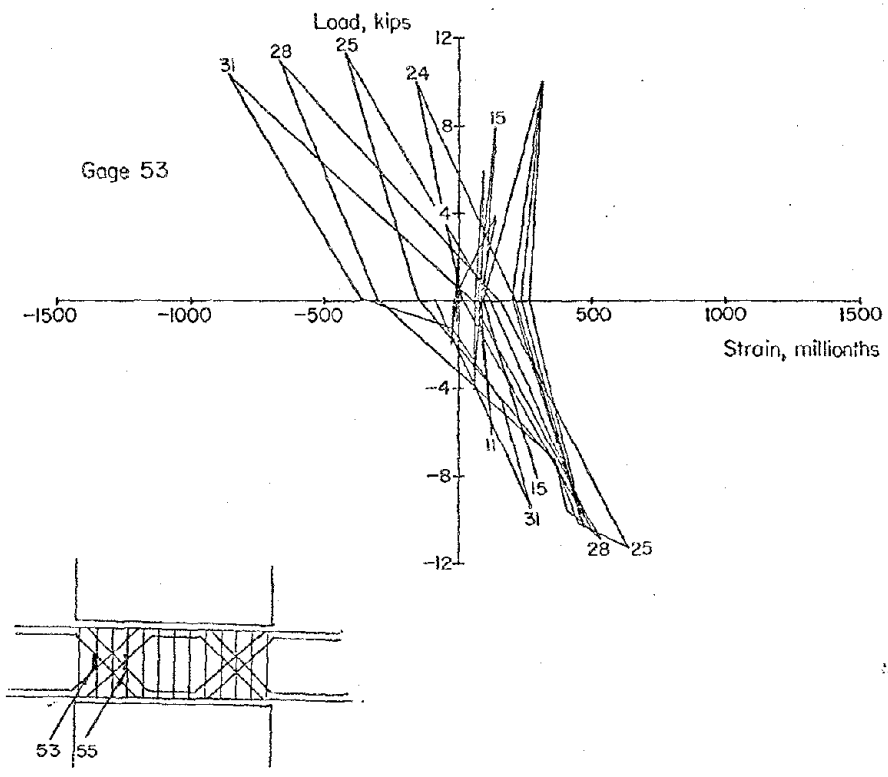
Fig. A-44   Load versus Stirrup-tie Steel Strains
for Specimen C4 (West Beam)

Fig, A-45   Load and Deflection Histories for Specimen C5

A-47

Fig. A-46   Load versus Deflection for Specimen C5
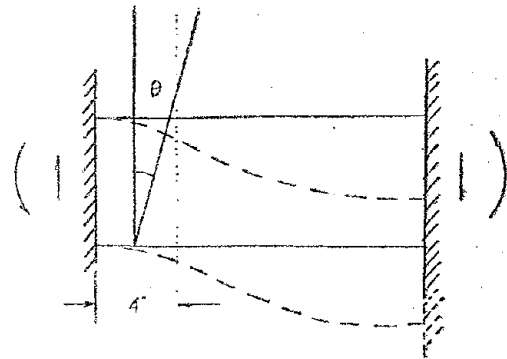
a) East Beam

b) West Beam

Fig. A-47 Moment versus Rotation for Specimen C5
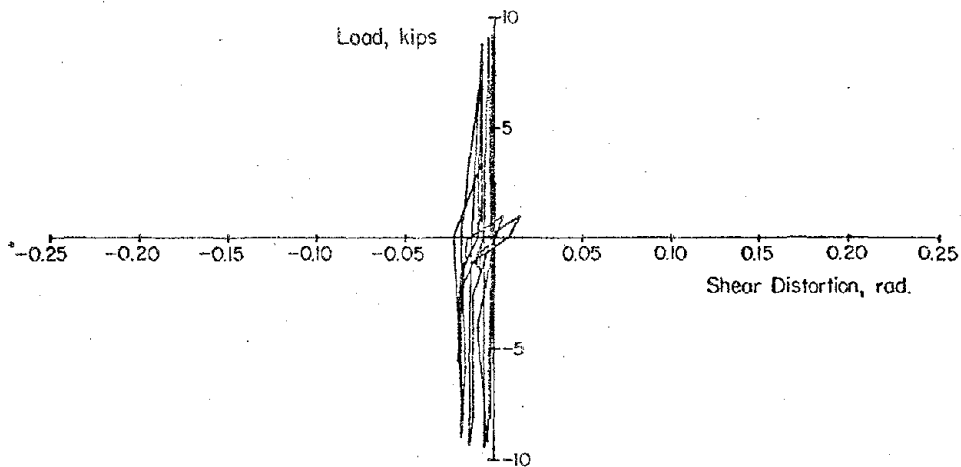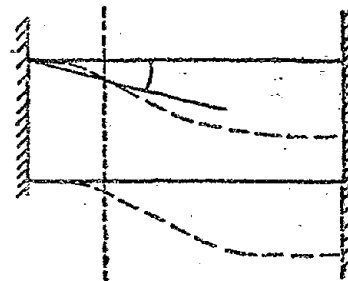
a) East Beam

b) West Beam

Fig. A-48 Load versus Shear Distortion for Specimen C5

Gage 31

Load, kips

Strain, millionths

Gage 33

Load, kips

Strain, millionths

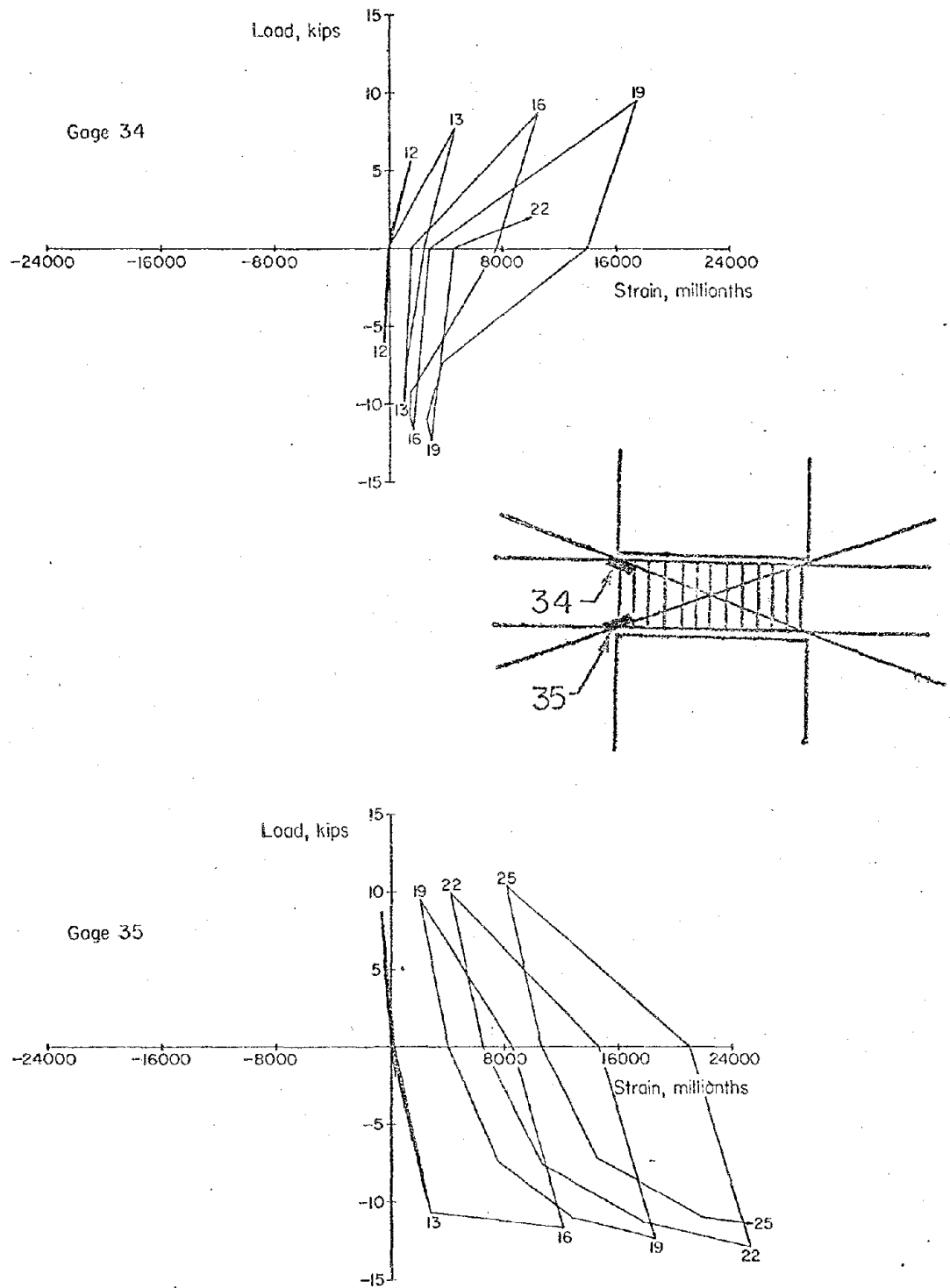Fig. A-49   Load versus Flexural Steel Strains
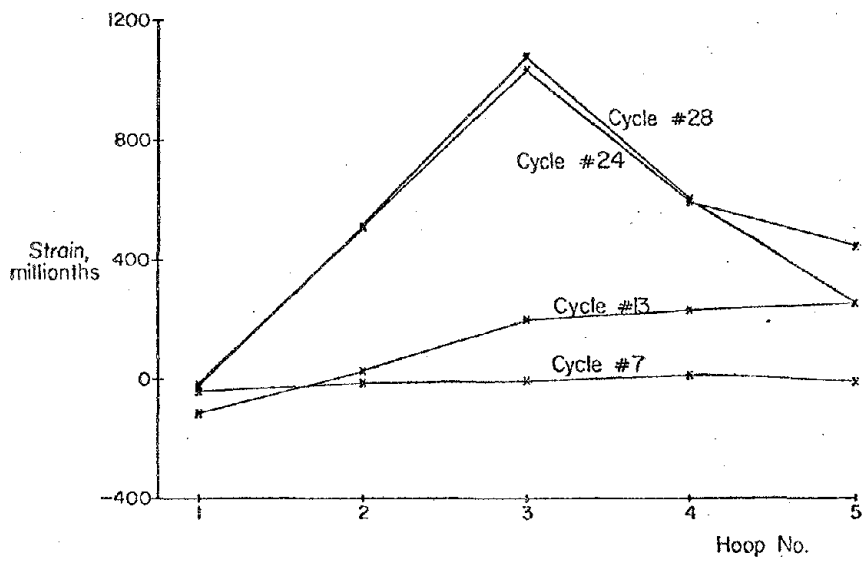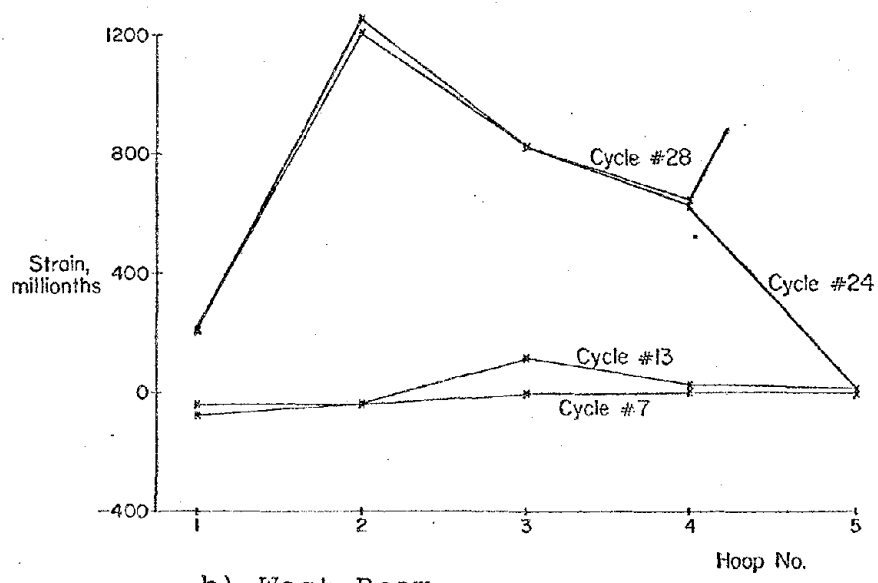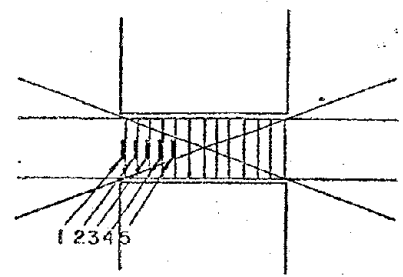for Specimen C5 (East Beam)

A-51

Fig. A-50   Load versus Flexural Steel Strains
for Specimen C5 (West Beam)

a) East Beam

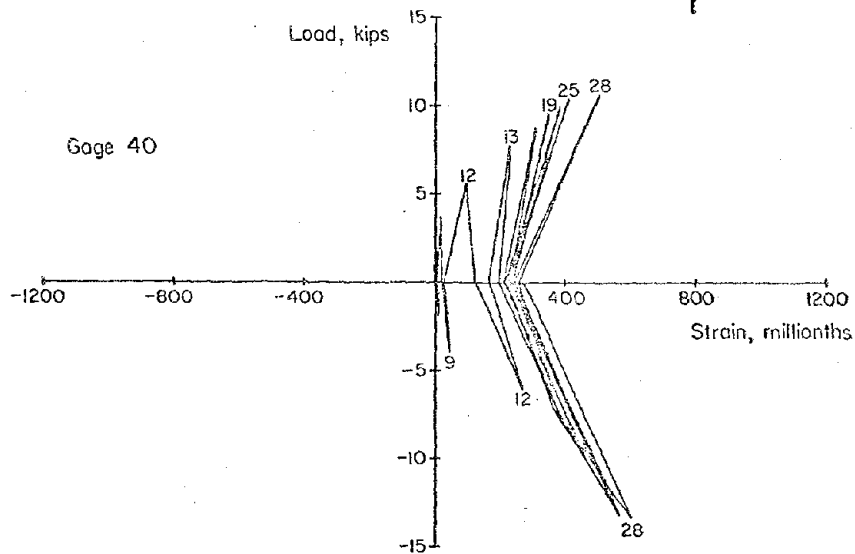b) West Beam

Fig. A-51 Stirrup-tie Steel Strains for Specimen C5

Fig. A-52   Load versus Stirrup-tie Steel Strains
for Specimen C5   (East Beam)
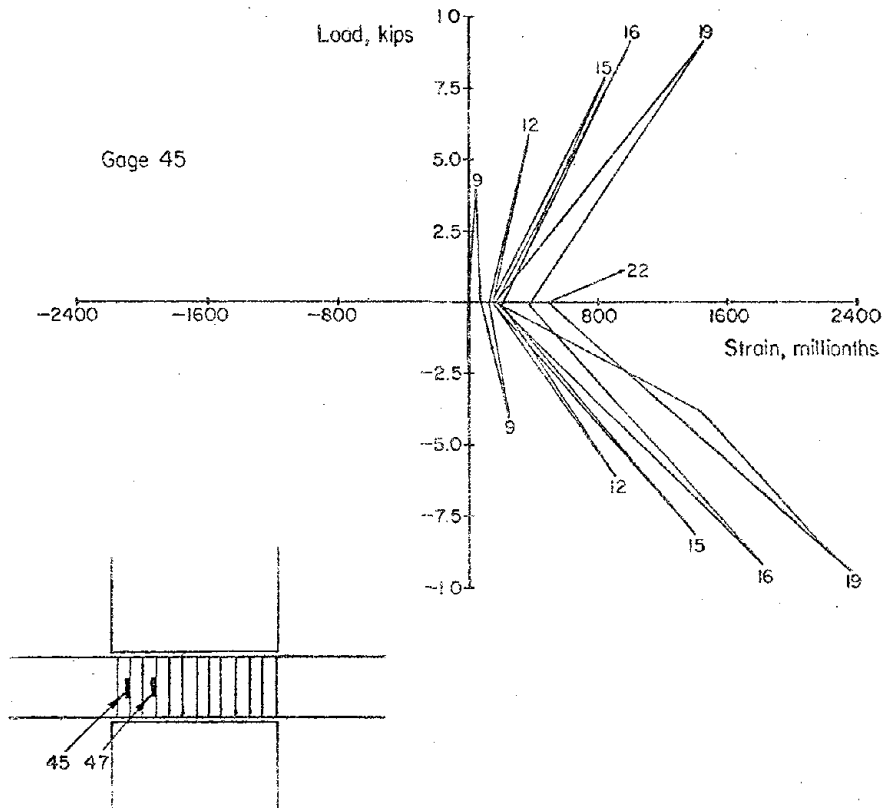
Fig. A-53 Load versus Stirrup-tie Steel Strains
for Specimen C5 (West Beam)

A-55

Fig. A-54   Load and Deflection Histories for Specimen C6

A-56

Fig. A-55   Load versus Deflection for Speciment C6

a) East Beam

b) West Beam

Fig. A-56 Moment versus Rotation for Specimen C6

A-58
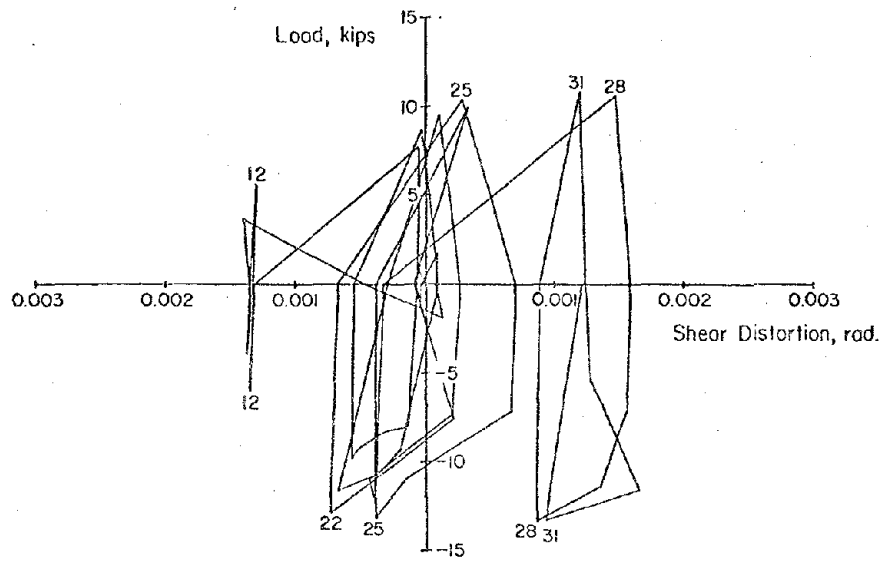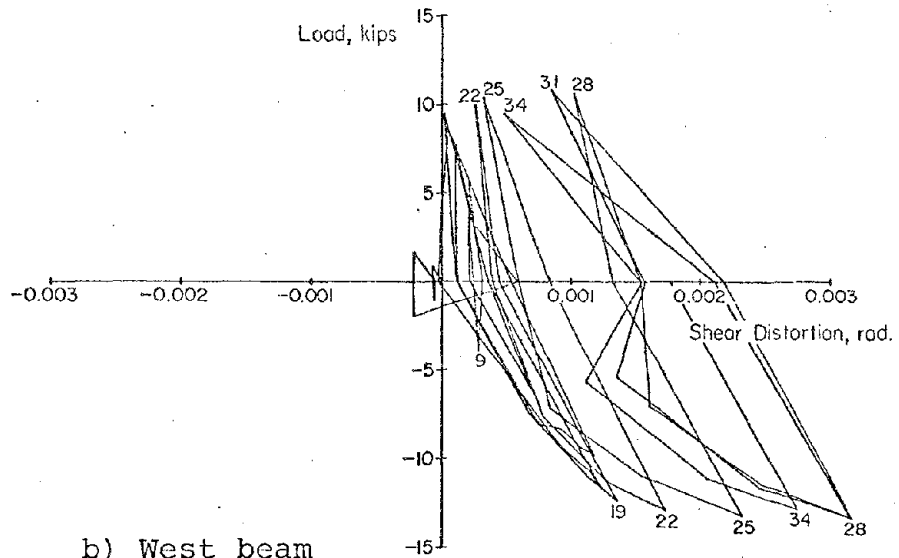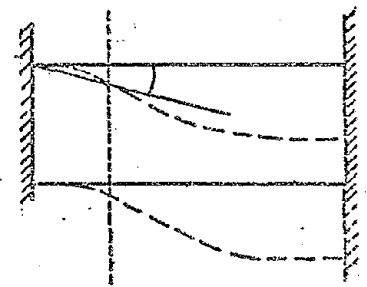
a) East Beam

b) West beam

Fig. A-57   Load versus Shear Distortion for Specimen C6
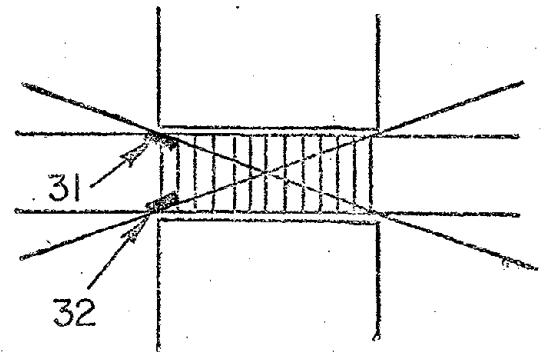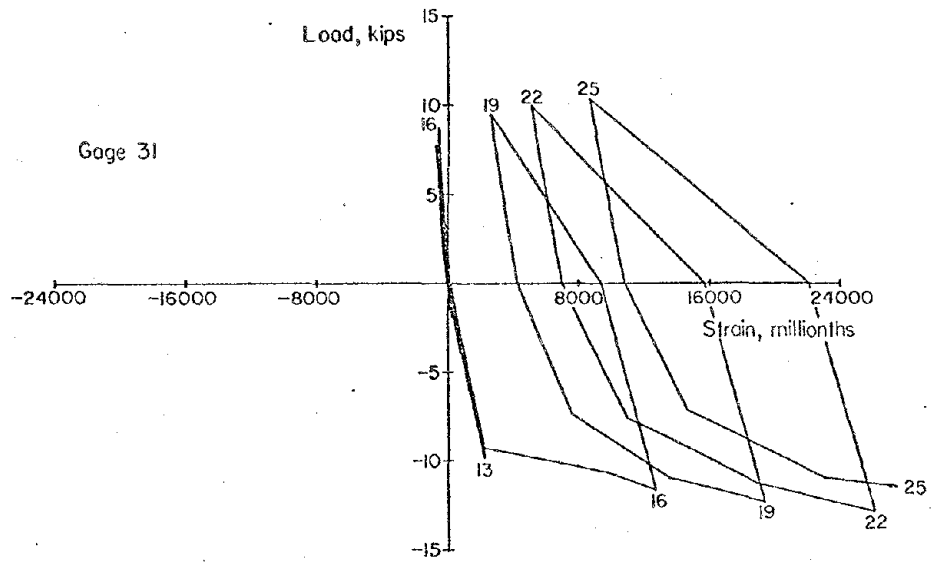
Fig. A-58   Load versus Diagonal Steel Strains
for Specimen C6 (East Beam)

Fig. A-59   Load versus Diagonal Steel Strains
for Specimen C6 (West Beam)

a) East Beam

b) West Beam
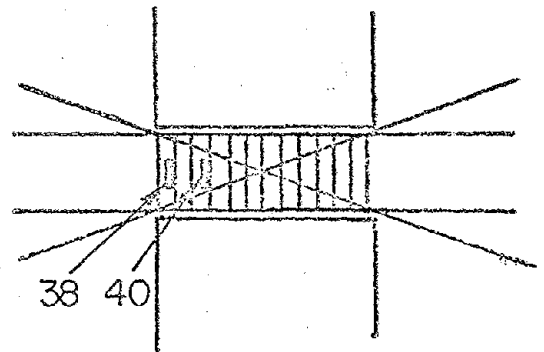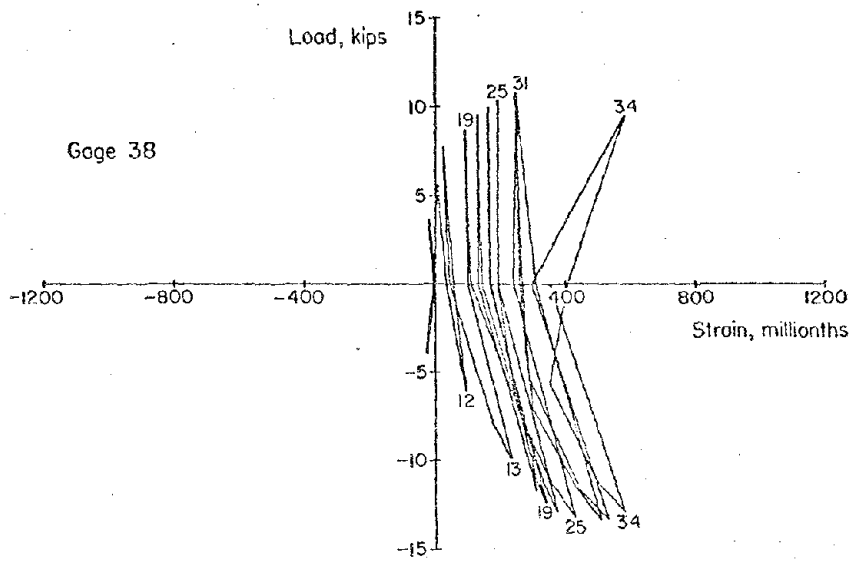
Fig. A-60   Stirrup-tie Steel Strains for Specimen C6

Fig. A-61   Load versus Stirrup-tie Steel Strains
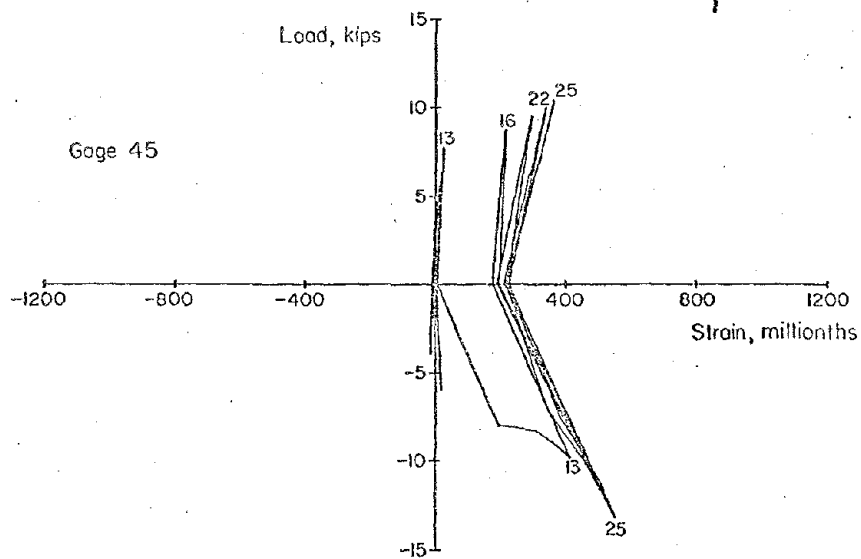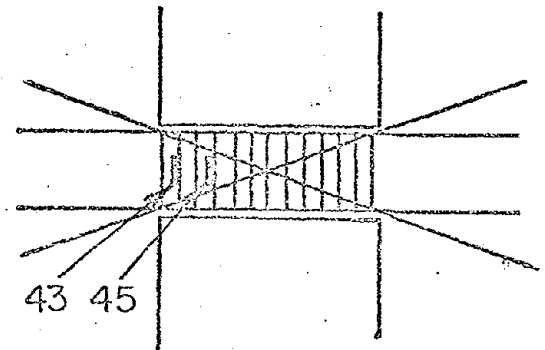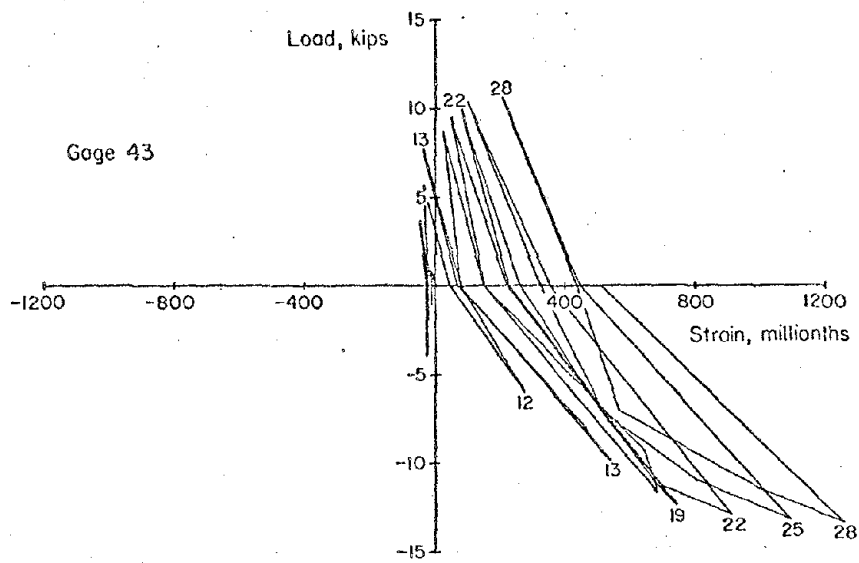for Specimen C6 (East Beam)

Fig. A-62   Load versus Stirrup-tie Steel Strains
for Specimen C6 (West Beam)